Island System Operation with High Degree of Renewable Energy Resources

Proposing solutions for smaller power systems to ease the transition to clean energy generation

by
Mohammad Rajabdorri

supervised by
Enrique Lobato Miguélez
Lukas Sigrist

A document submitted in partial fulfillment of the requirements for the degree of
Doctor of Philosophy
at
ICAI School of Engineering
Comillas University

برای مامان و به یاد بابا

To my mom and in memory of my dad

Declaration

I declare that this thesis was composed by myself, that the work contained herein is my own except where explicitly stated otherwise in the text, and that this work has not been submitted for any other degree or professional qualification except as specified.

Mohammad Rajabdorri
Madrid, September 2022

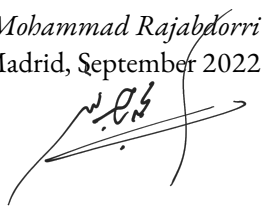

Acknowledgment

Probably Lukas and Enrique don't know to what extent they changed the course of my life just by hiring me at IIT. From the beginning, I promised myself not to let them down. They only made things easier for me by being supportive and helpful. I enjoyed my time and learned a lot of things here. It hasn't been an easy journey tho. From leaving my home country to starting a new life here in Spain, to dealing with the pandemic at the same time, I've been facing some tough challenges. But I guess that's what makes life more exciting.

I have to thank my mom for always being there for me. It wouldn't be possible without her help and constant support. I thank my brother for all the sacrifices that he made after we lost our father. I would also wish the best for the people of my country, as they are fighting these days for their freedom. I'm sure that they will earn what they're looking for. They deserve better.

Abstract

Island power systems, and in general smaller power systems, have specific characteristics that make the transition to renewable energy generation even harder. There are different challenges that are hindering the operation of a bigger share of renewable energy sources. These challenges are acknowledged in this thesis and novel solutions are introduced, that can help operators to ease the transition and also contributes to the current state-of-the-art. To tackle the reserve scarcity, the economic and technical impacts of storing renewable energy by deloading are assessed. Deloading enables renewable sources to offer some reserve as their headroom. The results show that providing online reserve by deloading is always beneficial for small power islands, and beneficial for medium and big islands when renewable energy is abundant. As renewable generators are uncertain, storing energy for periods with generation surplus and releasing it when necessary has been recognized and studied a lot in the literature. Storage devices should be scheduled alongside with the thermal and renewable generators, to be used efficiently. A formulation is presented in this thesis, that makes it possible to include liquid air energy storage in the unit commitment problem. Another issue that small power systems have been suffering from and it's getting worse by increasing the share of renewable energy sources is inertia scarcity. Any contingency can lead to a fast frequency decay when inertia is low. To prevent contingencies that will cause poor frequency response, it's been tried to include frequency dynamics in the scheduling process. It's challenging because frequency dynamics are highly non-linear and non-convex, making it very hard to add them to the unit commitment problem, which is usually solved as a mixed integer linear programming problem. In this thesis frequency constrained unit commitment is proposed with the help of machine learning, which keeps the size of the unit commitment similar to the conventional formulation. That also makes it suitable for more computationally demanding unit commitment formulations like robust and stochastic methods. This is important because systems with a high share of renewable generation are also uncertain. A robust frequency constrained unit commitment formulation is proposed in this thesis, which uses logistic regression to learn the frequency-related constraints. Then a machine learning process to learn the frequency nadir after outages as a constraint for the unit commitment problem is introduced and compared with an analytical state-of-the-art formulation. Results show that the proposed method based on machine learning is as effective as the analytical methods while having a considerably lower run-time.

Resumen

Los sistemas eléctricos insulares, y en general los sistemas eléctricos pequeños, tienen características específicas que hacen más difícil la transición ecológica a un mix de generación con mayor cantidad de energía renovable. Existen diferentes retos que dificultan aumentar la penetración de fuentes de energía renovable. En esta tesis se identifican estos retos y se proponen soluciones novedosas que pueden ayudar a los operadores a facilitar la transición ecológica contribuyendo al estado actual del arte. Para hacer frente a la escasez de reservas, se evalúan las repercusiones económicas y técnicas de permitir la participación de fuentes de energía renovable en el control de la frecuencia, ofrezciendo parte del producible eólico como reserva a subir. Los resultados demuestran que proporcionar reserva con energías renovables es siempre beneficioso en islas eléctricas pequeñas, y beneficioso para las islas medianas y grandes cuando la energía renovable es abundante. Dado que la producción de los generadores renovables es muy variable, los dispositivos de almacenamiento deben programarse junto con los generadores térmicos y renovables, para ser utilizados de forma eficiente. En esta tesis se presenta una formulación que permite incluir la tecnología LAES (almacenamiento de energía en aire líquido) en el problema de despacho económico. Otro problema que han sufrido los sistemas eléctricos pequeños y que se agrava con el aumento de la participación de las fuentes de energía renovables es la escasez de inercia. Cualquier contingencia puede provocar una rápida caída de la frecuencia cuando la inercia es baja. Para evitar que las contingencias provoquen una mala respuesta de la frecuencia, se ha incluido la dinámica de la frecuencia en el proceso de programación. Es un reto porque la dinámica de la frecuencia es altamente no lineal y no convexa, lo que hace muy difícil añadirla al problema de despacho económico, que normalmente se resuelve mediante un problema de programación lineal entera mixta. En esta tesis se propone un despacho económico con restricciones de frecuencia con la ayuda del aprendizaje automático, que mantiene el tamaño del problema de despacho económico similar a la formulación convencional. Esto también lo hace adecuado para formulaciones más exigentes desde el punto de vista computacional, como la optimización robusta o estocástica. Esto es importante porque los sistemas con una alta proporción de generación renovable tienen una gran variabilidad. En esta tesis se propone una formulación robusta del despacho económico con restricciones de frecuencia, que utiliza la regresión logística para modelar las restricciones relacionadas con la frecuencia. A continuación, se introduce un proceso de aprendizaje automático para representar la frecuencia mínima ante contingencias se compara con una formulación analítica previamente propuesta en el estado del arte. Los resultados muestran que el método propuesto basado en el aprendizaje automático es tan preciso como los métodos analíticos y tiene un tiempo de ejecución considerablemente menor.

Contents

List of Figures

List of Tables

1 Introduction

The general scope of this thesis and the main challenges involved in the topic under study are discussed. A summary of the next chapters, and how each chapter is relevant to the purposes of this thesis, is presented here. The corresponding literature review of each chapter is presented in the framework section of the following chapters.

Isolated electrical systems are different from large interconnected systems because they are smaller in size and usually not connected to other systems. The lack of technical and economic support from neighboring systems makes island systems more vulnerable to disturbances and causes higher system operating costs than in interconnected systems [1]. Currently, there are thousands of island electrical systems in the world [2]. The number of off-grid systems is increasing [3]. The isolated character affects island systems in two respects. On the one hand, the small size of island systems affects their stability and in particular frequency stability. Frequency stability depends fundamentally on the disturbance, the inertia of the system, and its frequency control capacities. The smaller size implies that there are fewer generating units connected, which implies that the system's inertia and its overall frequency control capacity are lower. Furthermore, the generation of each generating unit represents a high percentage of the total demand. The loss of a unit can lead to a rapid drop in frequency, causing a blackout if the frequency protections do not act in time. Current frequency protections shed predetermined amounts of loads if the frequency derivative exceeds certain thresholds [4], [5], and [6]. Adaptive advanced protections are also being developed [7].

On the other hand, island systems do not benefit from the economy of scale for electricity generation. For security reasons, the installed capacity per generation unit is limited, resulting in smaller and generally less efficient generator sets. The generation mix is based on gas, fuel oil, or Diesel. Their operating costs are higher than other conventional sources and must be added to the logistics costs of raw materials [8]. The profound reliance on imported fossil fuels is a challenging problem. This situation exposes the islands to external disturbances such as energy price volatility and the risks associated with the disruption in their energy supply chains. Taking such issues into account is an essential part of energy planning and management to come up with adequate solutions that would address the energy challenges [9]. Furthermore, the spinning reserve requirements are more demanding in relation to the size of the units, increasing the total operation cost. In order to lower operating costs and increase sustainability, an increase in the penetration of renewable energy sources (RES) is encouraged. However, non-synchronous RES (e.g., wind generation and photovoltaic generation) does not currently provide inertia or spinning reserve, therefore by incorporating more RES, the security of the system may decrease since RES

substitutes the conventional generators, further reducing system inertia and frequency control capacity. In addition, the portfolio effect (compensation for the variation in dispersed renewable sites) is lower in island systems due to their smaller geographic extension with the consequent spatial concentration of non-synchronous RES, so that RES usually vary simultaneously. As a result, rational renewable energy planning is needed to tackle these shortcomings [10].

This thesis focuses on addressing the challenges that the island power systems are facing, from the scheduling point of view. The scheduling of the operation of island systems is carried out by considering different time horizons: annual, weekly, daily, and intra-day time [11]. Most of the island systems operate under a centralized scheme (not under a wholesale market system) [12]. Currently, the operation of the generating units is scheduled by solving the unit commitment (UC) problem, which minimizes the dispatch costs and tries to ensure security by assigning a predefined amount of spinning reserve. Optimization models are used to do this. The UC problem is inherently a mixed integer optimization problem, which is usually solved as a mixed integer linear programming (MILP) problem, due to the computational limitations [13]. Ideally, UC should be able to handle the uncertainties of RES and should ensure that the frequency dynamics are within an acceptable range when a contingency happens.

1.1 Specific Challenges

The frequency dynamics of the power systems are highly non-linear, non-convex, and mathematically complicated to be incorporated in the UC problem directly [14]. Considering that the dynamics of the system and the scheduling of the system are both complicated and they have different time scales, in practice, these problems are addressed independently and not necessarily optimally in real island systems. On the one hand, the spinning reserve requirements incorporated in the planning level do not guarantee that the dynamic behavior of the frequency when a disturbance occurs (loss of groups, interconnections, etc.) is adequate [15]. On the other hand, current economic dispatch models do not include the possibility of load shedding as a measure to lower the cost of dispatch, nor do they consider restrictions associated with frequency dynamics indicators (minimum frequency, limits in derivative of frequency, etc.) [16]. Therefore, it would be possible to improve the dispatch of the system by means of a reserve value capable of preventing shedding (and their associated costs) and improving the frequency dynamics, or being able to activate shedding when the reserve necessary to avoid them involves a higher cost. In addition, it is imperative to review the planning process and the provision of the reserve service in the face of the high penetration of RES. With the aim of facilitating high penetration of RES at minimum cost in island systems, the challenge of jointly addressing operation planning and frequency stability is raised in this thesis. Both problems are closely related through the reserve and planning the operation considering frequency stability and its associated dynamics can lead to a more secure and efficient operation. Island power systems of the Canary Islands will be used to validate all developments during this research.

Island power systems are small and already suffer from inertia scarcity, so they are already vulnerable to frequency instability [17]. The fact that thermal synchronous generators are being replaced by RES aggravates the issue because not only RES is decoupled from the grid and does not introduce any inertia, but also it brings more uncertainty to the system [18]. Reserve provision is

expensive in small systems, because any outage is big comparing the total demand, so a relatively high amount of headroom should be always available. Traditionally, RES does not provide any reserve either. In traditional scheduling of the units, both frequency dynamics and the uncertainty of RES are ignored. Frequency dynamics are non-convex and complicated, which makes its inclusion in the UC computationally demanding. Uncertainty is also complicated and considering it in the scheduling process is computationally challenging.

When RES take a significant role in the generation of power, some challenges will arise, predominantly because of the inherent variability that these source have [19]. Specifically, the two main RES that are being vastly used currently, solar photovoltaic and wind power, are subjected to a lot of variability, with high penetration times and low penetration times for wind, solar cycles, cloudy or rainy days, and etc. With all of these specifications it's reasonable to assume that for covering the energy needs with RES, the system should be oversized and must include storage systems so it can store some of the excess when RES is abundant to be used later in times of need [20].

1.2 Solutions

Reserve scarcity can be improved by either adding more sources of the reserve or scheduling the allocation of reserve while ensuring a tolerable frequency response. Frequency stability can be improved by including the frequency dynamics in the scheduling process or introducing new sources of inertia. Uncertainty of the RES and other inputs can be handled by the methods that are introduced in the literature. It's important to keep in mind, that the scheduling process should remain computationally affordable.

Storing RES can be beneficial too, to cover the demand throughout the day. There are different types of storage devices, and each type has some advantages and disadvantages. To implement the storage effectively, it should be investigated, usually from an economic point of view to find the suitable storage capacity that is able to cover the energy needs at the lowest cost. On the other hand, storage devices are a potentially valuable tool to provide reserve for the system, especially in the small power systems with high share of RES, that suffer from both reserve scarcity and RES volatility [21].

This thesis addresses on the one hand the possible reserve scarcity by contemplating and adding more reserve resources such as enabling RES or installing liquid air energy storage (LAES). On the other hand and since reserve provision is related to frequency stability, the thesis addresses the problem of including frequency dynamics in the scheduling process. This is particularly challenging given the different times scales involved.

1.3 Thesis Roadmap

This thesis is trying to acknowledge the aforementioned obstacles and approaches each of them with a solution that contributes to the previous studies. Chapter 2, chapter 3, and chapter 4 mainly focus on reserve provision, by considering the current spinning reserve criteria and storage with a longer term planning horizon in mind. Whereas chapter 5 and chapter 6 tackle the problem

of including frequency stability constraints into the UC for short-term studies. The following chapters of this document are organized as listed below,

- **Viability of Providing Spinning Reserves by RES:** to address the online reserve scarcity in power systems with a high share of RES, the deloading of the wind turbines is investigated as a tool that enables RES to self-sufficiently provide reserve. The economic impacts of deloading are discussed in chapter 2. The chapter starts with a complete review of the relevant state-of-the-art. Then a short review of the current regulations of the Spanish islands is presented in section 2.3. The general UC model that is used throughout this thesis is formulated in section 2.4.3. Two islands of Tenerife and La Palma are used as case studies. Section 2.5 presents the details of these two systems. In section 2.6 the results of this chapter for both islands are discussed, and then in section 2.7, the conclusions are drawn.

When the economical aspects of enabling RES to provide reserve are clear, this question arises: with the proper controllers, how deloading affects the dynamic response of the system? The dynamic frequency response should be investigated separately with the help of system frequency response (SFR) models, to explore the technical benefits that deloading might bring.

- **Feasibility of Providing Spinning Reserves by RES:** following the studies in chapter 2, in chapter 3 the technical benefits of providing frequency regulation by RES in island power systems is investigated. Here the results of chapter 2 are used to analyze the frequency stability in terms of frequency deviations and amount of under frequency load shedding (UFLS) when the wind turbine generator (WTG) operates at a fixed and a variable deloading percentage under normal conditions. In section 3.2 the methodology of this chapter is presented. Then in section 3.4 and section 3.5 the results for both La Palma and Tenerife islands are provided and analyzed.

Now that the benefits of RES providing reserve by means of deloading are fully explored, other sources of reserve like energy storage system (ESS) can be focused. ESS not only can provide reserve, but also can reduce the cost of electricity by load-shifting. Including ESS in power systems, especially the ones with a high share of RES, has been seriously considered in recent years. A model to include a specific type of ESS (LAES) in the scheduling process is introduced in the following chapter, and the economical benefits of it, in the long run, are explored.

- **LAES Model for Scheduling Purposes:** storage devices are another potential to provide reserve and primary frequency response. LAES is one of the promising technologies for storing energy. A novel and more accurate formulation of LAES for scheduling purposes is introduced and realistic expectations of installing LAES in the island power system are explored. Chapter 4 starts with a comprehensive review of the related literature. The methodology of this chapter, including the MILP formulation of LAES is proposed in section 4.3. Then the results are presented and discussed in section 4.4. Conclusions are argued in section 4.5.

As mentioned before, in low-inertia systems like islands, securing frequency stability is necessary. One way to improve the frequency response of the system in case of contingencies is by

including the frequency dynamics in the short-term scheduling process. On the other hand and as opposed to long-term studies, in short-term studies like the day-ahead UC problem, uncertainties of RES sources can be considered, as more accurate forecasts are available. In chapter 5, a method is introduced to include frequency dynamics in the day-ahead UC problem while tackling the uncertainties of RES and keeping the formulation computationally affordable.

- **Robust FCUC Using an ML method:** when the share of RES grows, it's necessary to consider the uncertainties that they bring. To include the uncertainties in the UC problem, a robust formulation of the UC is presented. But still, considering both uncertainties and frequency dynamics in the UC problem is computationally demanding. In chapter 5 a data-driven constraint, with the help of logistic regression (LR), is used in a robust unit commitment (RUC) instead of the reserve constraint, which reflects the dynamics of the system while keeping the size of UC problem intact. At the beginning of the chapter, a complete review of the previous publications is presented. The fundamentals of a robust MILP optimization problem, the application of robust formulation in UC, the SFR model that is used to label the training data, and the proposed LR constraint are all discussed in section 5.3. Then the results of the simulations are argued in section 5.4, and the conclusions are drawn in section 5.5.

Although the data-driven approach that is introduced in chapter 5 is showing some merits, there is still room to improve some parts of the procedure, like the data generation or the learning model. Also, it would be interesting to compare data-driven and analytical methods of including frequency dynamics, in terms of their accuracy and their computational efficiency.

- **Comparing Analytical and ML-based Frequency Nadir in UC Problem:** a system with low inertia is very susceptible to frequency instability after contingencies. To prevent intolerable outages in the scheduling process, a novel frequency constrained unit commitment (FCUC) is developed in chapter 6. In comparison with chapter 5, here a new data generation process is proposed. Also in chapter 6 the focus is on learning the frequency nadir constraint, contrary to chapter 5 which is trying to reflect all the frequency metrics in one set of constraints. Both analytical approaches (based on the swing equation) and data-driven approaches (with the help of machine learning (ML)) are discussed and compared in chapter 6. The analytical MILP formulation of dynamic frequency metrics and the process of obtaining the frequency metrics with ML is discussed in section 6.2. Both methods are compared in section 6.3. Conclusions are presented in section 6.4.

2 Viability of Providing Spinning Reserves by RES

This chapter assesses the viability of providing down and up spinning reserves by RES in island power systems from an economic point of view. The process consists of evaluating the impact of providing spinning reserves on the system operation costs of different islands by simulating the UC problem. The proposed solutions in this chapter can help with the reserve scarcity of systems with a high share of RES. This chapter is published as a paper in [22].

Islands are facing considerable challenges in meeting their energy needs in a sustainable, affordable, and reliable way. This is mainly due to the isolated nature and the small size of island power systems. The geographic isolation also causes relatively high operation costs in comparison to large interconnected systems. Operation costs are not only higher because of expensive fuel transportation and lower efficiencies of the power generation technologies (e.g., Diesel), but also because of technical spinning reserve requirements to guarantee frequency stability. Actually, island power systems are more prone to suffer from frequency instability than larger interconnected systems, since they possess smaller inertia and each generating unit represents a significant fraction of the total generation in-feed [4].

2.1 Framework

According to local resource availability, RES offer an interesting solution to decrease the dependency on fossil fuels and increase island sustainability [23]. In [24], the possibility of achieving 100% renewable generation in the Canary Islands before 2050 is investigated. [25] and [26] determine the potential of offshore wind generation and solar photo voltaic (PV) roof-top installations in the Canary Islands. In current practice by operators, all available RES generation is directly injected into the power system, substituting thermal generation [27]. However, the increasing penetration of RES can negatively affect the frequency stability of island power systems even further ([28], [29]), by reducing control capacity and system inertia.

Spinning reserves denote sufficient power and energy reserves to contribute to frequency stability. Spinning reserves in power systems should be able to cover emergencies and non-emergency conditions. Non-emergency incidents include expected RES fluctuations (wind and solar fore-

cast error) or demand variations (demand forecast error). And emergency incidents include for instance the loss of generation units in case of generator trips or transmission line outages [30].

By increasing the injection of uncertain renewable power into the system, more reserve is required to balance the forecasted generation and real-time demands, hence an adequate sizing of the reserve is essential [31]. References [32] and [33] study the provision of reserve margins to hedge against real-time uncertainty and variability of wind power generation. The impact of forecasting horizon and amount of RES generation on reserve requirements have been analyzed in [34].

However, RES does not provide spinning reserves so far in Spanish island systems. RES generation can be curtailed to ensure system security. So, providing sufficient reserve to ensure frequency stability is becoming harder and harder by increasing the share of RES, especially in island systems. As a solution to this, researchers in this area have the general idea of using RES to provide reserve power. To exploit this idea on Spanish islands, first, we should find out what is the best approach for enabling RES to provide reserve. Then we can learn the economic impacts of it, by simulating the short-term scheduling problem. The economic analysis can give a good insight to the system operator about the cost-benefits of this approach. The other side of the story is the technical impact of substituting the spinning synchronous reserve with the reserve provided by RES. The economic analysis must be accompanied by a technical analysis to assess the impact on system security. The technical analysis will show whether and to what extent deloading actually improves frequency stability. Whereas for a given system inertia and perturbation, deloading will improve frequency response with respect to without deloading, the reality is more complicated since enabling deloading modifies the dispatch (inertia and perturbation). This is further investigated in chapter 3.

Synchronous generators have always been the main providers of inertia and frequency regulation in the power system. Traditionally in short-term planning (for example day ahead UC), they make sure that there is enough reserve in case of any contingency (generator or transmission line outage). In island power systems, usually, the number of online units is low, so each unit generates a big portion of the total demand. So, a considerable amount of reserve is always required to cover generator failures. Even when there is enough reserve available, some load shedding might happen in times of big failures, because the power imbalance would be very high, and frequency drops at a fast rate before the units have enough time to ramp up. Considering that more power is delivered by RES, it's expected that fewer synchronous units will be committed in future power systems. So, the current reserve criteria start to fall short, mainly because it does not identify available frequency regulation tools, like the amount of inertia, the ramp speed, and the time constants. On the other hand, RES is a big source of uncertainty itself, and to keep the frequency deviations within a reliable range, those uncertainties should also be taken into account. Finally, different islands have different characteristics. It would be insightful for the operators of Spanish islands, to see how these new approaches can improve the operation of the power systems in Spanish islands, which are mostly either medium size (like Tenerife) or small size (like La Palma).

When RES does not provide spinning reserves, there should be some thermal generation above minimum power to serve as a down reserve. The same or different thermal units should keep some headroom below maximum power to serve as an up reserve. Thus, RES providing down and up reserve can change the commitment status of units to reduce the operation costs.

Synchronous generators have always been the main providers of inertia and frequency regulation in the power system. Non-synchronous RES is unable to increase the inertia of the system

unless appropriate controls are in place because the converters decouple them from the grid [35]. Researchers have been trying to find ways of enabling wind turbines to contribute to primary frequency regulation and deliver inertia to the system. In [36], various reserve allocation methods are compared and a practice to assess immediate wind primary reserve is presented. Reference [37] has tested various control strategies of active power to investigate their effectiveness in times of high wind injection. It concludes that inertial and power frequency response controllers can be implemented on wind turbine generators and enhance the overall frequency response of the system. In [38] an aggregated frequency response model for wind generators is presented, considering the different operational modes of wind power turbines. Then an analytical approach is employed to aggregate the low-order frequency response model of all wind power plants into one model. In [39] a stochastic UC formulation is proposed, to evaluate the advantages of synthetic inertia and primary frequency response provision from wind turbines in the Great Britain power system and concludes that it potentially can mitigate operation costs of the system. Reference [40] has mentioned some inertia and frequency regulation approaches for RES and has divided them into two groups: The first one is the deloading technique, which lets the RES to keep some reserve power. And the second one includes inertia emulation, fast power reserve, and droop techniques, which are used to release the RES reserve power in times of under-frequency.

Among them, deloading brings more economic and technical benefits and provides a better frequency response [41]. Although deloading practice enables wind turbines to take part in frequency regulations, it contradicts the principle of acquiring the highest possible amount of power from wind sources [42]. RES such as wind power or solar generation is technically able to provide reserves by deloading a percentage of their maximum power point tracking (MPPT) operation [43]. This can be achieved by appropriately adjusting rotor speed in wind turbines or the direct current (DC)-link voltage in photo voltaic systems. Typically, the deloading rate is less than 20% of the actual available RES power, depending on the circumstances [44]. An extensive review of the deloading of wind turbines in power systems is presented in [45], and different control modes are compared. A stable operation of wind turbine generators is introduced in [46], which guarantees the optimum contribution of each wind turbine to improve the primary frequency response of the system. A dynamic strategy of active power control is presented in [41], to maximize the role of variable speed wind turbines in primary frequency regulation. The authors employ a fuzzy control method to sense the frequency deviations and adjust the amount of deloading subsequently. In [47], the authors argue that existing linear deloading techniques lack accuracy, and the nonlinear relation between rotor speed and output power during deloading practice should not be overlooked. Then they proposed a nonlinear formulation to enhance the stability and frequency regulation participation of wind turbines in microgrids. The control of wind turbines that enables them to utilize deloading is further discussed and used in chapter 3.

According to the Canary Islands Energy Yearbook, [48], there's been 9, 282.8 GWh of annual energy production, consisting of around 10% renewable generation, 90% thermal generation, and less than 0.01% refinery and cogeneration in 2018. Only in 2018, an amount of 1819.8 kilotons of fuel (including gasoline, diesel oil, and fuel oil) was imported to the Canary Islands, for the purpose of electricity generation. They're planning to add 200% to the renewable resources by 2025 and add 400% renewable capacity by 2030. Under such scenarios, the question arises whether reserve should be still provided by synchronous generators only or whether non-synchronous RES should participate as well. For this purpose, the islands of Tenerife (medium size) and La Palma

(small scale) are chosen for simulations because they are representative of the Spanish isolated systems. Further, the results shown here can be extrapolated to other islands to a good extent, since these two islands seem to fit in two of the five prototype islands identified through clustering techniques in [49]. The summary of the reviewed literature is presented in fig. 2.1.

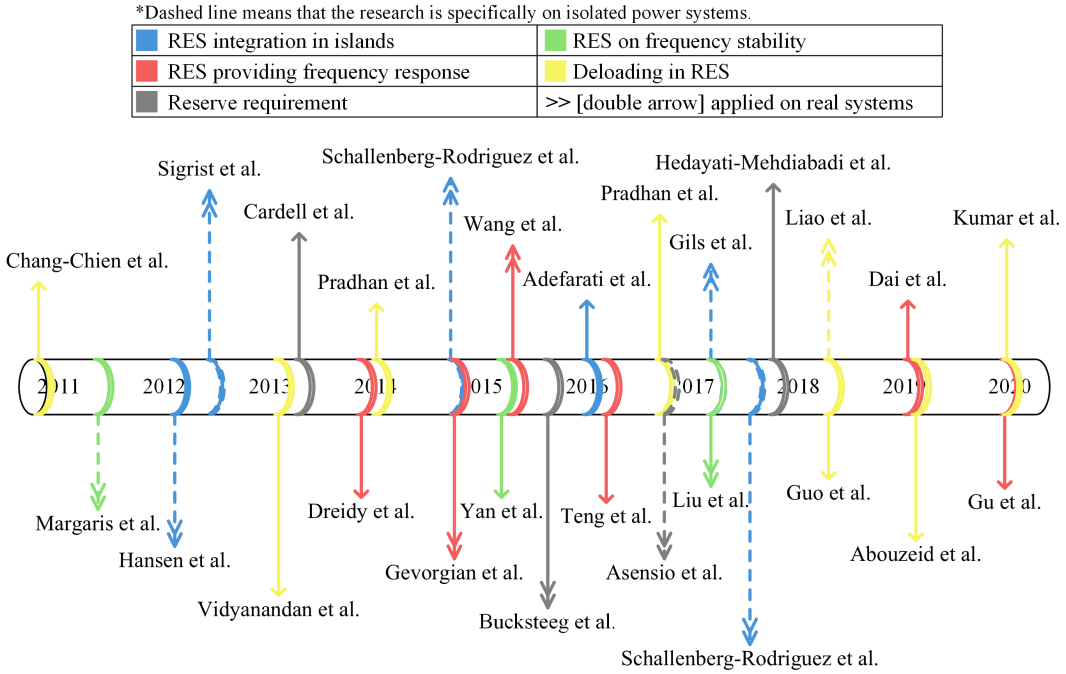

Figure 2.1: Summary of references ([4], [5], [6], [7], [23], [24], [25], [26], [27], [28], [29], [30], [31], [32], [33], [34], [35], [36], [37], [38], [39], [40], [41], [42], [43], [44], [45], [46], [47])

2.2 Gaps and Contributions

The main objective of this chapter is to evaluate the contribution of providing up and down spinning reserves by RES generation. The assessment consists of determining the impact of providing spinning reserve on the system operation costs by simulating its economic operation. As most island systems are operated under a classical centralized scheme, hourly UC on a weekly basis is proposed for this purpose. The focus is on analyzing whether reserve provision by RES generation is beneficial, whereas the actual implementation of the corresponding operation planning is out of the scope of this chapter. The actual implementation is affected by the variability of RES and might require operation planning methodologies under uncertainty, but to highlight the economic aspects of providing reserve by RES, a deterministic approach considering different scenarios (seasons and years) would be sufficient. Note that in this study the benefits of deloading in the long term are explored. To take the forecasting error of RES into the account, short-term studies should be conducted. To further contribute to the previous publications, the methodology of this chapter is applied to two real islands, La Palma and Tenerife, with factual input

data. Four different approaches to reserve provision are considered (RES providing no reserve, RES providing only down a reserve, RES providing up and down reserve with a fixed constant deloading factor, and RES providing up and down reserve with a dynamic optimum deloading factor) as different cases and are applied for various seasonal scenarios (summer, autumn, winter, and spring), both for current and future time-frames (years 2020, 2025 and 2030). Up reserve and down reserve are distinguished, then the impacts of each on the operation cost are included. Deloading is defined as a variable in the UC problem, and the amount of deloading is optimized for each hour in the last approach of RES reserve provision. A total number of 240 UC weekly simulations are performed for each island.

The rest of this chapter is organized as follows. Section 2.3 summarises the regulations of Spanish isolated systems. Then in section 2.4, the methodology used in this chapter is explained. In section 2.4.3, the UC formulation of the optimization problem is introduced and the corresponding constraints are presented. In section 2.6, the obtained results for both islands are fully analyzed. Conclusions for this chapter are drawn is section 2.7.

2.3 Regulation of Spanish Isolated Power Systems

This section provides a short review of the regulation of Spanish isolated power systems [50]. The Spanish isolated power systems are the power systems of the Canary Islands, Balearic Islands, and the Spanish towns in North Africa. These systems are of very different sizes. The most extensive system is the Mallorca-Menorca system with a peak demand of around 1100 MW and the smallest system is the El Hierro system with a peak demand of 7 MW.

2.3.1 Reserve Requirement

The technical regulatory framework of the Spanish isolated power systems is defined in a set of operational procedures [51]. Among others, operation procedure number 1 (section 8.1) describes the spinning reserve requirements in the isolated Spanish power systems. It points out that the up-spinning reserve, including primary and secondary frequency control reserves, should be greater than the largest online unit, greater than the expected RES power generation variations, and greater than the largest interconnection infeed. In addition, the down-spinning reserve must be at least 50% of the upward primary reserve. The operational procedure also recognizes that during the outage of a large unit, primary frequency control makes use of both primary and secondary reserves.

2.3.2 Economic Regulation

Isolated power systems can be operated either under a classical centralized scheme or under a market-driven scheme. Spanish isolated power systems are operated under a centralized scheme. In a classical centralized scheme generating units are programmed according to economic dispatch rules that consider the security of supply. The generation program is sequentially determined over different time horizons: weekly, daily, intraday, and real-time. The weekly generation program is initially determined by a UC and security of supply criteria. The UC contemplates standardized variable operation costs. In the second step, technical restrictions of the network are imposed and

generation units are re-scheduled if needed. The determination of the daily generation program is similar to the determination of the weekly program. Generators in Spanish isolated power systems are divided into two categories: category A includes hydro (excluding run of the river) and thermal generators and cogeneration power plants with net power greater than 15 MW, whereas category B refers to renewable energies and cogeneration power plants with a net power equal or lower than 15 MW. Renewable sources and high-efficiency cogenerators (of both category A or B) have priority of dispatch under equal economic conditions, considering that the security of supply requirements is maintained [51].

Generators of category A that have been included in the additional remuneration scheme (regimen retributivo adicional), are remunerated according to fixed costs and variable generation costs in function of the generation technology. The additional remuneration scheme repays investments and exploitation expenditures. Generators of category A that are not included in this scheme perceive a payment according to the hourly energy selling price and the energy produced. Generators of category B are remunerated according to the hourly energy selling price and the energy produced plus a specific remuneration as well as a payment for their contribution to ancillary services (if any). Note that the hourly energy selling price of the Spanish isolated systems depends on the daily or intra-day market price of the mainland system weighted by the relation between actual hourly demand and average daily demand of the isolated system of interest.

2.4 Methodology

This section presents the methodology to assess the viability of providing spinning reserves by RES in island power systems. First, the main benefits behind the provision of spinning reserves by RES are illustrated. Second, an overview of the proposed methodology is given. The assessment is based on the simulation of the economic operation by means of an hourly UC on a weekly basis.

2.4.1 Illustration of the benefits of providing reserves by RES

To provide spinning reserves, conventional units are connected and operated below the maximum power generation. The amount of required spinning reserve can be substantial in comparison with the total generation, increasing operation costs significantly. Operation costs could be reduced by providing spinning reserves by RES.

Figure 2.2 illustrates the main idea and benefits in terms of cost reduction of providing spinning reserves by RES. Suppose a hypothetical power system with two conventional units G1 and G2, and two wind farms, W1 and W2, feeding a certain demand at a given instant. G1, G2, W1, and W2 have the same size in terms of maximum generation at that given instant. In fig. 2.2 (a), the demand is covered by the generation of units G1 and G2, and spinning reserves are also provided by G1 and G2. Note that both units operate at the same power level to cover their possible individual outages. In fig. 2.2 (b), the demand is covered mostly by the wind farm W1 but also by G1, whereas reserve is mostly provided by unit G1. Note that unit G1 operates at the minimum power generation level. In fig. 2.2 (c), the demand is covered by the two wind farms W1 and W2, and spinning reserves are also provided by W1 and W2. Since operation costs of wind farms are usually much lower than those of the conventional generation, it is reasonable to assume that the operation cost decreases from fig. 2.2 (a) to fig. 2.2 (c).

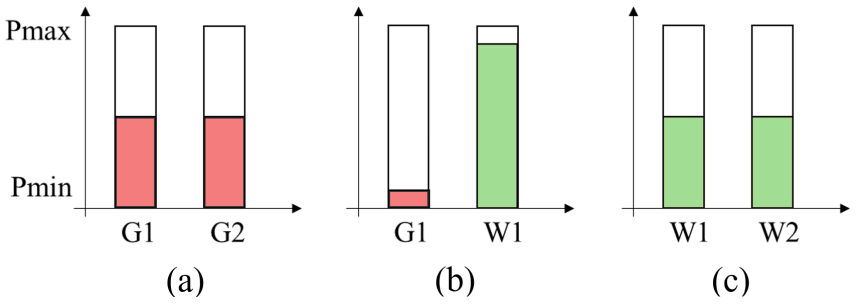

Figure 2.2: Illustration of the benefits of providing spinning reserves by RES: (a) Covering demand and providing reserves by G1 and G2. (b) Covering demand by W1 and providing reserves by G1. (c) Covering demand and providing reserves by W1 and W2.

Although the example is only illustrative and highly hypothetical, it shows the benefits of providing reserves by RES. It also insinuates that this provision makes sense under high RES penetration scenarios, where the exceeding available RES energy is not simply spilled, but reserved. The difference with respect to spilling is that an appropriate primary frequency controller is required to release the reserved energy.

2.4.2 Overview of the methodology

The methodology is based on simulations of the economic operation of islands under different demands, RES penetration scenarios, and cases with different approaches of providing reserve. The economic operation is simulated with an hourly UC on a weekly basis. The UC determines the hourly generation set point as well as the hourly start-up and shut-down decisions.

For a given weekly demand profile, the corresponding current RES profiles are scaled up according to the considered future installed capacity. Scaling-up current profiles is a proxy for future profiles under higher penetration scenarios since the current installed RES and RES spillage are low. For each weekly demand and RES generation profile, the simulation of economic operation is performed, considering whether RES is controllable (the subset of controllable RES is denoted as *cres* in this chapter) and able to provide up or down reserves or not. Different cases are considered which are introduced in section 2.6.

Figure 2.3 shows a flowchart of the methodology of this chapter. The input of the weekly UC includes the weekly hourly demand, wind and solar generation forecast, list of thermal generators, and their data sheet for each island and each sampling week under study. Considered scenarios are further discussed in section 2.6.

2.4.3 UC model

The UC is formulated as a minimization problem where generation set points and start-up and shut-down decisions are such that the total weekly operation cost is minimized while ensuring technical constraints. The objective function as well as associated constraints are summarized

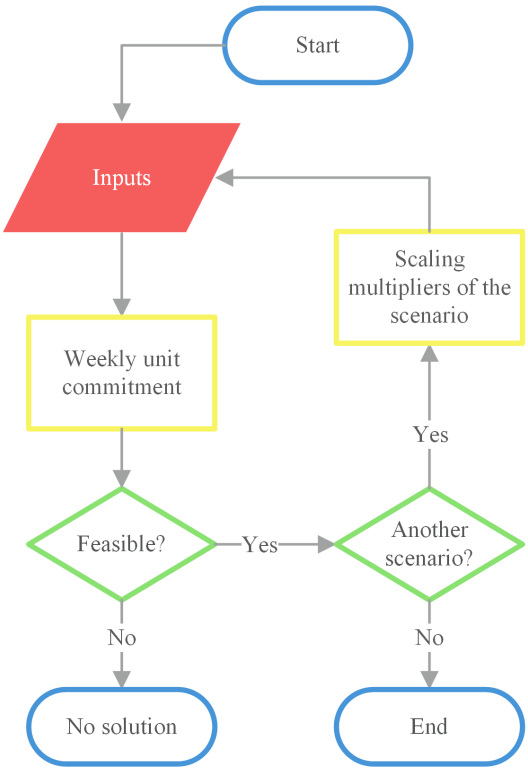

Figure 2.3: Flowchart of the methodology of chapter 2.

next. A description of the full UC but without constraints related to reserve provision by RES can be found in [1].

$$\min_{u,p} \; suc(u_{t,i}) + gc(p_{t,i}) \tag{2.1}$$

$$u_{t,i} - u_{t-1,i} = v_{t,i} - w_{t,i} \qquad t \in \mathcal{T},\ i \in \mathcal{I} \tag{2.1a}$$

$$v_{t,i} + w_{t,i} \leq 1 \qquad t \in \mathcal{T},\ i \in \mathcal{I} \tag{2.1b}$$

$$\sum_{tt=t-UT_i+1}^{t} v_{tt,i} \leq u_{t,i} \qquad t \in \{UT_i, \ldots, T\},\ i \in \mathcal{I} \tag{2.1c}$$

$$\sum_{tt=t-DT_i+1}^{t} w_{tt,i} \leq 1 - u_{t,i} \qquad t \in \{DT_i, \ldots, T\},\ i \in \mathcal{I} \tag{2.1d}$$

$$p_{t,i} \geq \underline{\mathcal{P}}_i u_{t,i} \qquad t \in \mathcal{T},\ i \in \mathcal{I} \tag{2.1e}$$

$$p_{t,i} \leq \overline{\mathcal{P}}_i u_{t,i} \qquad t \in \mathcal{T},\ i \in \mathcal{I} \tag{2.1f}$$

$$p_{t-1,i} - p_{t,i} \leq \underline{\mathcal{R}}_i \qquad t \in \mathcal{T},\ i \in \mathcal{I} \tag{2.1g}$$

$$p_{t,i} - p_{t-1,i} \leq \overline{\mathcal{R}}_i \qquad t \in \tau,\ i \in \mathcal{I} \tag{2.1h}$$

$$\text{generation} = \text{demand} \qquad t \in \mathcal{T} \tag{2.1i}$$

Equation (2.1) is subjected to eqs. (2.1a) to (2.1i). $suc(.)$ and $gc(.)$ are the start-up and generation cost functions in euros, respectively. u, v, and w are binary variables of commitment, start-up, and shut-down, respectively. p is the power generation variable. t is the index for time intervals. i is the index of generators. $\overline{\mathcal{P}}$ and $\underline{\mathcal{P}}$ are maximum and minimum power output of generators, respectively. $\overline{\mathcal{R}}$ and $\underline{\mathcal{R}}$ are ramp-up and ramp-down limitation of generators, respectively. All of the terms that are used in the equations in this thesis are defined in the nomenclature section. Quadratic generation cost curves in eq. (2.1) have been approximated by piece-wise linear functions. The binary logic of the status of the thermal units is defined in eq. (2.1a) and eq. (2.1b). Minimum downtime and up-time constraints in eq. (2.1d) and eq. (2.1c) are from [52]. It's further confirmed in other research like [53], that this approach improves the solving time of UC problems. Concerning thermal technical operation, eq. (2.1f) and eq. (2.1e) make sure that thermal units are generating between their maximum and minimum capability. Equation (2.1h) and eq. (2.1g) impose the ramping limitation. Any increment or decrement of power between two consecutive hours should not exceed the generator's ramp-up/down limits. Equation (2.1i) only shows the general concept of power balance. These are the most common UC constraints that are mentioned in [54]. Then depending on the specification of the system, the power generation units and the ones that consume energy can be different. The following equation defines the power balance constraint for the considered system in this chapter,

$$\sum_{i \in \mathcal{I}} p_{t,i} + P_t^{RES} - \sum_{dw \in DW} p_{t,dw}^{deloading} = \mathcal{D}_t + p_t^{spilled} \qquad t \in \mathcal{T} \tag{2.2}$$

Where $\mathcal{D}$ is the demand. In the MPPT approach, all available energy is instantly used for generation. But in deloading control mode, a percentage of available energy is stored as a reserve to support the system when a contingency happens. The maximum power is reduced by the de-

loading factor in the optimization problem. However, the wind turbine should be controllable (receive set point variations). As an example, a general control strategy is showed in fig. 2.4 [44]. Reserves are activated through appropriate proportional and derivative frequency controls. Note

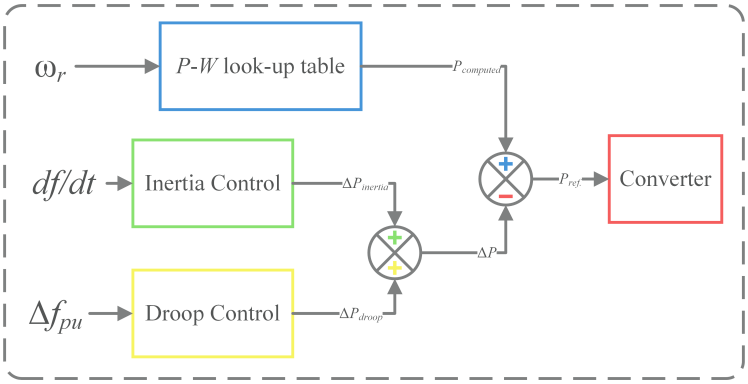

Figure 2.4: General control strategy of the deloaded wind turbine.

that this chapter does not focus on the details of control strategies, but it tries to study the economic impacts from the operator's perspective.

$$p_{t,dw}^{deloading} = P_{t,dw} DF_t \quad t \in \mathcal{T}, dw \in DW \tag{2.3}$$

Where DF is the deloading factor. In other words, net RES generation can be reduced by spilling energy with respect to the available wind generation as long as it is controllable. Typically, RES generation under the current scenarios is only spilled in case of possible issues with respect to system stability (like over-generation).

As specified by Spanish regulations for isolated systems, up spinning reserve in each hour should be bigger than the maximum of the largest operating unit and the expected RES variations. Also following Spain regulations, the total down-spinning reserve must be greater than k_{DR} (here 50%) of the up-spinning reserve. Equation (2.4) and eq. (2.5) compute the required up and down reserves. k_{RV} is set to 30% in this chapter.

$$URR_t = \max\left(p_{t,i}, (P_t^{RES} - p_t^{spilled} - \sum_{dw \in DW} p_{t,dw}^{deloading}).k_{RV}\right) \tag{2.4}$$

$$DRR_t = URR_t.k_{DR} \quad t \in \mathcal{T} \tag{2.5}$$

Where URR is up reserve requirement, k_{RV} is the expected renewable output variation coefficient, DRR is down reserve requirement, and k_{DR} is down reserve requirement coefficient. Up and down reserve are defined as follows,

$$r_{t,i}^{up} = \max\left((\overline{\mathcal{P}}_i u_{t,i} - p_{t,i}), \frac{\overline{\mathcal{R}}_i}{4}\right) \tag{2.6}$$

$$r_{t,i}^{down} = \max\left((p_{t,i} - \underline{\mathcal{P}}_i u_{t,i}), \frac{\mathcal{R}_i}{4}\right) \tag{2.7}$$

Where r^{up} is the up reserve and r^{down} is the down reserve. The thermal unit should be able to accomplish active power increase or decrease in 15 minutes [55]. Equation (2.6) limits the amount of scheduled reserve to the extent that the ramp-up rate of the unit allows (15 minutes is a quarter of an hour, so the ramp-up rate is divided by 4). Same explanation for ramp-down rate and eq. (2.7). Up reserves can be provided by renewable sources if the final generation set point is below the available RES power and the proper control mechanism is implemented on them. Wind turbines can participate as up-reserve providers if they benefit from the deloading control mechanism. There are different control strategies in the literature (see [44], [45], and [56]), mainly possible by conventional PI controllers and small read-only memory (ROM) memories to form the required look-up tables. The cost of adding a deloading control mechanism, tuning, and maintenance is ignored in the cost function. Still, the objective function is able to reflect the opportunity cost of providing reserve by deloading wind generation instead of using the associated energy to cover demand. RES can provide down reserve if they are able to sense the frequency of the system and curtail their generation in case of high frequency. Considering the deloading wind turbines and those controllable renewable sources that can participate as down reserve providers, up and down reserve criteria are defined as follows,

$$\sum_{i\in\mathcal{I}} r_{t,i}^{up} + \sum_{cw\in CW} p_{t,cw}^{deloaded} \geq URR_t \quad t\in\mathcal{T} \tag{2.8}$$

$$\sum_{i\in\mathcal{I}} r_{t,i}^{down} + \sum_{cres\in CRES} (P_{t,cres} - p_{t,cres}^{spilled}) - \sum_{dw\in DW} p_{t,dw}^{deloaded} \geq DRR_t \quad t\in\mathcal{T} \tag{2.9}$$

Equation (2.8) makes sure that the available up-spinning reserve which is the summation of reserve provided by thermal units and deloading of wind turbines, meets the requirements. Equation (2.9) states that the summation of the down reserve provided by thermal units plus the scheduled amount of controllable RES should be higher than the required amount. Note that the deloaded power, is the amount of power that is not extracted from the wind turbine and is kept as the headroom, so in case of any frequency drop it can be extracted. On the other hand, spilled power is scheduled to be curtailed. That can be achieved by stalling some of the wind turbines entirely.

2.5 Case studies

The methodology to assess the viability of providing spinning reserves by wind power generation has been applied to La Palma and Tenerife, both belonging to the Canary Islands. First, a brief description of the features of the island power systems is given. Next, the scenarios of demand and RES generation profiles are presented. Finally, the results of simulating the weekly economic operation for the considered scenarios are shown.

2.5.1 Description of the case studies

La Palma: the yearly demand in 2018 is about 277.8 GWh (average hourly demand of 31.7 MWh), supplied by eleven Diesel generators pre-dominantly. According to [48], the installed capacity of the La Palma island power system mounts to 117.7 MW, where about 6% of the installed

capacity belongs to wind power generation. Renewable generation covers about 10% of the yearly demand. Data of the units is presented in table 2.1.

Table 2.1: Generator capacities in La Palma

#	$\underline{\mathcal{P}}_i[MW]$	$\overline{\mathcal{P}}_i[MW]$
1	2.35	3.82
2	2.35	3.82
3	2.35	3.82
4	2.82	4.30
5	3.30	6.70
6	3.30	6.70
7	6.63	11.50
8	6.63	11.20
9	6.63	11.50
10	6.63	11.50
11	4.85	21

Tenerife: Total yearly demand in 2018 mounts up to 3,686.2 GWh (average hourly demand of 420.8 MWh). Two combined cycle units (gas and steam), cover around 45.5% of annual demand. 4 thermal steam units generate around 35.5% of the annual demand. There are 5 diesel units that cover 7% of annual demand. More recently some of these diesel units are being decommissioned. 5 thermal gas units generate 3.5% of annual electricity demand. The rest is delivered by RES. Operators are planning to decommission some of the more expensive thermal units and add to the renewable capacity before 2025. In table 2.2 the data of the units is presented. Figure 2.5

Table 2.2: Generator capacities in Tenerife

#	$\underline{\mathcal{P}}_i[MW]$	$\overline{\mathcal{P}}_i[MW]$
1	4.85	21.6
2	4.85	21.6
3	4.85	24.3
4	4.85	24.3
5	14.8	19.1
6	29.3	74.2
7	29.3	74.2
8	6.8	39.2
9	9.7	186.1
10	9.7	206.5

shows how much power is delivered from 1 unit of wind or solar in different seasons of the year from all RES sites in Tenerife island.

The Energy Strategy for the Canary Islands in 2025 aims to drive the system to a low-carbon economy. Among others, strategic objectives for the 2015-2025 period regarding RES involve achieving a 45% of RES participation in final electricity generation by 2025. This would require multiplying the amount of installed RES capacity, at least by five. In the case of wind power generation, not only on-shore but also off-shore wind farms are contemplated. In fact, authors

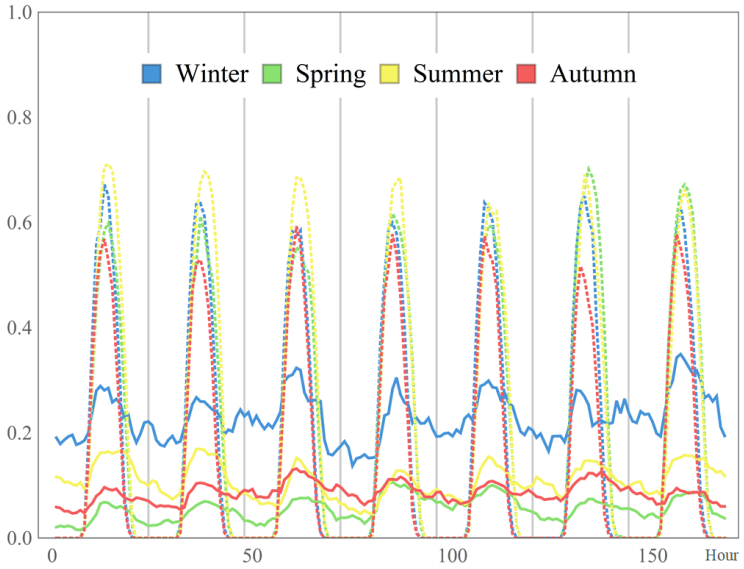

Figure 2.5: Cumulative generation of wind and solar in Tenerife island per unit during weeks of different seasons. Solid lines denote wind generation and dashes denote solar generation.

in [26] have estimated the wind offshore potential of the Canary Islands and concluded that 420 MW of offshore wind power generation can be installed in La Palma, about 40 times the current installed capacity of RES.

To achieve realistic results, in this study the most recent actual demand and RES generation of Tenerife and La Palma are used as the inputs. For future cases, the demand is scaled up by forecasted multipliers for the corresponding year. Other required inputs, including available power plants and their technical specifications like cost functions, up and down time limitations, capacities, ramping limitations and etc. are updated real data, obtained from the operators.

2.5.2 Scenario definition

The impact of wind penetration levels on providing spinning reserve has been analyzed by contemplating different scenarios of increasing installed capacity, in sample weeks of winter, spring, summer, and autumn. Scenario I denotes the current amount of installed wind capacity. For scenarios II to V, the initial amount is multiplied by 2, 5, 10, and ∞, respectively. All the seasons and scenarios are considered for forecasted electricity demand for the years 2020, 2025, and 2030 to acknowledge the economic benefits of each scenario in near future.

For each scenario, four cases with different capabilities of providing spinning reserve by RES are defined.

- **Case A:** This case is the current practice of operators in Spanish islands. RES cannot provide a spinning reserve. Both up and down reserves should be provided by thermal units. This case serves as a reference case.

- **Case B:** renewable sources are able to provide down-reserve, but they're unable to offer any up reserve.
- **Case C:** wind and solar sources provide the down spinning reserve. A deloading factor of 10% is applied for the entire time horizon to available wind power. So, in each hour, 10% of available wind generation is deloaded and specified as up reserve. Although choosing the percentage of deloading is arbitrary, 10% has been used in the literature consistently ([57], [58], [59]).
- **Case D:** The possible amount of deloading is defined as a coefficient between 0 and 15% of available wind generation. The UC optimization problem will decide the optimal amount of deloading in each hour. The scheduled amount of RES serves as down-reserve. The maximum percentage of dynamic deloading is also arbitrary. 15% is used in some previous studies like [60].

Figure 2.6 shows all of the considered states. Weekly UC is performed for 4 different cases, 4 sample weeks of different seasons of a year, and 5 wind penetration scenarios for each; composing 80 weekly UC for each year. This approach is employed for three different years: 2020, 2025, and 2030. For each island, a total of 240 simulations have been completed.

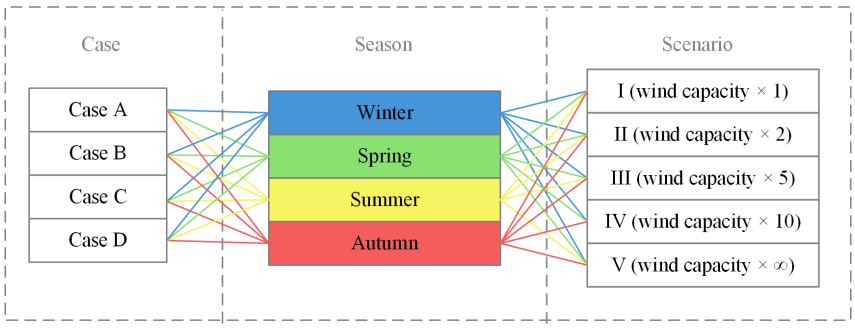

Figure 2.6: Considered states.

2.6 Results

In the following, the result obtained for La Palma and Tenerife island is presented and analyzed.

2.6.1 La Palma

The seasonal average results of different scenarios and cases for La Palma island are shown in fig. 2.7.

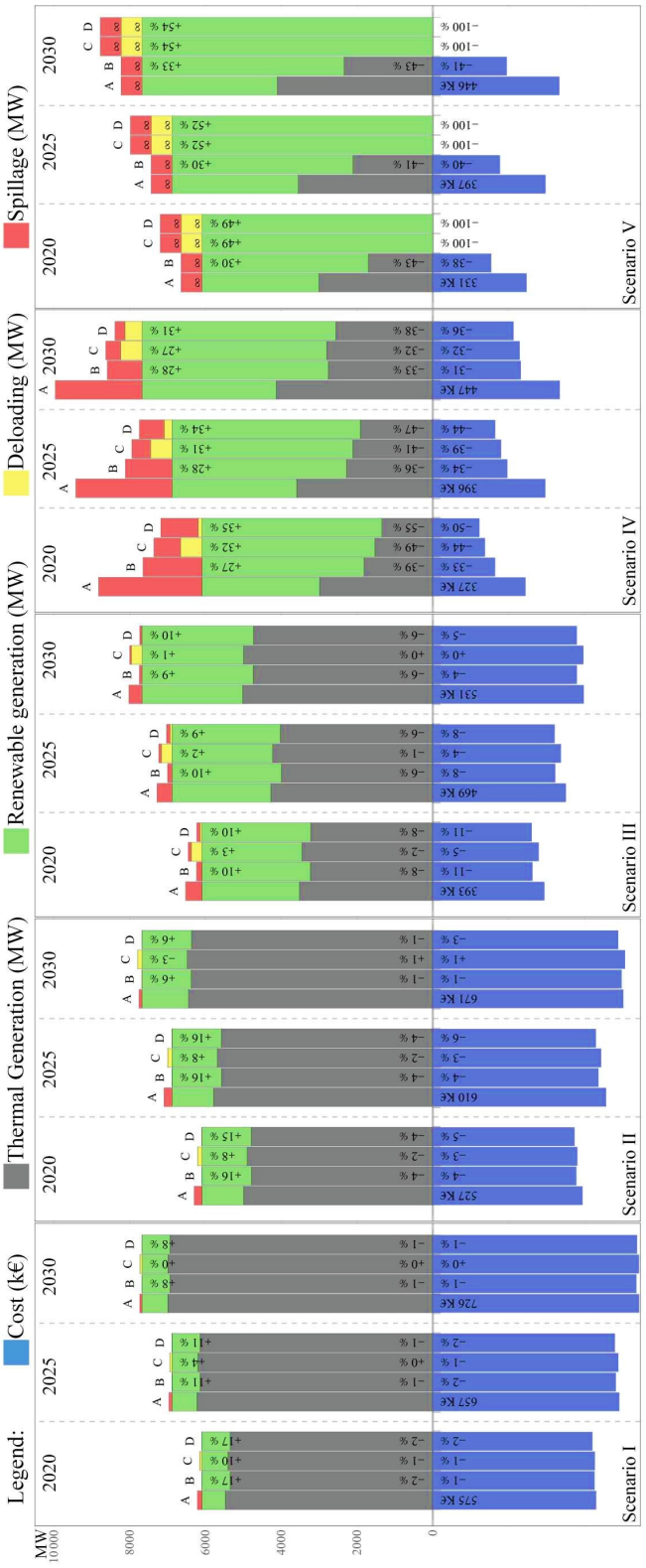

Figure 2.7: The average results of 4 seasons is shown here for La Palma island. Different cases are specified above each bar. The number of scenarios is stated at the bottom corner. Obtained results for the years 2020, 2025, and 2030 are separated with dashed lines.
*Above zero is the energy in megawatts and below zero is the cost in kilos Euros.

Different input states are compared, regarding their total cost, scheduled thermal generation, scheduled RES, spilled RES, and deloading of wind turbines. Case A is considered as the base case, then an incremental or decremental percentage of thermal energy, renewable energy, and the cost is inscribed in the figure, compared to the base case. As the results confirm, mostly the final weekly cost of thermal generation is less for the cases with deloading capability. The amount of spillage is considerably higher in the case of A, compared to cases B, C, and D. The reason is that case A only depends on the thermal sources to provide both up and down spinning reserves. Because of that every hour there should be enough generation above minimum capacity to cover down reserve and enough headroom in online units to cover up-reserve. This makes it really hard to dispatch renewable energies, hence so much renewable spillage happens even in scenarios with a low amount of renewable availability. It can be concluded that without enabling renewable sources to provide up and down-reserve, increasing renewable capacity is not a smart move, as the rating of spillage is high. The results of case A in fig. 2.7 confirm the poor performance of case A to use available renewable energy. By doubling the wind injection, the amount of spillage is also approximately doubled in every state for case A.

Enabling RES to provide down reserve in case B, has made considerable improvements in RES scheduling. Even for scenario I, where only the current installed RES is available, around 17% more renewable is scheduled and spillage is totally avoided. The results for scenarios with more RES injection confirm that the effect of providing down reserve by RES is considerably high and always reduces the thermal generation. In scenario IV (multiplying wind capacity by 10), a reduction of 33% of thermal generation and 31% of cost is expected for the year 2030, only thanks to adding the capability of providing down reserve to RES. These reductions even reach 40% for the extreme scenario V for the year 2030.

In case of C with a fixed percentage of deloading, less spillage has occurred, which has led to a decrement in the weekly cost of thermal generation, compared to the base case. But the obtained results of scenarios I to III (scenarios with lower availability of wind), suggest that there is no economic justification for imposing constant deloading of wind for every hour. For case C, cost and thermal generation reduction are apparent in scenario IV. Scenario V is an extreme hypothetical scenario that assumes an infinite amount of wind source is available. This means that the amount of deloading for cases C and D are also unlimited. Here the incapability of cases A and B to deploy the full potential of RES is better shown. Although infinite RES is available, the weekly expenses of thermal generation cannot be less than a certain amount for case A. The reason is that the up-spinning and down-spinning reserve constraints will keep some of the thermal generators online to satisfy the required reserve criteria. Case B manages to reduce the costs by around 40%, but still, some units should stay online. So, a 100% injection of RES will not be possible, unless RES is also capable of coping with the reserve constraints. The problem with case C from an economic point of view is that it does not choose the deloaded amount optimally. In some hours the up-reserve provision from thermal units might be sufficient, and more renewable generation is needed. In these circumstances, it's more cost-efficient to deliver more power to the grid and reduce or cut the deloading (also confirmed by fig. 2.8, which is explained later). Note in fig. 2.8 that unnecessary deloading occurs on days 1, 2, 3, and 6 of the week in Case C. That's exactly what case D is trying to prevent. It is worth noting that the allocated amount of deloading for case C, has never helped to fulfill reserve criteria in this sample week. As expected, case D achieves the most cost-efficient weekly results, compared to the other cases. In fact, in scenarios with low RES avail-

ability (Scenarios I, II, III), the economic results of a fixed deloading are even worse than when RES only provides down-reserve. In these scenarios, the possibility of an optimum variable deloading slightly reduces the final cost compared to the case with RES providing only down reserve, but the gap starts to grow by going towards scenarios with more renewable injection (Scenarios IV and V). Considering the tendency of operators of Spanish island to reduce thermal generation in the future and add more RES, it seems essential to implement the necessary controllers on the wind turbines to enable the reserve provision capability of wind generators.

On a small island like La Palma, operators should enable RES to participate as down reserve providers, even in the current actual situation, to considerably reduce the spillage of RES. Then they should start adding deloading capability to wind turbines, when the installed capacity of wind generation exceeds 5 times the current capacity (scenarios IV and V), to be as cost-efficient as possible.

In fig. 2.8, it's shown how the reserve is provided in each hour for different cases. This figure

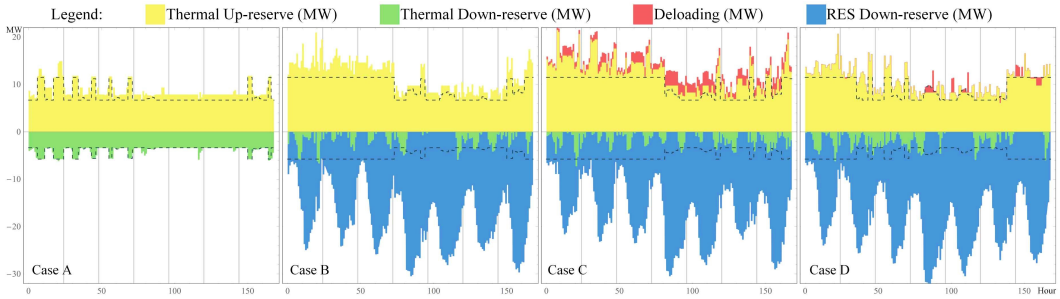

Figure 2.8: Reserve provision by different sources in the system for spring sample week 2020, scenario IV. Dashed lines are up and down reserve requirements in each hour. The days of the week are separated by vertical gray lines.

contains the results for a spring sample week of 2020, scenario IV. As La Palma is a small island, every unit provides a considerable percentage of the whole demand, hence in the majority of hours, the biggest online unit is the boundary for reserve criteria of eq. (2.4). In case A, thermal generation is the only provider of up and down-reserve. So, the units are scheduled to generate power and keep enough headroom to satisfy both up and down reserve constraints. Providing up and down reserve is troublesome to the extent that bigger units are online only in some limited hours, just to keep the reserve requirement low. Then in low-demand hours, mainly after midnight and in the afternoon (gray lines in the figure divide different days of the week), only smaller units are committed. This is one of the reasons that the cost is higher for case A; the solver is forced to turn off big units, even though they are cheaper, to avoid reserve violation. In case B, with help of RES providing down reserve bigger and cheaper units are online for more hours. Less thermal generation is scheduled to serve as down-reserve, which leads to accessing more headroom to serve as up-reserve. Also, for cases C and D, there is enough reserve to avoid unnecessary thermal generation. It's deduced from the results of case C that in many hours deloading is unnecessary from an economic point of view and just eliminates some of the available wind generations, which could be used instead of thermal generation. Then in case D, wind generation is only deloaded in the hours that not enough thermal generation up reserve is scheduled. The results for case D

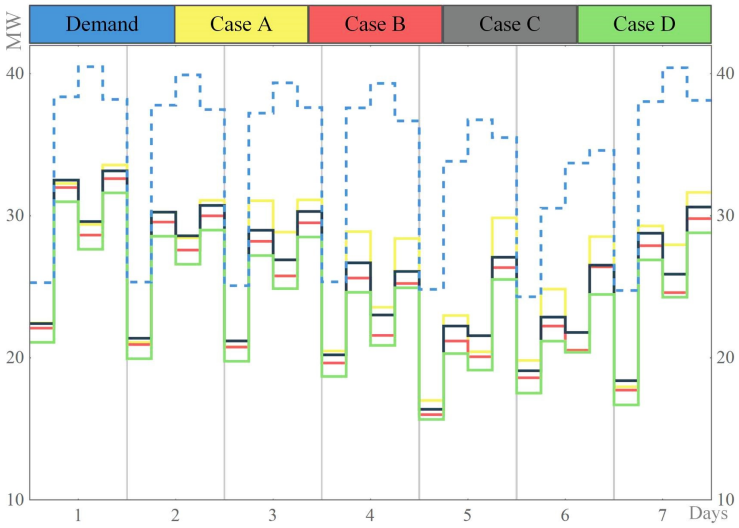

Figure 2.9: Power balance for a spring sample week, 2020, scenario III. The dashed line is the 6-hour power demand. Solid lines are the aggregated thermal power generation for corresponding cases A to D.

show how thermal generation can be minimized and the same time smartly allocates the amount of deloading to participate in the up-reserve provision, when needed. In cases, B and C, at some hours, the amount of available up reserve is much more than the required dashed line. Case D has managed to satisfy the up-reserve criteria and also not leave much unnecessary headroom.

Figure 2.9, shows the weekly power balance for a sample week. For the sake of clarity, 6-hour power demand is shown instead of hourly. The aggregated amount of thermal generation is illustrated with solid colors. Enabling RES to provide down-reserve, increases the share of renewables and reduces the overall thermal generation. As can be seen in the figure, case D is able to minimize the use of thermal generation.

2.6.2 Tenerife

For a bigger island like Tenerife, the main qualitative conclusions obtained for La Palma can be also verified. The average results of winter, spring, summer, and autumn are presented in detail in fig. 2.10.

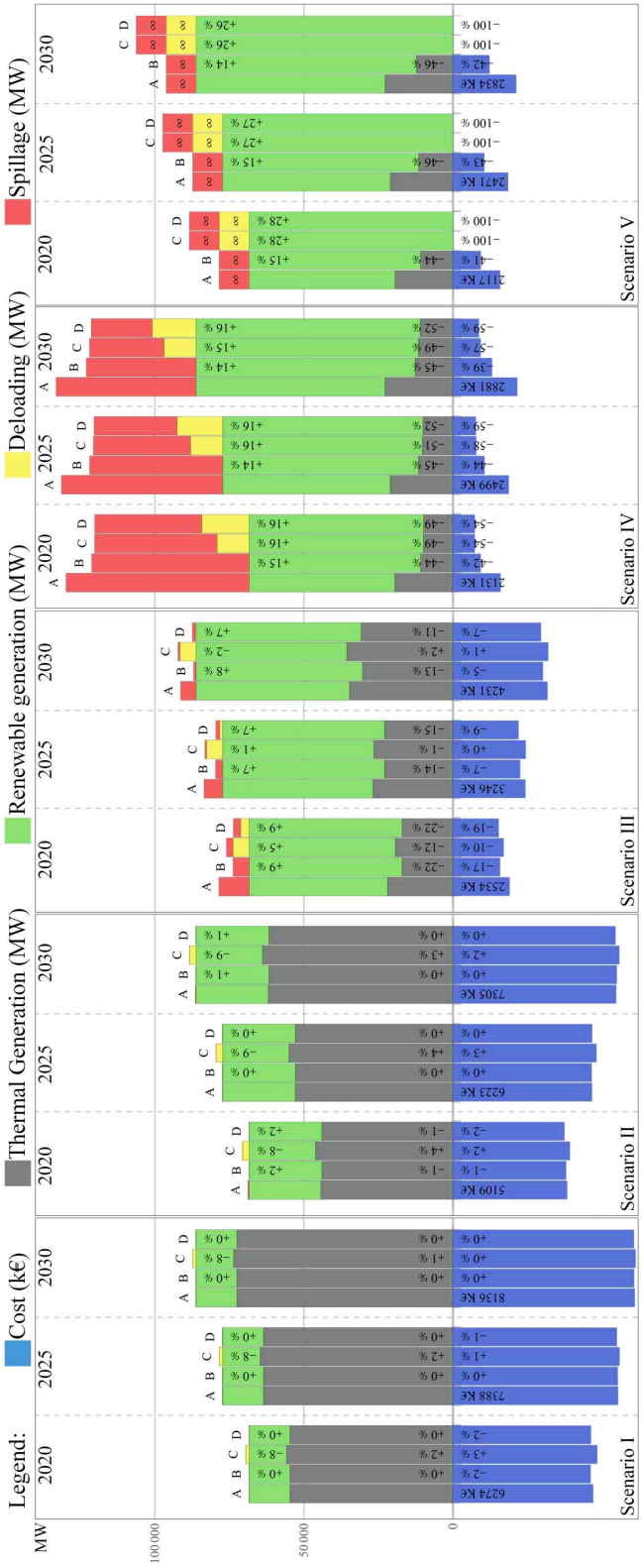

Figure 2.10: The average results of 4 seasons is shown here for Tenerife island. Different cases are specified above each bar. The number of scenarios is stated at the bottom corner. Obtained results for the years 2020, 2025, and 2030 are separated with dashed lines.
*Above zero is the energy in megawatts and below zero is the cost in kilo Euros.

Enabling renewable sources to provide down-reserve, which is the only difference between cases A and B, has always led to a reduction in cost and thermal generation. Also, for case B the amount of spillage is decreased for all scenarios, hence more renewable energy is scheduled. The improvement is negligible for the first scenarios, but as the available RES increases, the benefits become more noticeable. In scenario IV (multiplying the wind actual wind capacity by 10), a 45% reduction in thermal generation and a 39% of cost reduction are expected for the year 2030, only by adding the capability of providing down reserve to RES. These reductions even reach 40% for extreme scenario V for the year 2030.

The results show that imposing a constant percentage of deloading is not economically advisable on a big island like Tenerife when the penetration of RES is low (economic results are even worse for case C than for case B). However, starting from scenario IV, this approach starts to pay off and leads to more cost saving with respect to cases A and B. With the current amount of RES or for low RES scenarios in general, enabling them to provide down reserve seems futile. This is especially true for future years (2025 and 2030), where demand also grows and the share of thermal generation slightly increases. The most cost-efficient results stem from case D. In scenarios I and II, no deloading is scheduled. Then when enough wind power is available, deloading is advisable to minimize cost and thermal generation. In extreme situations, when wind energy is abundant, cases A and B are unable to use the potential, but as expected for cases C and D, a 100% renewable generation is possible.

Figure 2.11 shows how different energy sources are participating to satisfy reserve constraints. As Tenerife is a bigger island, the amount of scheduled RES is the boundary of reserve criteria in

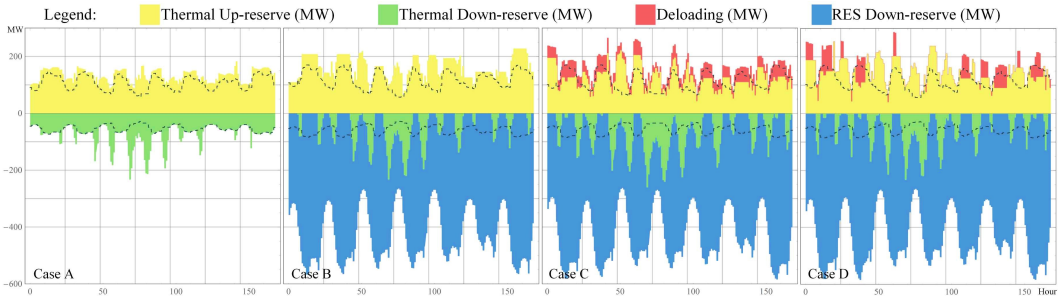

Figure 2.11: Provision of up and down reserve for different cases. The positive dashed lines are the amount of up reserve requirement and the negative dashed lines are the amount of down reserve requirement. Spring, 2030, scenario III.

(8). So, when a higher amount of RES is injected, the required reserve also goes higher. Implementing deloading is beneficial to meet the reserve requirement when the share of RES grows. In both cases C and D, it is noticeable from fig. 2.11, that deloading plays an important role in times of high RES injection. It is also evident that in some hours the wind power is unnecessarily deloaded in case C. In case D, deloading is employed more efficiently.

Figure 2.12, shows the weekly power balance for a sample week. For the sake of clarity, 6-hour power demand is shown instead of hourly. The aggregated amount of thermal generation is illustrated with solid colors. The dependency of the system on thermal units is considerably higher

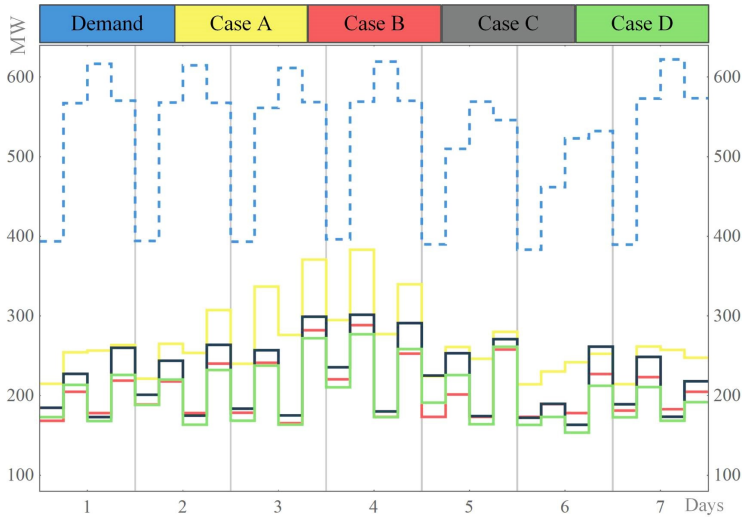

Figure 2.12: Power balance for a summer sample week, 2030, scenario III. The dashed line is the 6-hour power demand. Solid lines are the aggregated thermal power generation for corresponding cases A to D.

for case A. Enabling RES to provide reserve increases the ability of the system to benefit from available wind power, as much as possible.

2.7 Conclusions

This chapter has evaluated the impact of providing spinning reserves on the system operation costs. Simulations are conducted for La Palma (small size) and Tenerife (medium size) islands with various samples of actual and future scenarios to assess the economic benefits deriving from enabling RES to provide up and down-reserve. Up and down-reserve are considered separately in both formulation and assumed cases. The economic operation has been simulated by means of an hourly UC on a weekly basis.

Results show that using RES as down reserve providers is always beneficial for a small size island such as La Palma where the scarcity of reserve is more severe, where installed RES should immediately be able to provide down reserve to avoid unnecessary spillages and reduce costs. In contrast, it is beneficial only for high wind capacity scenarios for a medium size island such as Tenerife. For high penetration levels, providing down reserve reduces more than 40% the amount of thermal generation and more than 30% the system's cost on both islands.

For low penetration levels, up spinning reserve provision by wind generation is not justified, but as the penetration of wind generation becomes higher, the benefits of deloading wind generation to provide up reserve becomes more apparent making 100% renewable generation possible. Deloading a constant percentage of wind for all hours (case C) is not advisable, since it imposes extra expenses and leads to more thermal generation, and can even make economic results worse compared to only providing down reserve (Case B). However, if deloading is treated as a variable (case D), the optimization problem will be able to schedule deloading by deloading RES gener-

ation only when it has positive economic impacts. Implementing controllers on RES to enable them to provide down-reserve (case B), always leads to cost reduction. This cost reduction increases, when RES injection goes higher. Considering the future scenarios, the results suggest that providing reserve by RES is vital to inject more renewable energy when a high share of renewables is available in the system and helps lead to a 100% demand coverage by RES. In smaller islands, the scarcity of reserve is more severe and the installed capacity of RES should immediately be able to provide down reserve to avoid unnecessary spillages and reduce costs. For bigger islands like Tenerife, enabling RES to provide down reserve is not urgent, but will be required when the share of RES grows in the future. Future research will tackle the technical benefits of RES reserve provision on the dynamic frequency response of the system.

3 Feasibility of Providing Spinning Reserves by RES

This chapter investigates the technical benefits of providing frequency regulation by RES in island power systems. In the previous chapter, the economic aspects were studied. Following the findings in [22], here the results of the previous chapter are used to analyze the frequency stability in terms of frequency deviations and amount of load shed when the WTG operates at a fixed and a variable deloading percentage under normal conditions. This chapter shows that deloading can make improvements in frequency dynamics to some extent. The findings of this chapter are also submitted as a paper.

The improvements in renewable generation technologies together with a growing concern about the environmental impact of thermal generation and a boost in the global energy demand, are leading to an increasing interest in investigating new initiatives to evolve toward electric power systems that are more dependent on renewable energies, with wind power being the preferred option in the case of island systems [61], [2]. RES offers an attractive solution not only to minimize the use of fossil fuels and increase island sustainability but also to achieve cost-optimal electricity systems [62]. Spinning reserves denote those power and energy capacities that can be deployed in a relatively short time by means of the primary and secondary frequency controls. The amount of reserve needed in the island power system is significant with respect to the demand, so it is essential to adapt the size optimally so that they are sufficient to cover both emergency and non-emergency situations [31]. The common practice among island system operators is to establish a value of minimum spinning reserve requirement to be able to cover the loss of the largest online generating unit, expected RES variations, and loss of interconnections to other island power systems. Currently, RES generation does not provide spinning reserve. In addition, non-synchronous RES does not provide inertia by default, as they are connected to the grid through a power electronic converter that decouples the WTG's inertia [35]. Under this common practice, thermal generators are the providers of spinning reserve and inertia, functioning below their maximum power to provide the required amount of up reserve in some periods, thus increasing system operation costs. Further background studies that are related to this chapter are already reviewed in chapter 2, so it's skipped here.

3.1 Gaps and Contributions

The objective of this chapter is to investigate under what circumstances the provision of spinning reserves and inertia by RES provides technical benefits to real island power systems. The assessment is carried out by analyzing the impact of WTG when they operate at a fixed and at a variable deloading percentage under normal conditions. The UC problem is simulated, and the system frequency dynamics are analyzed in terms of security and stability. The assessment is carried out for real island power systems by considering different wind source availability scenarios for sample weeks of different seasons in current and future years. The islands of Tenerife (medium size) and La Palma (small scale) are chosen for simulations because they are representative of the Spanish isolated systems. These two islands fit in two of the five prototype islands identified through clustering techniques in [49].

In [22] (chapter 2) it's shown that the system operational costs of these two real islands can be reduced when RES provides up and down reserve. By taking the optimal UC schedules obtained in the previous chapter, this chapter simulates the dynamic responses of the system to thermal generator and wind outages and assesses the system response by a set of key performance indicator (KPI)s, such as frequency nadir or the amount of UFLS. This chapter complements the findings in chapter 2 by contemplating the actual impact of providing reserve on frequency stability.

Finally, this chapter also evaluates the appropriateness of the commonly used spinning reserve criterion to foster the development of RES in future demand scenarios. This criterion only sets the reserve requirement in terms of megawatt (MW), but it ignores the dynamic features (such as the speed or inertia) of the units providing reserve and thus can lead to increased UFLS under contingencies. Results show that a fixed deloading factor improves the frequency dynamics better than the variable deloading factor in most cases.

The rest of the chapter is organized as follows. In section 3.2, the methodology used in this chapter is explained. In section 3.3, the description of the case studies and the scenarios are presented. In section 3.4 and section 3.5, the obtained results for la Palma and Tenerife under no UFLS and under the current UFLS schemes are analyzed. Conclusions are drawn in section 3.6.

3.2 Methodology

The regulations of the Spanish Islands are already discussed in section 2.3. This section presents the methodology to assess the technical impacts of providing frequency regulation by WTG in island power systems and details the KPIs that will be used to evaluate the dynamic frequency response. The assessment is based on the simulation of the economic operation by means of an hourly UC on a weekly basis, which determines the hourly generation set point as well as the hourly start-up and shut-down decisions. Then the operation points are used as the input of the SFR model. This model simulates the dynamic system response in terms of frequency to the outage of every generator (including WTG) in every hour of the week. Dynamic simulations are conducted both with and without UFLS schemes. The simulations of the economic operation of the islands consider different scenarios for demands and RES penetration and cases of reserve provision capabilities. For a given weekly demand profile, the corresponding current wind pen-

etration profiles are scaled up according to the considered future installed capacity. The cases of reserve provision differ in the ability of WTG to provide reserves and frequency regulation.

Figure 3.1 shows a flowchart of the methodology. The input of the weekly UC includes the weekly hourly demand, wind and solar generation forecast, list of thermal generators, and their data sheet for each island and each sampling week under study. Considered scenarios and reserve provision cases are further discussed in section 3.3.

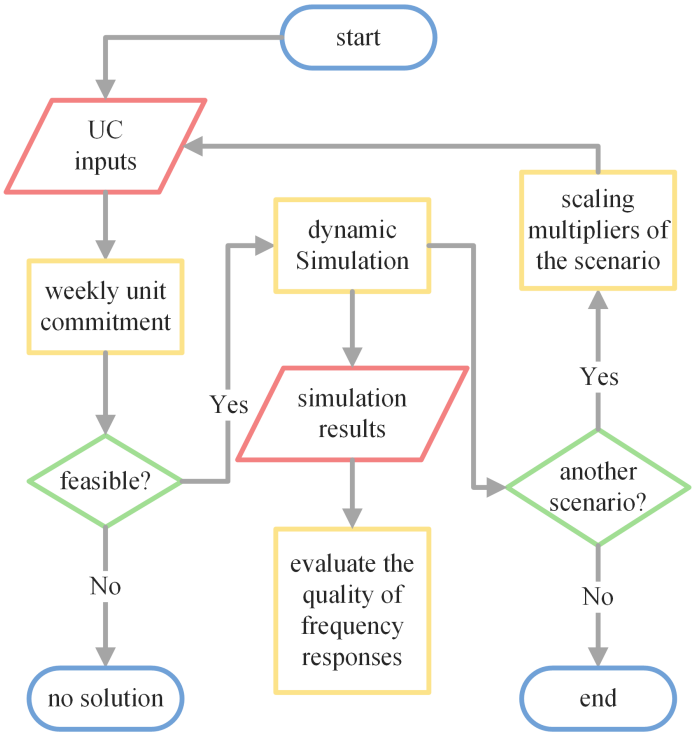

Figure 3.1: Flowchart of the methodology.

The UC model used in this chapter is the same as what is defined in chapter 2.

3.2.1 SFR Model

This section briefly presents SFR model used to analyze the frequency stability of small isolated power systems. These models are able to reflect the underlying short-term frequency dynamics of small isolated power systems. Figure 3.2 details the power-system model used to design UFLS schemes of a small isolated power system, consisting of I generating units. Each generating unit i is represented by a second-order model approximation of its turbine-governor system. In fact, frequency dynamics are dominated by rotor and turbine-governor system dynamics. Excitation and generator transients can be neglected for being much faster than the turbine-governor dynamics. Since frequency can be considered uniform, equivalent system inertia H can be defined. The overall response of loads can be considered by means of a load-damping factor D if its value is known.

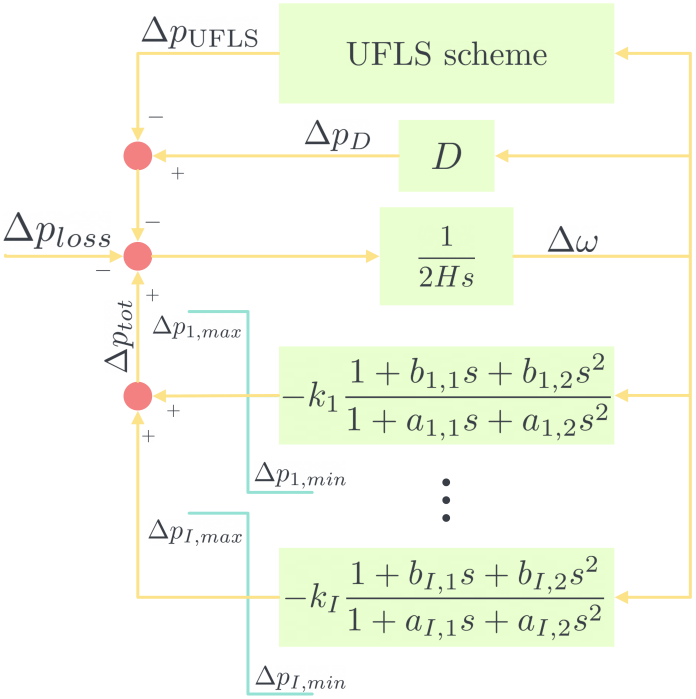

Figure 3.2: SFR model schematic.

The gain k_i and parameters $a_{i,1}$, $a_{i,2}$, $b_{i,1}$ and $b_{i,2}$, of each generating unit i can be deduced from more accurate models or field tests. Since the primary spinning reserve is finite, power output limitations $\Delta p_{i,min}$ and $\Delta p_{i,max}$ are forced. So the units can only participate as much as their available reserve. The complete model is explained in [1]. The inclusion of converter-connected generation can be realized if emulated inertia and parameters of the second-order generating unit model are given. In [1] wind turbines are modeled as thermal units with zero inertia H_i and zero gain k_i unless they emulate inertia or operate below the MPPT. In hours with enough wind production where deloading is considered, wind units work below the MPPT and are able to participate in the recovery of the frequency response when an outage happens. The control strategy of wind turbines is presented in fig. 3.3 and has been applied in different literature studies such as [46],[44],[63], and [64]. This configuration implements the inertia emulation control loop and is

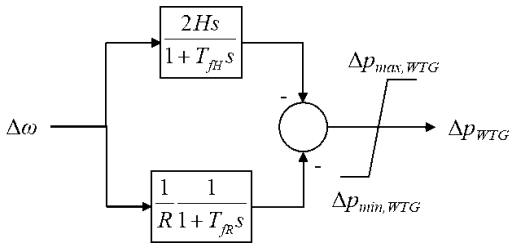

Figure 3.3: Control strategy of wind turbines ($H = 3s, R = 0.05, T_{fH} = 0.01$).

capable of steady-state power-sharing. The same method is used here. Wind systems provide both reserve and inertia emulation, where parameters for dynamic simulation are taken from [65].

For the purpose of this work, a 10% outage of wind power generation has been considered ($k_{\text{outage}} = 0.1$), following the information provided in the analysis of real wind patterns [48] for Tenerife and La Palma wind farms. Wind generation is modeled as two conventional units. One of them represents the remaining power and the other one represents the outage. P_s is the total forecasted amount of wind generation. In this way, the actual RES production after deloading is $P_s \times (1 - k_{\text{deloading}})$, and $P_s \times k_{\text{deloading}}$ is the amount of wind that can be used as reserve.

3.2.2 Key Performance Indicators

In order to analyze the results from a technical point of view, different input states are compared regarding a set of KPIs. When the simulations are executed without UFLS schemes, the following KPIs have been defined according to the frequency ranges. According to technical requirements of frequency stability for Spanish isolated power systems, a generating unit must be able to remain connected to the grid if the frequency falls below $47.5Hz$ for less than 3 seconds. The minimum frequency is $47Hz$. Rate of Change of Frequency (RoCoF) that an online unit must stand is $2Hz/s$, measured over a moving time window of $750ms$.

- The number of severe cases per state: it counts the number of times in all the simulations of a particular state that the frequency reaches a value lower than $47.5Hz$ for more than 3 seconds.
- The number of minimum frequency violations: it counts the number of times that the frequency reaches a value under $47Hz$.
- The number of online units in the whole week: it counts every unit that is online during the simulations of the considered state.
- The frequency violation percentage: calculated as the percentage of simulations in which the minimum frequency is violated [66].

When UFLS schemes are activated, UFLS prevents the frequency violations. Instead, the summation of UFLS for all contingencies in all of the hours will be measured in each state. In addition, the total load shedding cost (LSC) will also be obtained by adding the load shedding cost in each hour (C_t^{UFLS}), which is computed by multiplying the load shedding caused by the outage of every online generator in every hour (LS) by the forced outage rate (FOR) of each generator and the outage cost (OC) [66].

$$C_t^{UFLS} = LS_t \times \text{FOR} \times \text{OC} \tag{3.1}$$

$$\text{LSC} = \sum_{t \in \tau} C_t^{UFLS} \tag{3.2}$$

Where LS is the total UFLS in megawatts and C^{UFLS} is the cost of UFLS in euros. According to [66], the FOR of each type of generator listed in table 3.1 and the OC is 3000€/MWh to quantify the LSC. The actual cost of load shedding is difficult to assess. It depends on the time of

the incident, the spread, etc. In addition, penalization can be imposed on system operators and gencos. As another example, in [67] OC is assumed to be 11000€/MWh.

type of generator	FOR
diesel	0.004%
steam	0.002%
gas	0.0045%
wind	0.007%

Table 3.1: Forced outage rate of the generators in La Palma and Tenerife, according to their type

3.3 Case Studies and Scenarios

This chapter builds on the economic analysis presented chapter 2 and extends its findings by simulating the technical impact of providing reserve by RES. In this section, the case studies are described and the scenarios are defined.

3.3.1 Case Studies

The Energy Strategy for the Canary Islands in 2025 aims to reduce carbon dependency. Among others, strategic objectives for RES is achieving 45% of RES participation in final electricity generation by 2025. This would require multiplying the amount of installed RES capacity. In the case of wind power generation, not only on-shore but also off-shore wind farms are contemplated. To achieve realistic results, in this study the most recent actual demand and RES generation of Tenerife and La Palma are used as the inputs. The demand is scaled up for future cases by forecasted multipliers for the corresponding year. Other required inputs, including available power plants and their technical specifications such as cost functions, up and down time limitations, capacities, and ramping limitations are updated real data, obtained from the operators. The details of the islands under study and their units are presented in section 2.5. Figure 3.4 shows the weekly generation of wind and solar, per unit of installed capacity.

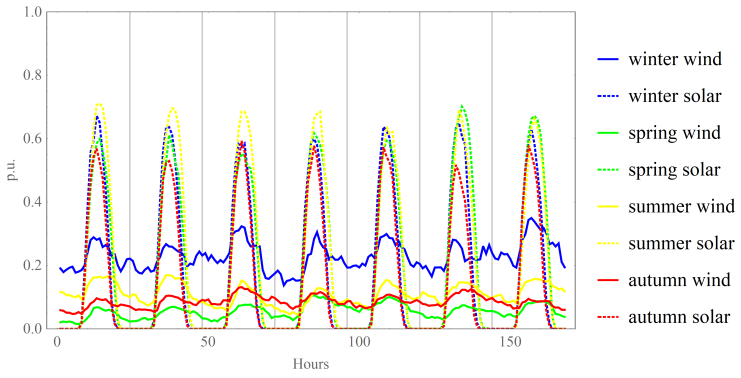

Figure 3.4: Solar and wind generation per installed unit.

The weekly demand for each season in 2020 on Tenerife island is shown in fig. 3.5.

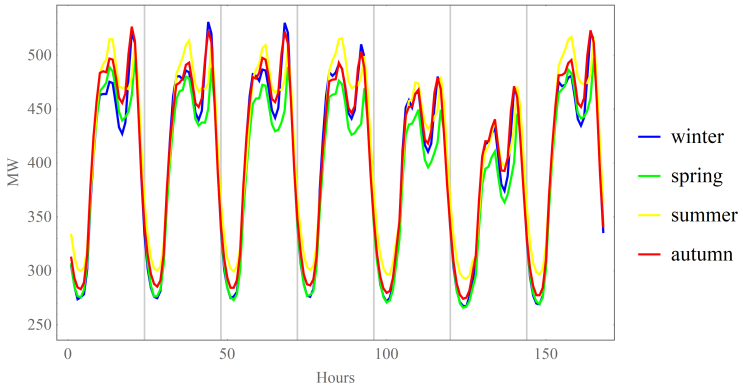

Figure 3.5: Weekly demand for each season of the year 2020.

3.3.2 Scenario Defenition

The impact of wind penetration levels on providing spinning reserve is analyzed by contemplating different scenarios of increasing installed capacity, in sample weeks of each season (winter, spring, summer, and autumn). The inputs here are the same as chapter 2. Scenario I denotes the current amount of installed wind capacity. For scenarios II to IV, the initial amount is multiplied by 2, 5, and 10, respectively. All the seasons and scenarios are considered for forecasted electricity demand for the years 2020, 2025, and 2030 to acknowledge the economic and technical impacts of each scenario in near future. For each scenario, three cases with different capabilities of providing spinning reserve by RES are defined.

- **Case A:** This case is the current practice of operators in Spanish islands where RES can provide neither spinning reserve nor inertia. The total reserve should be provided by thermal units. This case serves as a reference case.

- **Case B:** wind and solar sources provide up spinning reserve. A constant deloading factor of 10% is applied for the entire time horizon to available wind power. So, in each hour, 10% of available wind generation is deloaded and specified as up reserve. Emulation of inertia is also included.

- **Case C:** The possible amount of deloading is defined as a coefficient between 0 and 15% of available wind generation. The UC optimization problem will decide the optimal amount of deloading in each hour. Emulation of inertia is also included.

Figure 3.6 shows all of the considered states. Weekly unit commitment is solved for 3 different cases (A, B, and C), 4 sample weeks of different seasons (winter, spring, summer, and autumn), and 4 wind penetration scenarios (I, II, III, IV) for each year; composing 48 weekly UCs for each year. This approach is employed for three different years: 2020, 2025, and 2030. For each island, a total of 144 weekly UC simulations have been completed. For each hour of the 144 weekly UC, the outage of every generator including WTGs is simulated with the SFR model.

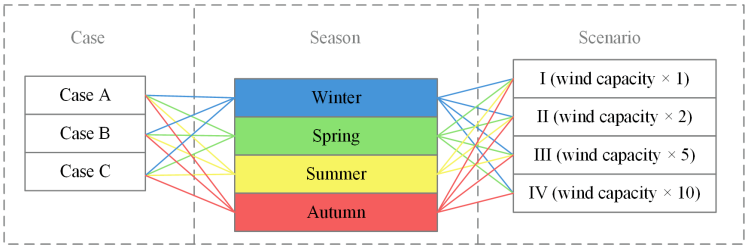

Figure 3.6: Considered states.

3.4 Results for La Palma

When the simulations are executed without UFLS schemes, the weekly KPI and the total weekly operation cost for the different scenarios and cases for the La Palma island are shown in Table 3.2. Weekly KPIs have been averaged over the four seasonal sample weeks. In addition, it shows in the dynamic simulations under current UFLS schemes, the expected weekly cost of UFLS for the different scenarios and cases. For a better analysis of the results, data from table 3.2 are depicted in fig. 3.7, where average weekly results for 4 seasons are shown. Different cases are specified above each bar. The number of scenarios is stated in the bottom corner. Obtained results for the years

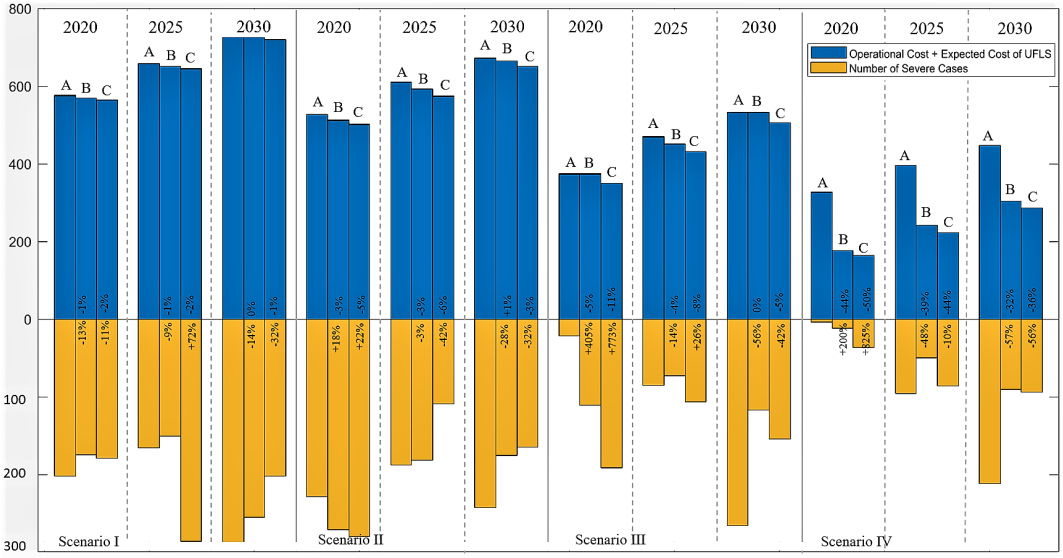

Figure 3.7: The average weekly results of 4 seasons in La Palma island.

2020, 2025, and 2030 are separated with dashed lines. Above zero is the total cost in k€ and below zero is the number of severe cases.

In fig. 3.7, blue bars represent the weekly UC dispatch cost from section 2.6.1 plus the expected cost of UFLS. Yellow bars represent the number of severe cases under no UFLS schemes. Case A is considered as the base case, then the incremental or decremental percentage of the KPIs is inscribed in the table and in the graphic, compared to the base case. It should be noted that as

Table 3.2: Results for La Palma.

			SFR with no UFLS				UC simulations	SFR with UFLS
			online units in whole week (#)	severe cases (#)	min frequency violations (#)	frequency violation (%)	weekly operation cost (K€)	weekly Cost of UFLS (K€)
scenario I	2020	A	1329	202	199	15	575	0.35
		B	1358 (+2%)	175 (-13%)	169 (-15%)	12.4 (-17%)	-1%	-13%
		C	1289 (-3%)	179 (-11%)	175 (-12%)	13.6 (-9%)	-2%	-4%
	2025	A	1467	166	144	9.8	657	0.37
		B	1477 (+1%)	151 (-9%)	127 (-12%)	8.6 (-12%)	-1%	-9%
		C	1420 (-3%)	286 (+72%)	224 (+56%)	15.8 (+61%)	-2%	22%
	2030	A	1452	295	215	14.8	726	0.53
		B	1533 (+6%)	255 (-14%)	192 (-11%)	12.5 (-15%)	0%	-12%
		C	1544 (+6%)	202 (-32%)	141 (-34%)	9.1 (-38%)	-1%	-16%
scenario II	2020	A	1294	229	217	16.8	527	0.37
		B	1165 (-10%)	271 (+18%)	257 (+19%)	22.1 (+32%)	-3%	-6%
		C	1206 (-7%)	280 (+22%)	283 (+30%)	23.5 (+40%)	-5%	1%
	2025	A	1438	188	178	12.4	610	0.37
		B	1373 (-5%)	182 (-3%)	159 (-11%)	11.6 (-6%)	-3%	-5%
		C	1487 (+3%)	109 (-42%)	113 (-37%)	7.6 (-39%)	-6%	-18%
	2030	A	1452	243	187	12.9	671	0.46
		B	1460 (+1%)	176 (-28%)	140 (-25%)	9.6 (-26%)	1%	-15%
		C	1516 (+4%)	165 (-32%)	122 (-35%)	8 (-38%)	-3%	-15%
scenario III	2020	A	1308	22	11	0.8	393	0.21
		B	1077 (-18%)	111 (+405%)	132 (+1100%)	12.3 (+1357%)	-5%	-15%
		C	1051 (-20%)	192 (+773%)	209 (+1800%)	19.9 (+2265%)	-11%	32%
	2025	A	1374	85	81	5.9	469	0.27
		B	1288 (-6%)	73 (-14%)	83 (+2%)	6.4 (+9%)	-4%	-25%
		C	1215 (-12%)	107 (+26%)	128 (+58%)	10.5 (+79%)	-8%	12%
	2030	A	1266	266	247	19.5	531	0.44
		B	1308 (+3%)	117 (-56%)	108 (-56%)	8,3 (-58%)	-44%	-40%
		C	1302 (+3%)	154 (-42%)	145 (-41%)	11.1 (-43%)	-50%	-25%
scenario IV	2020	A	1241	4	4	0.3	327	0.25
		B	807 (-35%)	12 (+200%)	13 (+225%)	1.6 (+389%)	-44%	-85%
		C	781 (-37%)	37 (+825%)	45 (+1025%)	5.8 (+1660%)	-50%	-58%
	2025	A	1232	96	90	7.3	396	0.33
		B	913 (-26%)	50 (-48%)	57 (-37%)	6.2 (-15%)	-39%	-73%
		C	818 (-34%)	86 (-10%)	97 (+8%)	12.2 (+67%)	-44%	-52%
	2030	A	1206	212	205	17	447	22
		B	937 (-22%)	91 (-57%)	99 (-52%)	10.6 (-38%)	-32%	-62%
		C	965 (-20%)	94 (-56%)	109 (-47%)	11.3 (-34%)	-36%	-51%

the KPIs under no UFLS scheme (except for the number of online units) are correlated, only the number of severe cases is represented in fig. 3.7.

As shown in chapter 2, the weekly operation cost of thermal generation is less for the cases with deloading capability. In case A, the UC solver is forced to turn off big units, even though they are cheaper, to avoid reserve violation. When deloading is considered, wind generators have the capacity of providing up reserve in the system. As a result, the economic dispatch changes, and the number of online units decreases because some thermal units that in case A are only connected to cover the reserve requirements can now be disconnected. In case B and C, less spillage occurs which leads to a decrement in weekly cost, compared to the base case. In some of the hours of case B more power than the amount to cover the reserve requirements is deloaded. In these circumstances, it is more cost-efficient to deliver more power to the grid and reduce or cut the deloading and as a result, the total operation cost of case B increases with respect to case C.

3.4.1 Analysis of Simulations Without UFLS Schemes

When UFLS schemes are not activated, there is a high number of severe cases and frequency violations. The comparison of the metrics between these cases yields a clear picture of how and when the provision of inertia and reserve by RES improves or worsens the dynamic frequency behavior of the system. Results show that for the current demand (the year 2020), the frequency response only improves for the cases with deloading capability (cases B and C) if the wind penetration is low (Scenario I). For instance, in 2020 the number of severe cases for case B diminishes 13% for Scenario I, and increases +18%, +405%, and +200% with respect to base case A for scenarios II, III, and IV respectively. As with low demand in a small island like La Palma the number of online units is very low, and the outage of one of them has a big impact on the frequency response of the system. If the wind generation increases, fewer conventional units are connected and when the considered wind outage occurs, the impact on the frequency response is considerable. It is important to highlight that comparing different cases implies comparing different economic dispatches, as the online units for the same demand and wind penetration vary from one case to another. Figure 3.8 shows the frequency response of the system in hour 69 of one sample week (summer) with the current demand and low wind penetration scenario (scenario I). Each response represents the frequency response of the system to the outage of one of the online units. The outage of every thermal unit, as well as the loss of 10% of RES, is shown. The legend specifies the amount of power that is lost in each contingency of the generators dispatched by the UC in cases A, B, and C. This graphic illustrates how the frequency response can improve for the cases with deloading, especially if the deloading factor is constant (case B). This figure also shows the limits for severe cases and minimum frequency. UFLS schemes are essential in this case to avoid the violation of the frequency ranges required by the Spanish regulation.

It is also worth mentioning that in the year 2020, the number of severe cases is always better for case B (fixed deloading factor) than for case C (variable deloading factor). This proves that the deloading factor that is optimal from the UC economic point of view (case C) is not necessarily optimal for the frequency response enhancement. In fact, case C can improve or worsen the frequency response of the system with no clear correlation with the demand and the wind penetration (for instance, in 2030 case C improves case B in scenarios I and II, and worsens in III and IV). Since the UC schedules a minimum spinning reserve requirement neglecting frequency

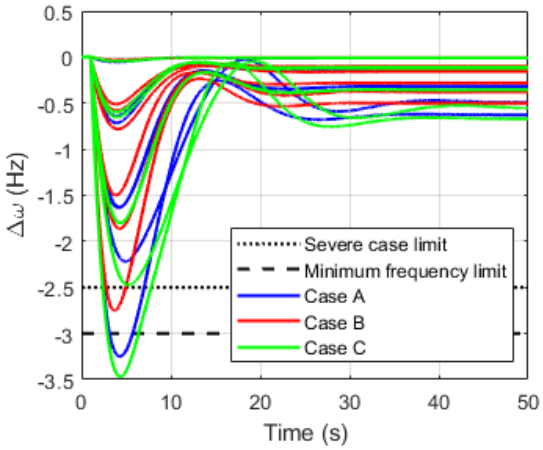

Figure 3.8: Frequency response in hour 69 of summer in La Palma 2020, scenario I for case A, B and C under no UFLS.

dynamics, wind generation is only deloaded in the hours that thermal generation up reserve is not enough. When a contingency occurs, it has less power to serve as reserve and can result in a worse frequency response. Figure 3.9 shows the frequency response of the system in hour 69 of the summer week with the current demand (the year 2020) and a high wind penetration scenario (IV). For each case, the frequency response of every committed unit is presented. For instance, there

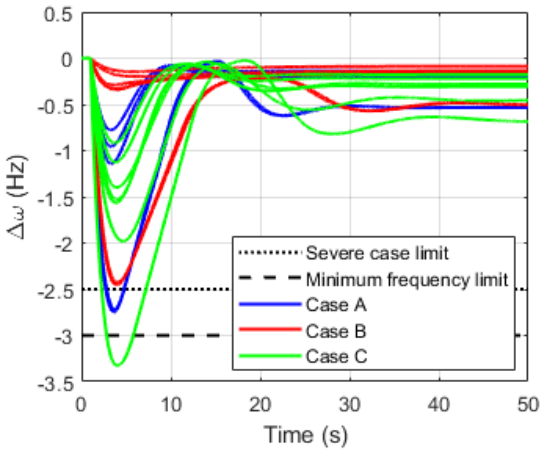

Figure 3.9: Frequency response in hour 69 of summer in La Palma 2020, scenario IV for cases A, B and C under no UFLS scheme.

are five green responses because, for case C, 5 thermal units were scheduled. The figure shows also the thresholds of severe frequency response (47.5 Hz for more than 3 seconds) and minimum allowable frequency (47 Hz). It can be seen that variable deloading does not improve the response, since a violation of the minimum frequency and thus a severe case only occurs for case C. When

the demand increases (the years 2025 and 2030) more online units are connected, and their outage does not have such a high impact on the frequency response. It can be seen that a fixed deloaded capability (case B) always improves base case A, for every wind penetration scenario (Scenarios I, II, III y IV). In the increased demand scenarios of 2025 and 2030, for high wind penetration scenarios (III and IV), case C worsens the dynamic response with respect to case B.

3.4.2 Analysis of Simulations Under Current UFLS Schemes

When the UFLS scheme is considered, table 3.2 outlines that a better dynamic performance translates into less load shedding and in this way less UFLS system cost. However, due to the low values of FOR of generators, the total expected cost of UFLS is negligible compared to the system operations cost. For example, the total operation cost for the year 2020, scenario I and case A, is 575 k€ while the expected UFLS cost is 0.35 k€. When checking the total system cost (dispatch operations cost + expected UFLS cost in fig. 3.7) case B outperforms case A regarding the operation cost, and case C outperforms case B.

Even though reserve provision in actual demand scenarios (the year 2020) might be counterproductive, in future scenarios it allows increasing RES penetration. In addition, it becomes clear that neglecting the dynamic response when considering reserve provision in the UC model leads to an overestimate of the benefits of providing reserve. In order to improve the dynamic performance of the system and in this way reduce the UFLS, it is advisable to implement a fixed deloading percentage of RES in wind generators and not a variable deloading as decided by the UC only. However, from a strictly economical point of view with the assumed cost of load shedding, a variable deloading factor is advisable since the expected cost of UFLS is not significant compared to the operational cost. It seems also quite interesting that in order to capture both the minimum system cost and best frequency dynamic behavior, system operators of real systems should move to the use of UC models that include frequency-related constraints (more on this in chapter 5 and chapter 6).

3.5 Results for Tenerife

The seasonal average weekly KPI and the total operation cost for different scenarios and cases for Tenerife island without UFLS scheme are shown in table 3.3 and in fig. 3.10 (which follows the same pattern as fig. 3.7).

For a bigger island like Tenerife, the main qualitative conclusions obtained for La Palma are verified only for high wind penetration scenarios. For low wind penetration scenarios (I and II), deloading (fixed or variable) might not be advisable both from an economic or a dynamic frequency quality point of view. For instance, in Scenario II and the year 2030, case B increases the number of severe cases by 10% and the total system cost by 2%, while case C increases the number of severe cases by 15% not being able to reduce the total system cost. For future wind scenarios, case B always diminishes the number of severe cases with respect to case A, and case C can improve or not frequency quality with respect to case B. For future high demand and wind scenarios (scenario IV, years 2025 and 2030) RES frequency regulation removes all severe cases meaning that UFLS is not activated.

Table 3.3: Results for Tenerife.

			SFR with no UFLS				UC simulations	SFR with UFLS
			online units in whole week (#)	severe cases (#)	min frequency violations (#)	frequency violation (%)	weekly operation cost (K€)	weekly Cost of UFLS (K€)
scenario I	2020	A	1604	159	147	9.2	6274	7.02
		B	1629 (+2%)	154 (-3%)	144 (-2%)	8.8 (-4%)	3%	-9%
		C	1625 (+1%)	149 (-6%)	145 (-1%)	8.9 (-3%)	-2%	-3%
	2025	A	1706	244	236	13.8	7388	11.07
		B	1738 (+2%)	232 (-5%)	215 (-9%)	12.4 (-11%)	1%	-13%
		C	1729 (+1%)	244 (+0%)	230 (-3%)	13.3 (-4%)	-1%	-3%
	2030	A	2005	255	234	11.7	8136	10.09
		B	2069 (+3%)	238 (-7%)	225 (-4%)	10.9 (-7%)	0%	-14%
		C	2072 (+3%)	246 (-4%)	220 (-6%)	10.6 (-9%)	0%	-10%
scenario II	2020	A	1403	167	166	11.8	5109	8.01
		B	1402 (+0%)	165 (-2%)	163 (-2%)	11.6 (-2%)	2%	-9%
		C	1401 (+0%)	163 (-2%)	163 (-2%)	11.6 (-2%)	-2%	-3%
	2025	A	1644	122	107	6.5	6233	4.65
		B	1602 (-3%)	140 (+15%)	129 (+21%)	6.3 (+24%)	3%	36%
		C	1562 (-5%)	112 (-8%)	98 (-8%)	8.1 (-4%)	0%	24%
	2030	A	1788	165	146	8.2	7305	8.25
		B	1723 (-4%)	181 (+10%)	159 (+9%)	9.2 (+9%)	2%	1%
		C	1773 (-1%)	174 (+5%)	154 (+5%)	8.7 (+5%)	0%	-1%
scenario III	2020	A	1179	49	15	1.3	2534	0.31
		B	834 (-29%)	5 (-90%)	5 (-67%)	0.6 (-53%)	-10%	-89%
		C	809 (-31%)	23 (-53%)	24 (+60%)	3 (+133%)	-19%	-48%
	2025	A	1309	27	25	1.9	3246	1.06
		B	1108 (-15%)	9 (-67%)	9 (-64%)	0.8 (-57%)	0%	-71%
		C	1094 (-16%)	7 (-74%)	7 (-72%)	0.6 (-66%)	-9%	-87%
	2030	A	1416	21	21	1.5	4231	1.08
		B	1297 (-8%)	17 (-10%)	17 (-19%)	1.3 (-12%)	1%	-74%
		C	1283 (-9%)	11 (-48%)	11 (-48%)	0.9 (-42%)	-7%	-60%
scenario IV	2020	A	1150	51	17	1.5	2131	0.33
		B	674 (-41%)	1 (-100%)	0 (-100%)	0 (-100%)	-54%	-100%
		C	672 (-42%)	0 (-98%)	1 (-94%)	0.1 (-90%)	-54%	-98%
	2025	A	1282	14	9	0.7	2499	12
		B	681 (-47%)	0 (-100%)	0 (-100%)	0 (-100%)	-58%	-100%
		C	684 (-47%)	0 (-100%)	0 (-100%)	0 (-100%)	-59%	-100%
	2030	A	1266	0	0	0	2881	9
		B	716 (-43%)	0	0	0	-57%	-100%
		C	701 (-34%)	0	0	0	-59%	-96%

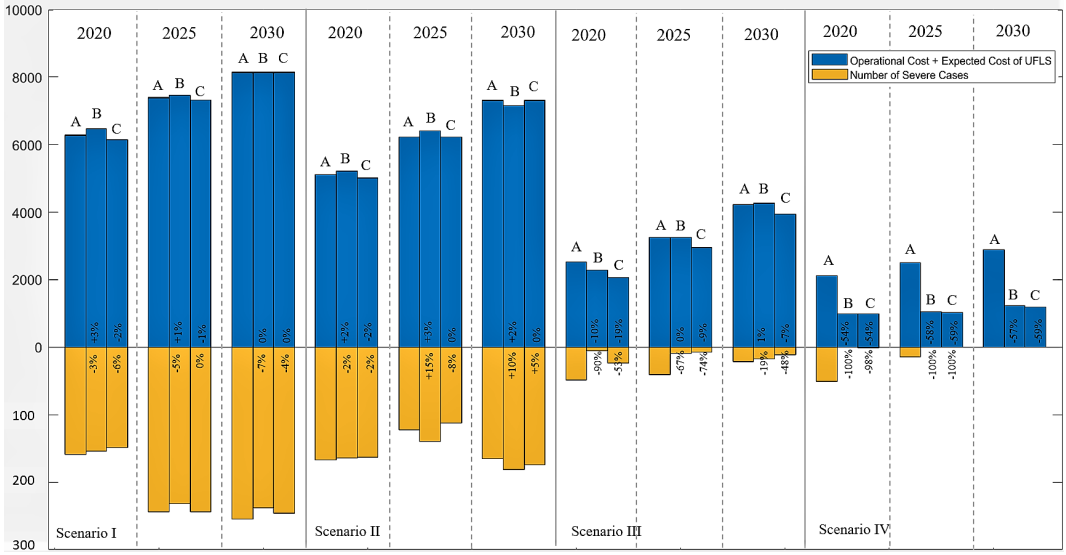

Figure 3.10: The average results of 4 seasons in Tenerife island.

Figure 3.11 shows the frequency response of the system in the first hour of a summer week with high demand (the year 2030) and a high wind penetration scenario (scenario III). It shows that

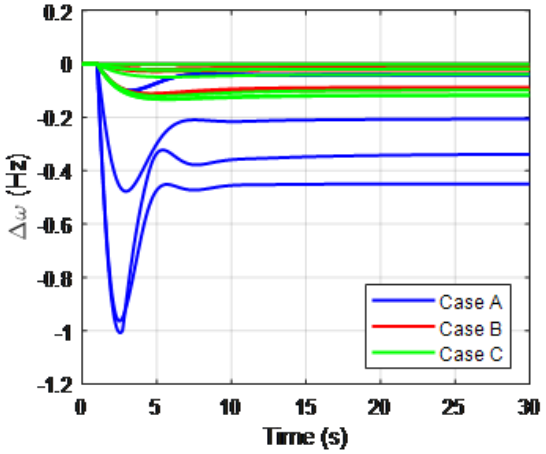

Figure 3.11: the frequency response in the first hour of summer in Tenerife 2030, scenario III for case A, B, and C.

deloading (either fixed deloading -red- or optimal -green-) clearly improves the frequency response of case A represented by blue lines. Because of its big size, Tenerife has more units connected than smaller islands, and the contingency of each of them has a smaller impact on the overall frequency response. The number of severe cases, minimum frequency violation, and frequency violation percentage are better than in La Palma, and in fig. 3.11, none of the frequency limits are reached. It can be concluded that the size of the island power system is essential for the frequency response.

More online units participating in the recovery of the system translates into a lower impact on the frequency dynamics. From the analysis of simulations run under UFLS schemes, it is clear from table 3.3, that total expected UFLS cost is also negligible for Tenerife island, and from a strictly economical point of view, variable deloading is best, especially for high wind scenarios (III and IV) and can reduce case A total system cost up to 60%.

3.6 Conclusion

This chapter has evaluated the impact of providing frequency regulation by wind turbines on the system frequency response. Simulations are carried out for La Palma (small size) and Tenerife (medium size) islands with various samples of actual and future scenarios to recognize what technical impacts are expected from enabling RES to provide reserve and frequency regulation. Simulations without UFLS schemes are presented to evaluate the frequency response quality, whereas simulations under current UFLS schemes are conducted to assess the impact on UFLS size and cost. For future scenarios of a small island like La Palma, fixed deloading enhances the frequency quality behavior compared to variable deloading in most scenarios. However, since the expected cost of UFLS schemes is negligible due to typical values of FOR of generators, variable deloading is preferable from a strictly economical point of view. In a bigger island like Tenerife, variable deloading is only recommended for high demand and wind scenarios, since it improves both dynamic response and total system cost.

In order to achieve both the minimum system cost and the best dynamic behavior, system operators of real systems should move from the common practice of establishing a value of minimum spinning reserve requirement to the use of the UC models that include frequency-related constraints. Future research will tackle the use of these advanced UC models on island systems in chapter 5 and chapter 6.

4 LAES Model for Scheduling Purposes

This chapter presents a detailed mixed integer linear model of LAES, to be used in scheduling and planning problems. A comprehensive cycle diagram of different processes of liquid air energy storage is presented, and the model has been developed accordingly. Installing LAES in the power system can help with storage scarcity problems and storage requirements. In line with the previous chapter, the operation planning is carried out by considering a static reserve requirement only. Inertia has not been included explicitly, although they can provide inertia with their flywheels. The findings of this chapter are published as a paper in [68].

Generating electricity has been reliant on burning fuels for decades. Although thermal generation is cheap, it emits a considerable amount of greenhouse gasses, which has negative environmental impacts. To go towards cleaner ways of generating electricity, the share of RES is increasing in the power systems in recent decades. Contrary to the thermal generation that can provide as much as it's demanded, renewable sources only produce energy when it's available. The abundance of available renewable energy might happen in low-demand hours, or there might be a lack of renewable production in high-demand hours. To use available RES more efficiently, it's wise to store energy when there is extra and use it when required.

4.1 Framework

Different types of ESS are used in the power system, including electrochemical and battery, thermochemical, flywheel, compressed air, liquid air, magnetic, etc [69]. There is a wide range of benefits that can be expected from energy storage systems, including load balance when the demand changes, providing additional energy to end-users during overload situations, and storing the excess energy of RES to minimize CO2 emission [70]. In [71] a demand management model for industrial parks considering the integrated demand response of combined heat and power (CHP) units and thermal storage is proposed, to reduce the peak demand charge.

Although the use of LAES in the islands is not specifically studied in the literature, extensive analysis has been done in [72] to scrutinize the performance of underwater compressed air energy

storage (CAES) in island power systems. A round-trip efficiency of 58.9% is promised with both energy and exergy analyses. In [73] adiabatic CAES is investigated, which is not dependent on fossil fuels. Low-temperature adiabatic CAES can address some of the current limitations that restrict process temperature for higher flexibility and the use of cheaper components to lower the overall expenditure.

Among different technologies, LAES seems promising for large-scale energy storage. Chemical energy storage systems, like batteries, have the highest efficiency, but their short lifetime makes them expensive. Also, they should be recycled when their life is over, which has negative environmental impacts. Large-scale mechanical storage systems like pumped pumped hydroelectric energy storage (PHES) and CAES have geographical limitations, as they need big vessels or underground caverns. These disadvantages of other technologies have led LAES to get more attention in the research field recently, although the round-trip efficiency of LAES is lower than some of the other competing technologies [74]. Innovations are being proposed to enhance the efficiency of LAES ([75] and [76]). As stated in [75] disadvantages of LAES are the relatively high investment cost, large-scale requirements, and low round-trip efficiency. On the other hand, the advantages of LAES are high energy density, low storage losses, and not having geographical limitations. LAES can contribute to reverse provision and load shifting from the operational planning point of view, and to frequency and voltage control from the technical point of view.

A hybrid system of LAES combined with high-temperature thermal energy storage (HTES) is presented in [77]. HTES is used as an alternative to the conventional combustion chamber in LAES. In [78] and [79] liquefied natural gas (LNG), is integrated with LAES, achieves better generation flexibility, increases operating profits from electricity arbitrage, and enhances energy efficiency. LNG is regasified depending on the amount of demand: LNG cold energy is recovered and stored during peak times, and during off-peak times transfers high-grade cold energy to LAES for energy storage. A combination of gas-steam combined cycle unit and LAES is proposed in [80], to better utilize the exhaust heat of the combined cycle unit and the high-grade cold energy from the LNG terminal. It is demonstrated that the integrated system is economically more efficient and also prevents temperature increases.

While innovative solutions are being proposed to make energy storage systems more feasible, it is necessary to also incorporate them into the power production scheduling and planning process. This requires an appropriate model of the energy storage system. In [81], the methods of incorporating ESS in the UC problem are reviewed. A general formulation of additional constraints for ESS in UC is presented, including state of charge of storage, maximum charge and discharge, binary logic, and ramping. While this general model is usually used for battery ESS, more accurate models for pumped hydro storage (PHS), hydrogen storage system (HSS), and superconducting magnetic energy storage (SMES) are also presented. An interval unit commitment (IUC) model for optimal energy and reserve scheduling in a system with CAES is introduced in [82], which also considers frequency dynamics. A robust optimization approach is employed in [83], to achieve the offering and bidding curves of CAES. In both of these studies with CAES, a general MILP model is used, that overlooks the charging and discharging start energy of CAES and transitions. Reviewed literature is categorized and summarized in fig. 4.1.

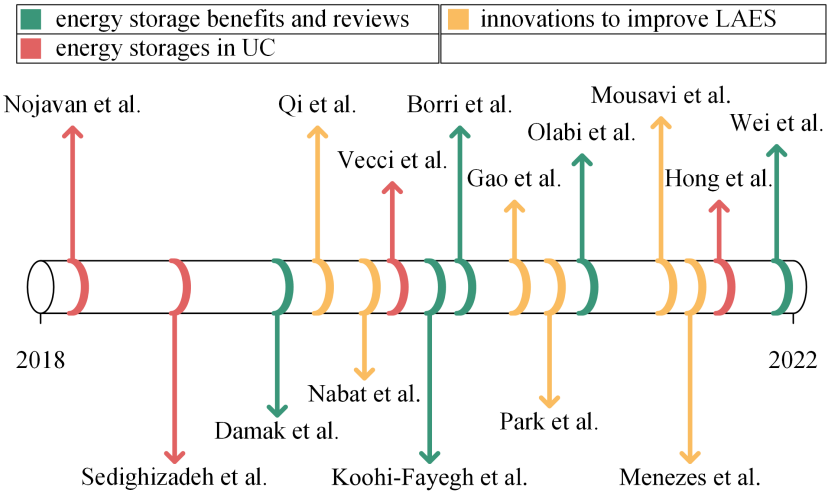

Figure 4.1: Summary of references ([69], [70], [71], [74], [75], [76], [77], [78], [79], [80], [81], [82], [83])

4.2 Gaps and Contributions

This chapter introduces a detailed MILP model for LAES to incorporate into the UC problem. The contribution of this chapter is presenting a MILP formulation of LAES, that includes charging start energy (CSE) and discharging start energy (DSE). Realistic future scenarios of Tenerife island for the years 2026 and 2030 are used to validate the proposed model, by solving weekly UC. As wind and solar availability vary from season to season, weekly sample scenarios of winter, spring, summer, and autumn are used, to provide a better insight over each year. The model is compared with the general formulation, and the differences are pointed out.

The methodology, including basic and proposed LAES formulation, is presented in section 4.3. Scenarios and obtained results are presented in section 4.4. Then conclusions are drawn in section 4.5.

4.3 Methodology

4.3.1 UC formulation

The short-term scheduling is often solved by the mixed integer linear formulation of UC problem. The general formulation of UC was introduced in the previous chapter with eqs. (2.1a) to (2.1i). The additional constraints to define power balance and reserve with LAES are as follows,

$$r_t = \sum^{i\in\mathcal{I}} \left(r_{i,t}^{Ther}\right) + r_t^{LAES} + r_t^{BESS} \qquad t \in \mathcal{T} \tag{4.1a}$$

$$\sum^{i\in\mathcal{I}} \left(p_{t,i}\right) + wg_t + sg_t + p_t^{dischar} = \mathcal{D}_t + \mathrm{CSE}_t + \mathrm{DSE}_t + p_t^{char} \qquad t \in \mathcal{T} \tag{4.1b}$$

$$wg_t \leq \mathcal{W}_t \qquad t \in \mathcal{T} \tag{4.1c}$$

$$sg_t \leq \mathcal{S}_t \qquad t \in \mathcal{T} \tag{4.1d}$$

$$r_{i,t}^{Ther} = \max[\overline{\mathcal{P}_i}.u_{t,i} - p_{t,i}\ , \overline{\mathcal{R}_i}.u_{t,i}] \tag{4.1e}$$

$$r_t - r_{i,t}^{Ther} \geq p_{t,i} \qquad t \in \mathcal{T}, i \in \mathcal{I} \tag{4.1f}$$

$$r_t \geq (wg_t + sg_t) \times \mathrm{RRM} \qquad t \in \mathcal{T} \tag{4.1g}$$

Where r, wg, and sg are the online reserve power, wind generation, and solar generation variables in megawatts, respectively. Renewable reserve multiplier (RRM) is applied to eq. (4.1g). Equation (4.1a) is the total up reserve equation. Total up reserve is the summation of the generation headroom of thermal units, plus the amount of reserve that is provided by LAES and battery ESS. Equation (4.1b) is the power balance equation, considering LAES charge and discharge. It's later explained how to calculate CSE_t and DSE_t. Equation (4.1c) and eq. (4.1d) make sure that the scheduled wind power and solar power are always equal to or less than the forecasted amount. Equation (4.1e) calculates the amount of reserve that each unit can provide. Equation (4.1f) and eq. (4.1g) are stating that the available reserve should be always bigger than any outage of thermal units and estimated intra-hour variations of renewable infeed. RRM in eq. (4.1g) is a multiplier that can be adjusted depending on the expected volatilities or outages of RES forecast.

LAES model

Energy stored in the cryogen (liquefied gas) is different from other types of heat storage; It is obtained from decreasing internal energy and increasing its exergy. The principle of using liquid air to store energy is based on three steps:(a) liquefying air when energy is available, (b) storing it as a liquid in insulated vessels, and (c) expanding the air and pumping it to turbines to generate power [84]. The process is shown in fig. 4.2 schematically.

A detailed cycle diagram, that includes transitions and start-up energies is necessary to develop a MILP model of LAES. The cycle diagram of LAES is presented in fig. 4.3. The same duty cycle can be found in [85] for different operation modes. In this diagram, charge start time, charge duration, charge down duration, charge-discharge turnaround time, discharge start time, discharge duration, and discharge downtime are specified. In current technologies of LAES, charge start time and energy cannot be ignored. Charge down and discharge down duration is negligible, hence ignored in this chapter.

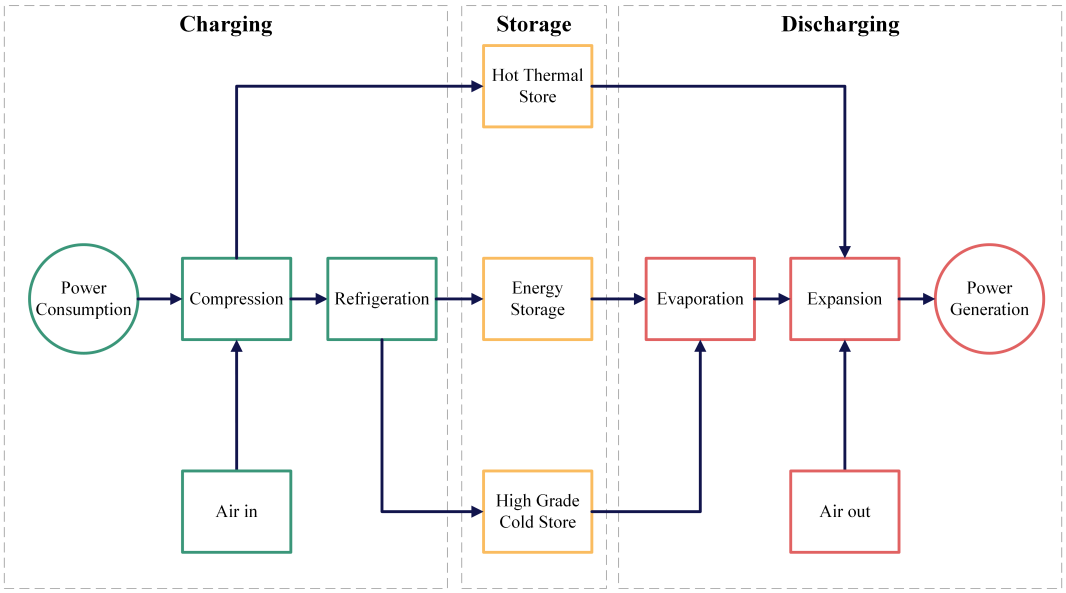

Figure 4.2: Liquid air energy storage process

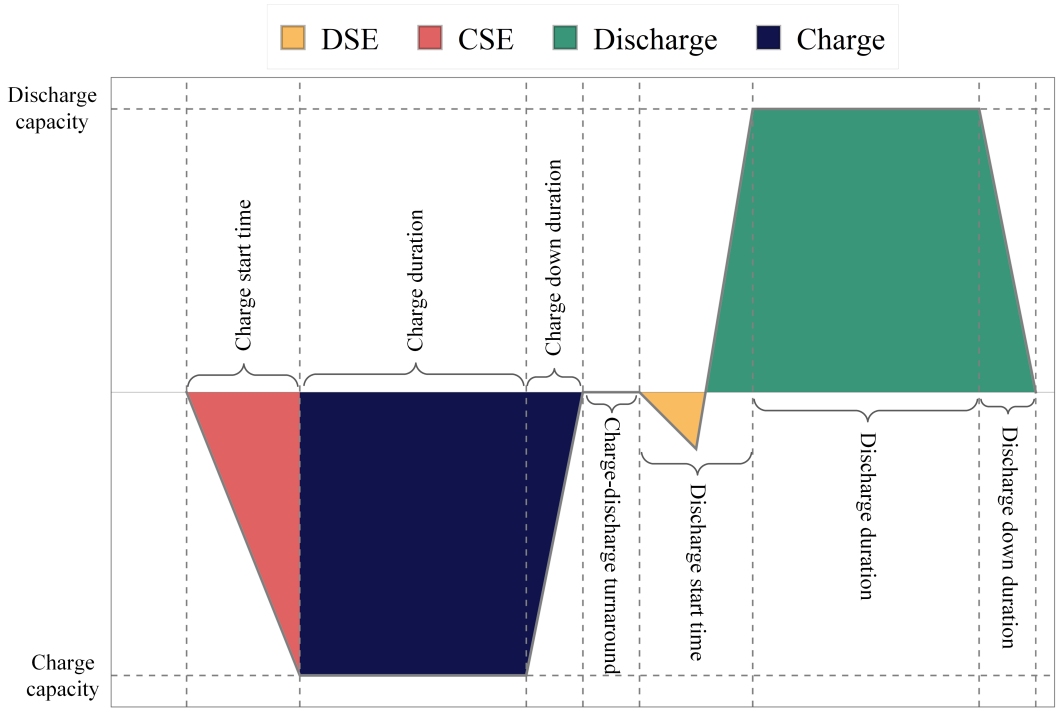

Figure 4.3: Liquid air energy storage cycle diagram

LAES basic formulation

Storage devices are usually modeled with a set of constraints, presented here.

$$u_t^{char} + u_t^{dischar} \leq 1 \tag{4.2}$$

$$p_t^{char} \leq \overline{\mathcal{P}}_{char}\left(u_t^{char}\right) \tag{4.3}$$

$$p_t^{dischar} \leq \overline{\mathcal{P}}_{dischar}\left(u_t^{dischar}\right) \tag{4.4}$$

$$e_t^{LAES} = e_{t-1}^{LAES} + p_t^{char}\xi^{LAES} - p_t^{dischar} \tag{4.5}$$

Where e and ξ are the energy state and round-trip efficiency of LAES, respectively. Equation (4.2) makes sure that only one of the charging or discharging modes is active. Equation (4.3) and eq. (4.4) are the maximum charging and discharging capacity of LAES, respectively. And in eq. (4.5) the energy state of LAES is defined.

Using this approach for LAES ignores the charging start-up energy, discharging start-up energy, transient ramp up and ramp down, the turnaround times, minimum charging, and minimum discharging. These differences can add up and lead to unrealistic conclusions regarding the planning and scheduling LAES.

LAES proposed formulation

Due to essential differences between liquid air systems and batteries, ignoring the characteristics of LAES may lead to unrealistic results. Here an accurate model of LAES is presented, that takes into account the unique characteristics of LAES. To define the binary logic, it should be noted that: (a) simultaneous charging and discharging are not allowed. (b) charge start energy and discharge start energy are imperative, so binary variables of charging start-up, charging shut-down, discharging start-up, and discharging shut-down should also be defined.

$$u_t^{char} + u_t^{dischar} \leq 1 \tag{4.6}$$

$$u_t^{char} - u_{t-1}^{char} = v_t^{char} - w_t^{char} \tag{4.7}$$

$$v_t^{char} + w_t^{char} \leq 1 \tag{4.8}$$

$$u_t^{dischar} - u_{t-1}^{dischar} = v_t^{dischar} - w_t^{dischar} \tag{4.9}$$

$$v_t^{dischar} + w_t^{dischar} \leq 1 \tag{4.10}$$

Simultaneous charging and discharging are avoided by eq. (4.6). In eq. (4.7) and eq. (4.8) the binary logic for start-up and shut-down of charging mode is defined. Same logic is defined for discharging mode in eq. (4.9) and eq. (4.10).

Other than maximum capacity for charging and discharging, LAES is limited with minimum charging and discharging boundaries too. Especially in the charging mode, LAES should always be charged close to maximum capacity. The capacity constraints are presented here. Also, LAES is unable to charge during charging start time (CST) or discharge during discharging start time (DST).

$$p_t^{char} \leq \overline{\mathcal{P}}_{char}\left(u_t^{char} - v_t^{char} \times \mathrm{CST}\right) \tag{4.11}$$

$$p_t^{char} \geq \underline{\mathcal{P}}^{char}\left(u_t^{char} - v_t^{char} \times \text{CST}\right) \tag{4.12}$$

$$p_t^{dischar} \leq \overline{\mathcal{P}}_{dischar}\left(u_t^{dischar} - v_t^{dischar} \times \text{DST}\right) \tag{4.13}$$

$$p_t^{dischar} \geq \underline{\mathcal{P}}^{dischar}\left(u_t^{dischar} - v_t^{dischar} \times \text{DST}\right) \tag{4.14}$$

Charging is limited by the maximum charge capacity of LAES in eq. (4.11). But it always takes a while to start up the charging process. Depending on the LAES technology, charging start time might vary from minutes to more than half an hour. CST indicates what fraction of an hour it takes for the charging process to start up. DST indicates what fraction of an hour it takes for the discharging process to start. Minimum charge capacity is imposed in eq. (4.12). Maximum and minimum discharge capacity is defined in the same manner in eq. (4.13) and eq. (4.14).

$$e_t^{LAES} = e_{t-1}^{LAES} + p_t^{char}\xi^{LAES} - p_t^{dischar} \tag{4.15}$$

$$e_0^{LAES} = e_T^{LAES} \tag{4.16}$$

Where e_0 and e_T are the initial and final energy state of LAES in megawatts. The energy state of LAES is calculated with eq. (4.15). Equation (4.16) makes sure that the energy state at the beginning and end of the time horizon is equal. As mentioned before the amount of charging start energy and discharging start energy are not negligible in LAES, and should be taken into account. The amount of this energy depends on the charging start power (CSP), discharging start power (DSP), and the duration of the start-up.

$$\text{CSE}_t = \text{CSP} \times \text{CST} \times \overline{\mathcal{P}}_{char} \times v_t^{char} \tag{4.17}$$

$$\text{DSE}_t = \text{DSP} \times \text{DST} \times \overline{\mathcal{P}}_t^{dischar} \times v_t^{dischar} \tag{4.18}$$

CSE is calculated in eq. (4.17) for each hour, considering CSP and CST. DSE is calculated in eq. (4.18) for each hour, considering DSP and CST. Compared to other fast storage devices, LAES does not contribute a lot to the primary reserve provision. Depending on the acceptable duration of the primary response, the reserve provided by LAES can be calculated as follows,

$$\begin{aligned} r_t^{LAES} =& \text{CSE}_t + p_t^{char} + \max[\overline{\mathcal{R}}_{dischar}.u_t^{dischar}, \\ & \overline{\mathcal{P}}_{dischar}.u_t^{dischar} - p_t^{dischar}] \times \text{PRD} \end{aligned} \tag{4.19}$$

The amount of reserve that LAES provides is the sum of charging power (because it can instantaneously stop charging) and the maximum between up ramp and capacity headroom, multiplied by primary response duration (PRD). The slower ramp-up speed of LAES in comparison with battery ESS is the main reason that it is usually implemented alongside a battery ESS with a low energy capacity. So LAES can store the curtailed RES in high penetration hours, and battery ESS can provide the fast response that is needed in case of any contingency.

The MILP formulation of LAES, that is presented in eq. (4.1) to eq. (4.19) are added to the UC optimization problem in eqs. (2.1a) to (2.1i), to schedule the LAES optimally.

4.4 Results

To point out the differences that the proposed LAES model can make, simulations are carried out for the Tenerife Island power system, with the forecasted data of 2026 and 2030. As the RES input is widely different throughout the year, sample weeks of each season are considered. The scaled amount of demand for 2026 is shown in fig. 4.4, numbers are scaled up for 2030 according to annual energy consumption forecasts. Wind and solar profiles are shown in fig. 4.5 and fig. 4.6 respectively, in per unit of installed capacity. Wind and solar capacities for 2026 and 2030 are in accordance with the most recent estimations of Red Eléctrica de España [86]. Note that the data that is used in this chapter as the input for wind availability, solar availability, and the demand is different from what was used in the previous chapters.

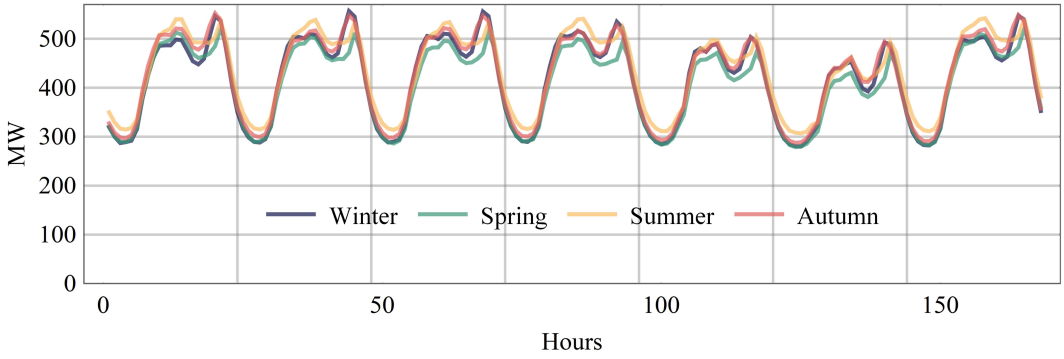

Figure 4.4: Estimated demand of 2026 for a sample week of winter, spring, summer, and autumn.

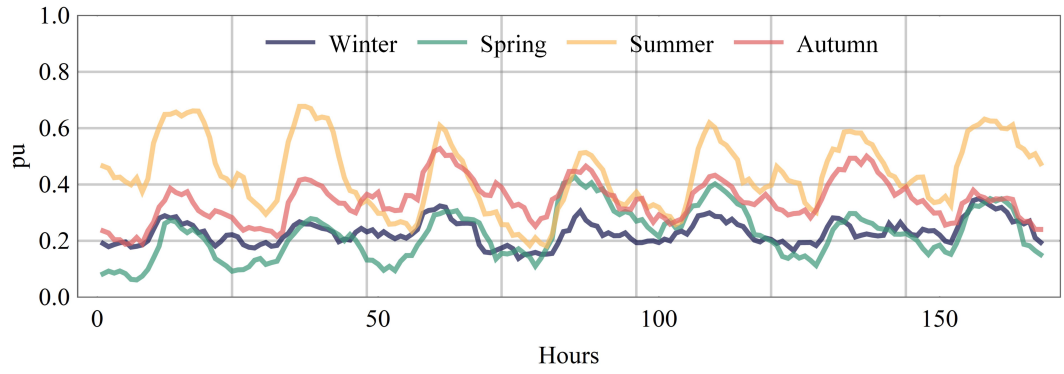

Figure 4.5: Estimated wind generation for sample weeks of winter, spring, summer, and autumn, in per unit.

Considering that the LAES is too slow to provide a significant amount of primary reserve, in practice, it's usually supported by a low-capacity, fast battery ESS. The idea is to perform load shifting and RES storage on high penetration hours with the LAES (because it has a big capacity) and put the low capacity battery ESS on hold for contingencies and moments with up reserve shortage. So in this study, we assume that every LAES is accompanied by a battery ESS as big as the LAES maximum charging capacity. To be able to fully capture the differences that a more

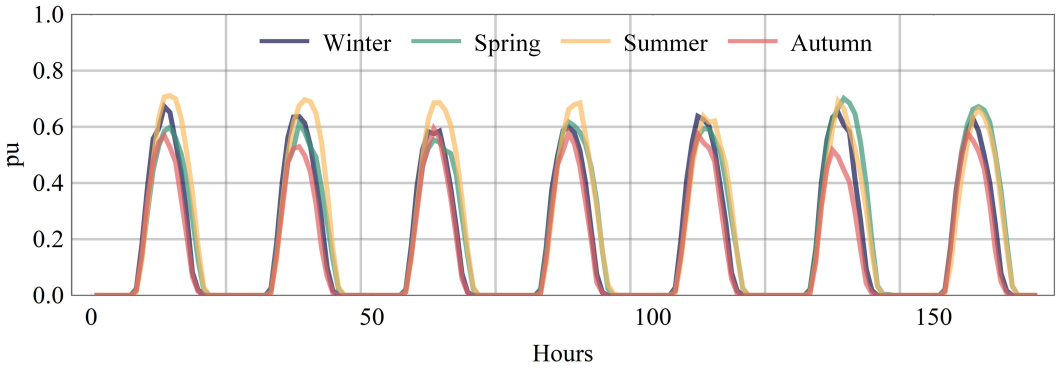

Figure 4.6: Estimated solar generation for sample weeks of winter, spring, summer, and autumn, in per unit.

accurate LAES formulation can make, for each time horizon (different seasons of 2026 and 2030), five scenarios are considered:

No LAES (base case): There is no LAES and no battery ESS in this scenario. It serves as the base case.

50MW LAES, basic model (50MW BM): in this scenario LAES with 50MW/h maximum charging capacity and 300MWh energy capacity is installed in the system, which is supported by a 50MWh energy capacity battery ESS. The battery ESS only provides reserve. The basic LAES model is used in the formulation.

50MW LAES, the proposed model (50MW PM): in this scenario LAES with 50MW/h maximum charging capacity and 300MWh energy capacity is installed in the system, which is supported by a 50MWh energy capacity battery ESS. The battery ESS only provides reserve. The proposed LAES model is used in the formulation.

100MW LAES, basic model (100MW BM): in this scenario LAES with 100MW/h maximum charging capacity and 600MWh energy capacity is installed in the system, which is supported by a 100MWh energy capacity battery ESS. The battery ESS only provides reserve. The basic LAES model is used in the formulation.

100MW LAES, the proposed model (100MW PM): in this scenario LAES with 100MW/h maximum charging capacity and 600MWh energy capacity is installed in the system, which is supported by a 100MWh energy capacity battery ESS. The battery ESS only provides reserve. The proposed LAES model is used in the formulation.

A summary of the input properties used for LAES is presented in table 4.1. How LAES participates in the power balance in different scenarios is shown in fig. 4.7, for a sample week of summer 2030. As expected there is much more curtailed RES when there is no LAES and battery ESS installed. Mainly because more thermal generation is forced to be online to provide the required up reserve. In the middle of the day when there is more solar power injection or windy hours, thermal generation goes down as much as possible, while there is enough headroom to comply with the

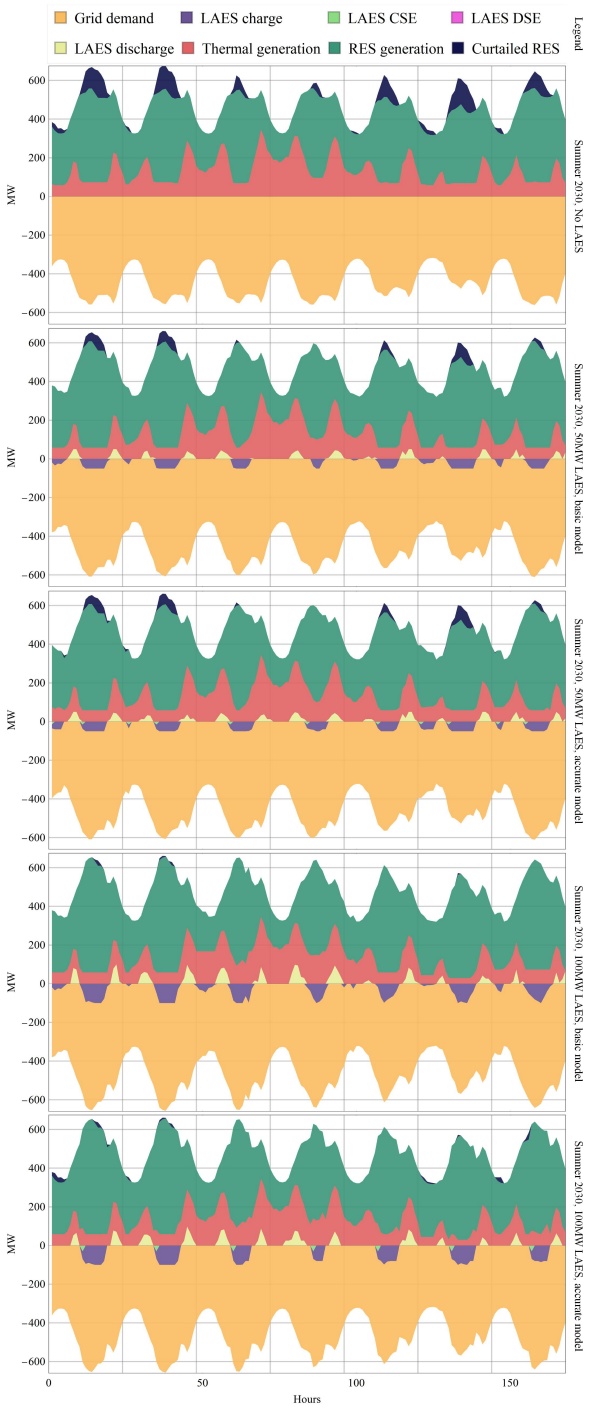

Figure 4.7: Power balance, sample week of summer 2030.

Table 4.1: LAES properties

ξ^{LAES}	55%
CST	30 minutes
DST	$\overline{\mathcal{P}}_{dischar}/5MW$ minutes
CSE	$60\% \times \overline{\mathcal{P}}_{char} \times CST$
DSE	$0.5\% \times \overline{\mathcal{P}}_{dischar} \times DST$
Charge and discharge rundown time	0

reserve criteria. And the rest of the available RES is curtailed. When LAES is added to save extra RES when necessary, and battery ESS is added to provide a reserve, thermal generation can go even lower, to better utilize available RES. 50 MW LAES is able to store some of the extra RES, but still at some hours with so much RES injection there would be curtailment. The main difference between the proposed model and the basic model is the amount of CSE. DSE is also calculated, but the amount is much less than the CSE. Comparing the cases with the proposed model, and cases with the basic model in fig. 4.7, the amount of curtailment in the proposed model seems more. Mainly because CSE and DSE consume extra energy. Also, the number of start-ups in the LAES is reduced with the proposed model, to avoid CSE as much as possible.

To see the differences that the proposed model makes, specifically in the charging and discharging pattern of LAES, the results for a sample summer week of 2030, with 100MW LAES installed, are depicted in fig. 4.8 and fig. 4.9. The DSE is so small that it cannot be seen in the figures. But

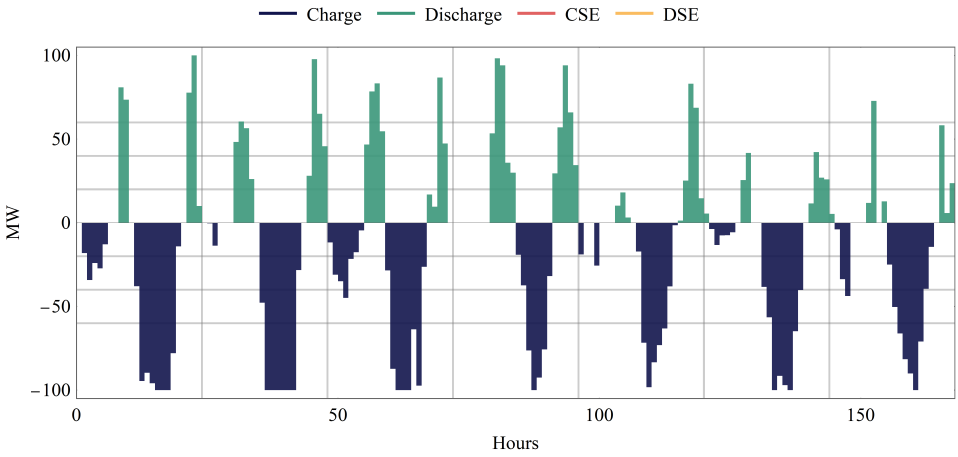

Figure 4.8: LAES charging-discharging, sample week of summer 2030, basic model.

considering CSE can effectively reduce the number of charging incidents to avoid unnecessary CSE as much as possible. Also, there are many hours in the basic model, and LAES is scheduled with a low amount of charging. In practice, the current technology of LAES is usually only able to charge close to maximum capacity (80% of maximum charging capacity of more).

From the weekly UC solutions of winter, spring, summer, and autumn sample weeks, an estimated yearly summary of results for years 2026 and 2030 is presented in tables table 4.2 and table 4.3. Although the operation cost is reduced for cases with storage systems compared to the

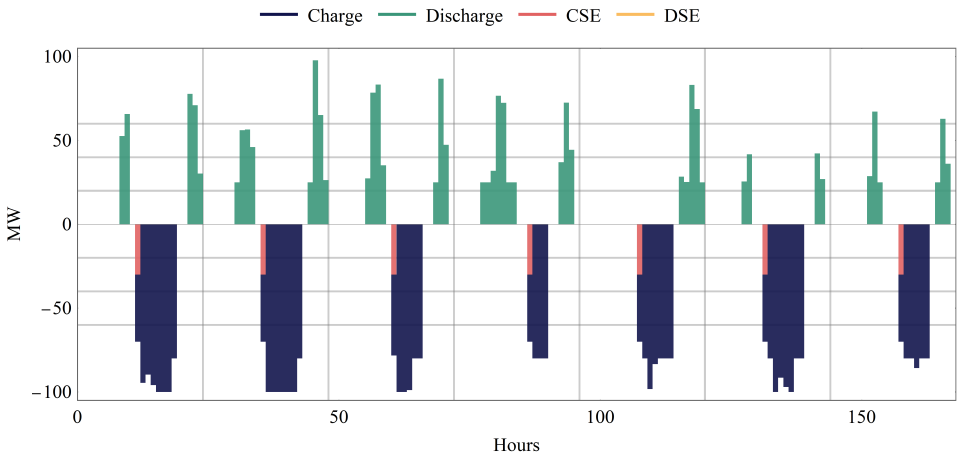

Figure 4.9: LAES charging-discharging, sample week of summer 2030, proposed model.

Table 4.2: Yearly Results of 2026

	operation cost (k€)	scheduled RES (GW)	number of charging	number of discharging
base case	205,600	1,877.3	-	-
50MW BM	181,215	1,898.8	912	847
50MW PM	188,434 (+3.4%)	1,898.7 (0.0%)	508 (-44.3%)	834 (-1.5%)
100MW BM	177,514	1,900.4	847	769
100MW PM	183,413 (+3.3%)	1,900.3 (0.0%)	365 (-56.9%)	730 (-5.1%)

Table 4.3: Yearly Results of 2030

	operation cost (k€)	scheduled RES (GW)	number of charging	number of discharging
base case	192,618	2,127.7	-	-
50MW BM	168,753	2,175.2	939	873
50MW PM	169,130 (+0.2%)	2,174.4 (-0.0%)	560 (-40.4%)	795 (-15.3%)
100MW BM	162,647	2,191.6	847	872
100MW PM	165,001 (+1.4%)	2,188.0 (-0.2%)	469 (-44.6%)	730 (-16.3%)

base case with no storage system, the basic model always underestimates the operation costs. With the detailed model, the operator will have a more accurate power balance schedule, and a better awareness of expected losses. An incremental or decreasing percentage is also provided in both tables, which compare the basic model and the proposed model. According to the tables, the basic model can be misleading in reflecting the realistic operation cost. Also, as the CSE and DSE are taken into account in the proposed model, the number of scheduled charging periods is diminished considerably in the proposed model. It also reduces the wear and tear of LAES in practice. It would also be interesting to see how much CSE consumption is overlooked by the basic model yearly. The corresponding numbers are presented in table 4.4. These yearly amounts might seem small. So for the long-term planning procedures that these orders are negligible, the simple model can be a good choice, as it's less complicated and that might affect the speed of big long-term problems. On the other hand, for short-term scheduling problems, the proposed model can help to avoid unnecessary real-time modifications. All of the UC problems in this chapter are solved by cplex solver in GAMS.

Table 4.4: Overlooked yearly CSE consumption in the basic model

	50MW BM (2026)	100MW BM (2026)	50MW BM (2030)	100MW BM (2030)
Yearly CSE	13,680 MW	25,410 MW	14,085 MW	25,410 MW

4.5 Conclusion

The benefits and ancillary services that LAES provides are manifold and are not limited to cost reduction. But to prevent the overestimation of the operation cost reduction with LAES in the system, a detailed representation of LAES in the UC problem is needed. A detailed model can take other characteristics of LAES, like CSE and DSE into account. This will give a more accurate insight to the operator or the planners. Also with a basic model, LAES will be scheduled to start up too many times, which in reality imposes a lot of charging and discharging start energy. The proposed model gives a realistic awareness of the cost and benefits of LAES, and by considering CSE, automatically prevents unnecessary start-ups to minimize unnecessary energy losses.

5 Robust FCUC Using an ML method

This chapter introduces a data-driven linear constraint to improve the post-disturbance frequency response in island power systems. A coherent initial dataset is obtained by simulating the SFR of single outages. Then logistic regression is employed as a predictive analytic procedure to differentiate the acceptable and unacceptable incidents. Including frequency metrics in the scheduling process can help with the frequency response quality, as it optimizes the resources in hand to prevent outages that might lead to unacceptable frequency responses. Also, the proposed method in this chapter takes the uncertainties of the RES into account. The methodology and findings of this paper are published [87].

Variability and uncertainty are becoming a bigger concern in power systems due to the ever-increasing penetration of RES as a source of power generation. Among power systems, island power systems suffer more as they inherently possess less inertia and primary frequency control capacity. Inertia scarcity in island power systems makes them more susceptible to power outages and fluctuations in uncertain RES. Traditionally, online reserve power provided by conventional units has been the main tool to tackle unforeseen sudden changes in power balance and to maintain the frequency within a tolerable range. The current reserve assignment is such that the N-1 criterion is covered and expected load and RES variations can be absorbed, but it ignores available inertia and system response speed. This practice is falling short as (1) the conventional units are less utilized by increasing the share of RES, (2) the amount of available reserve might not be enough depending on the changes in RES infeed, which is exposed to forecast errors, (3) the system is left with insufficient amount of responsive resources facing outages and forecast errors. It's reasonable to propose a scheduling method that can tackle the uncertainties that the RES is bringing while ensuring the quality of the frequency response after the outages. This is challenging, because both stochastic formulations and frequency constraints are quite complex, and impose a lot of computational burden on the scheduling procedure. This chapter tries to address both of these issues while keeping the size of the UC problem intact.

5.1 Framework

To address the volatile nature of RES and include the stochasticities in the scheduling process, usually stochastic and robust models are employed. Considering the pros and cons of different models, an adaptive robust UC is employed for the purpose of this chapter. Some of the more recent usages and developments in the formulation can be found in [88], [89], [90], and [91]. A robust formulation is employed in this chapter to include the uncertainties of RES. To ensure the provision of sufficient and fast reserves, different solutions are introduced in the literature ([92], [93], [94], [22]). While new sources of the reserve are being introduced, it's also essential to make sure that the quality of frequency transitions is guaranteed in the scheduling process, in case of any abrupt contingency.

Following the higher injection of RES to the grid, larger frequency deviations are expected after any power mismatch. The amount of frequency control that is needed depends on system inertia, generation loss, and the speed of providing reserve. More attention is being paid to this issue. One obstacle is that frequency-related constraints, like frequency nadir, are highly non-linear, so it's hard to implement them in the scheduling process, which is usually solved by mixed-integer linear programming methods. In [95], a linear formulation is introduced that equips the UC problem with information about inertial response and the frequency response of the system and makes sure that in case of the largest outage, there is enough ancillary service to prevent UFLS. To linearize frequency nadir constraint, first-order partial derivatives of its equation with respect to higher-order non-linear variables are calculated. Then the frequency nadir is presented by a set of piecewise linearized constraints. In [96], different frequency services are optimized simultaneously with a stochastic unit commitment (SUC) approach, targeting low inertia systems that have high levels of RES penetration. The stochastic model uses scenario trees, generated by the quintile-based scenario generation method. To linearize frequency nadir, an inner approximation method is used for one side of the equation, and for the other side, a binary expansion is employed and linearized using the big-M technique. In [97], a SUC approach is introduced for low inertia systems, that includes frequency-related constraints. The problem considers both the probability of failure events and wind power uncertainty to compute scenario trees for the two-stage SUC problem. An alternative linearization approach is used to make sure the nadir threshold is not violated. Instead of piece-wise linearizing the whole equation, relevant variables including the nonlinear equation are confined within a plausible range that guarantees frequency drop after any contingency will be acceptable. Reference [98] has proposed a forecasting approach to model the uncertainties of RES to define upper and lower bounds and further implement them in a RUC. This study has assumed that frequency deviation is a linear function of the RoCoF, and has added it as a constraint to the optimal classifier trees (OCT) problem. In [99], a reformulation linearization technique is employed to linearize the frequency nadir limit equation. To address the uncertainties of wind generation, an improved IUC is used. Results show that controlling the dynamic frequency during the scheduling process decreases the operation costs of the system while ensuring its frequency security. In [100], first, a frequency response model is developed that provides enough primary frequency response and system inertia in case of an outage. All frequency dynamic metrics, including the RoCoF and frequency nadir, are obtained from this model, as analytic explicit functions of UC state variables and generation loss. These functions are then linearized based on a pseudo-Boolean theorem, so they can be implemented in linear FCUC problems. To find

the optimal thermal UC and virtual inertia placement, a two-stage chance-constrained stochastic optimization method is introduced in [101]. Frequency nadir is first defined with a bi-linear equation and then it's linearized with the help of the big-M approach. Although these methods are directly obtained from the dynamic equations, they are based on assumptions, and they increase the computational complexity of the UC problem.

In [102], instead of extracting analytical formulas from swing equation, a ML-based method is used. Indeed, a data-driven multivariate OCT technique is used to extract linear frequency constraints. A robust formulation is proposed to address the uncertainties of load and RES. OCT is solved separately as an MILP problem. Because of that, the size of the training dataset should be moderately small, especially for deeper tree structures. A dynamic model is presented in [103] to generate the training data. The generated data is trained by the deep neural network. Trained neural networks are formulated so they can be used in an MILP problem and the frequency nadir predictor is developed, to be used in the UC problem. Then in [104] deep neural network (DNN) is trained by high-fidelity power simulation and reformulated as an MILP set of constraints to be used in UC. The number of constraints and variables that are required for MILP representation of DNN, can be overwhelming and increase the computational complexity of the problem. In [105], a revised support vector machine (SVM) based method is introduced to convexify the frequency nadir constraint. Then based on the method, an FCUC model is formulated as a tractable mixed integer quadratic problem. In [106] the gradient boosting decision tree algorithm is employed to build a frequency response model, which is then added to the UC problem to maintain the frequency within an acceptable range. In the same line of research, this chapter is presenting a data-driven constraint to enhance the frequency response quality after outages. A summary of the reviewed FCUC-related papers are provided in table 5.1. In the next chapter (chapter 6) an analytical approach is compared with a data-driven model and the advantages and disadvantages of both approaches are highlighted.

Analytical formulations for frequency metrics are usually based on simplified models with respect to fully detailed power system models or linearizing the nonlinear behavior of power systems during large active power unbalance and including them methodically in the UC problem To include the non-linear frequency metrics in linear UC, reviewed references are trying to employ a linearization technique. Eventually, the obtained linear lines are always a function of system dynamic constants, available inertia, and the amount of power imbalance. Although this serves the purpose of ensuring the quality of frequency response, it usually increases the size and complexity of the UC problem, in order to reach some level of accuracy. This chapter employs a ML-based method denominated LR as a dichotomous classification approach to classify the post-disturbance frequency drop as acceptable or unacceptable. LR is important in predictive analytics, as it's able to categorize the outcome [107]. Considering the problem at hand and the purpose of this chapter, this approach is promising. In [108], a framework is proposed that removes irrelevant features with no effect on classification and concludes that a training data-set with missing values can still generate sufficient explanations of LR classifications. These characteristics of LR make it an interesting option for FCUC application:

- A linear constraint is derived from LR that can be directly used in the MILP formulation of UC.

Table 5.1: A Summary of FCUC References

#/year	Uncertainty model	linearization technique	Case study
[95]/2018	Deterministic	First-order partial derivatives	Great Britain 2030
[96]/2019	Stochastic	Inner approximation and binary expansion	Great Britain 2030
[97]/2020	Stochastic	Extracting bounds on relevant variables	IEEE RTS-96
[98]/2016	Robust	Assuming nadir is a linear function of RoCoF	Northern Chile
[99]/2020	Improved interval	Reformulation linearization technique	IEEE 6-bus
[100]/2020	Deterministic	Pseudo-Boolean theorem	IEEE RTS-96
[101]/2021	Chance-constrained	Binary expansion	China 196-bus
[102]/2021	Robust	Data-driven optimal classifier trees	Rhodes island and IEEE 118
[103]/2021	Deterministic	DNN trained by dynamic simulation	Modified 33-node system
[104]/2021	Deterministic	DNN trained by high-fidelity generated data	IEEE 39-bus system
[105]/2022	Deterministic	Convexifying by support vector machines	IEEE 24 and 118 bus systems
[106]/2022	Deterministic	Gradient boosting decision tree algorithm	Taipower system in Taiwan

- In practice there are some generator outages that can be tolerated and some others that cannot. This type of dichotomous problem is what LR describes well.
- In contrary to [102], [100], and [104] the obtained constraint from LR does not introduce any additional binary variables to the formulation, making it viable for more computationally demanding methods like robust and stochastic UC.
- Training data with LR is very fast, even for a big number of inputs to better represent the system behavior.
- The LR gives a probabilistic interpretation of the classification. That helps the operator choose the margin of security, depending on the requirements.

All of the reviewed papers are categorized in fig. 5.1.

5.2 Gaps and Contributions

Considering the presented background, this chapter proposes a predictive analytic approach to enhance post-disturbance frequency quality in a robust UC model. The idea is to avoid dispatches that lead to poor frequency responses by scheduling only those generators whose outage would not violate acceptable frequency deviations, thus reducing the potential UFLS.

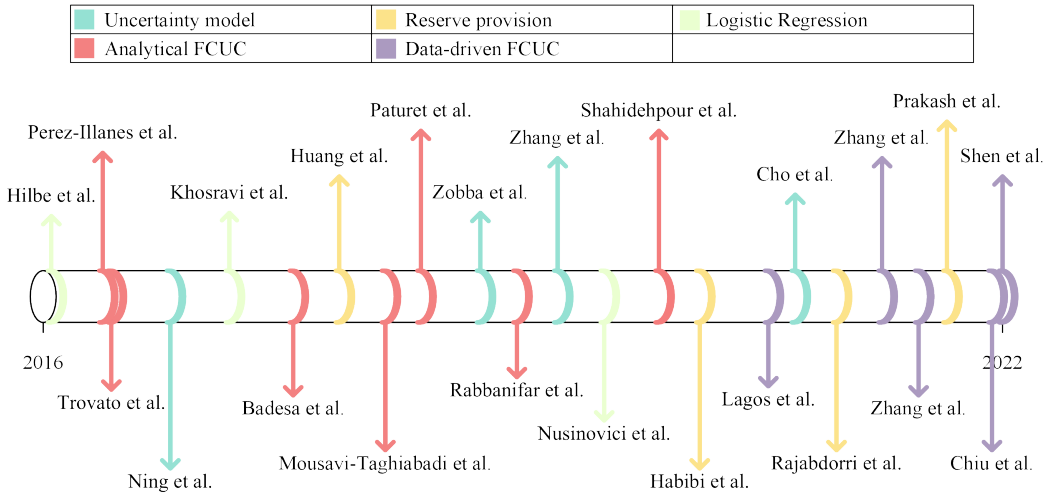

Figure 5.1: Summary of references ([88], [89], [90], [91], [92], [93], [94], [22], [95], [96], [97], [98], [99], [100], [101], [102], [103], [104], [105], [106])

This chapter proposes a novel data-driven constraint, by analyzing a coherent data-set and using a logistic regression procedure. To build an initial set of data to train the LR model, an adaptive robust UC formulation with reserve constraint is employed and solved for different levels of the reserve requirement. The idea of using different levels of the reserve is to simultaneously determine the level that is actually needed. The commitment variables of the robust UC solution for different levels of reserves are used to solve the economic dispatch (ED) problem for day-ahead stochastic scenarios. Every single outage of the obtained results is simulated by an SFR model, which makes the training dataset a proper representative of all acceptable and unacceptable frequency responses. From the training dataset, a new constraint is derived using the logistic regression procedure and then included in robust UC instead of conventional reserve constraint to ensure both frequency quality after outages, and feasibility of the result in case of any realization of the stochastic variable. Although the linearization happens in the training process, the new constraint does not add to the number of constraints in the UC problem, hence keeping the problem size intact. The system operators can use this method to include frequency dynamics in the short-term scheduling process (weekly UC, day-ahead UC, hours-ahead UC, etc.) while keeping the size of the UC problem unaffected. To compare the proposed approach with recent data-driven methods that are introduced in the literature, OCT is also used to train a linear constraint. Both methods are compared in the results and their computational run-time and improvements in the frequency quality are highlighted. To summarize the key contributions and merits compared to the current state of the art, this chapter introduces logistic regression as a tool to train output data of the SFR model and develops a new constraint to be used in UC problems instead of the reserve constraint. The proposed formulation does not add any new binary, integer, or free variables to the UC problem and does not enlarge the number of UC constraints, conserving the size and complexity of the problem. The procedure of training the new constraint is very fast and can be done, using any computer algebra system.

The rest of the chapter is organized as follows. In section 5.3 the required methodology of the proposed approach is presented, starting with the robust UC with reserve constraint in section 5.3.2. Then the SFR model is presented in section 5.3.3, which takes the UC solutions as input. The outputs of the SFR model are used as the training data set for the LR model. How the LR works, and how the LR constraint is obtained are presented in section 5.3.4. The adaptive robust UC formulation with LR can be found section 5.3.5. The results are demonstrated in section 5.4, and conclusions are drawn in section 5.5.

5.3 Methodology

This section presents the methodology. The main argument for using LR is that instead of trying to methodically linearize highly non-linear terms, it is possible to use historic or synthetic data to represent frequency metrics with a line that is a function of system dynamic constants, available inertia, available reserve, and the amount of lost power. Such a procedure does not jeopardize accuracy through linearization and does not introduce unnecessary complexity and computational burden. The methodology is valid for active power unbalances in general, including generation outages. The proposed method tries to distinguish between outages that potentially violate tolerable frequency levels and the ones that do not. This type of problem can be dealt with dichotomous classification approaches like LR. The first step is to build a comprehensive set of data to train an accurate constraint. An adaptive robust UC with reserve constraint is used in this chapter to obtain this dataset, which is explained in section 5.3.1 and section 5.3.2. The UC problem is solved for different levels of the reserve requirement, and ED is solved for all of the stochastic scenarios. The obtained results predominantly picture the possible feasible solutions that might be encountered in real-time. Using these data, dynamic simulations are carried out to see the quality of frequency response in case of all potential outages. To perform the dynamic simulations an SFR model including the UFLS scheme is used (section 5.3.3). As the inputs of the SFR model have different levels of reserve and the amount of inertia is ignored, the simulation results will be a broad-ranging mix of tolerable frequency responses, poor responses, and even unstable cases. Analyzing the correlation between inputs and outputs of the SFR model facilitates the training of the LR model (section 5.3.4), so it can distinguish the tolerable cases and the ones which will lead to poor frequency responses in case of outages. Note that any other power system simulation tool can be used instead of the SFR model. The obtained estimation of the LR model has been further used in an adaptive robust UC formulation as an alternative constraint instead of the current reserve constraint (section 5.3.5). Such formulation is inherently equipped with a constraint that is able to control the quality of frequency response of potential outages.

5.3.1 Fundamentals

A general representation of an MILP can be formulated as follows:

$$\begin{aligned} \min_{x,y(.)} \quad & c^\top x + d^\top y(.), \\ \textbf{s.t.} \quad & Ax \geq b, \\ & Bx + Dy(.) \geq g, \\ & x \geq 0,\ y \geq 0,\ x \in \mathbb{Z},\ y \in \mathbb{R} \end{aligned} \tag{5.1}$$

Being able to solve the problem by using Benders' decomposition is interesting because it can be helpful in solving MILP problems in power systems, when there is a hard-to-satisfy constraint, or when uncertain sources should be addressed. To be able to solve this problem by using the Benders' decomposition approach, eq. (5.1) is reformulated to eq. (5.2) with the help of a value function to obtain a problem only in x and the value function, $f(x)$, contains all other variables as well as the constraints. Reformulation is necessary to correspondingly perform a decomposition.

$$\begin{aligned} \min_{x} \quad & c^\top x + f(x), \\ \textbf{s.t.} \quad & Ax \geq b, \\ & x \geq 0,\ x \in \mathbb{Z} \end{aligned} \tag{5.2}$$

The primal problem is given by,

$$f(x) = \min_{y>0} \{ d^\top y(.) \mid Bx + Dy \geq g,\ y \in \mathbb{R} \} \tag{5.3}$$

Then by using the set of dual variables, θ, the dual formulation can be defined like this:

$$f'(x) = \max_{\theta>0} \{ \theta^\top (g - Bx) \mid D^\top \theta \leq d^\top,\ \theta \in \mathbb{R} \} \tag{5.4}$$

Note that each variable in the primal form corresponds to a constraint in the dual form, and each constraint in the primal form corresponds to a variable in the dual form. A generic method of taking the dual form of a linear program can be found here [109]. As the strong duality suggests, *the dual has an optimal solution if and only if the primal does, and the solutions are equal,* $f(x) = f'(x)$. Considering that the dual formulation, $f'(x)$, is now a maximization, an equivalent form of the (5.2) can be defined here.

$$\begin{aligned} \min_{x} \quad & c^\top x + \phi, \\ \textbf{s.t.} \quad & Ax \geq b, \\ & \phi \geq f'(x) \\ & x \geq 0,\ x \in \mathbb{Z} \end{aligned} \tag{5.5}$$

An interesting property of the dual form in eq. (5.4), is that only the objective function of $f'(x)$ depends on x, thus the feasible region is independent of x. So $f'(x)$ can be described as a set of

extreme points and extreme rays, i.e, $f(x)$ can be described as a set of *dual* extreme points and *dual* extreme rays. Let $\mathcal{O}$ be the complete set of possible extreme points, which lead to optimality cuts, and $\mathcal{F}$ be the complete set of possible extreme rays, which lead to feasibility cuts. Then the outer level (Benders' master problem) can be written as follows,

$$\begin{aligned} \min_{x} \quad & c^\top x + \phi, \\ \mathbf{s.t.} \quad & Ax \geq b, \\ & \phi \geq \hat{\theta}^\top (g - Bx) \;\; \forall \theta \in \mathcal{O} \\ & 0 \geq \hat{\theta}^\top (g - Bx) \;\; \forall \theta \in \mathcal{F} \\ & x \geq 0, \; x \in \mathbb{Z} \end{aligned} \tag{5.6}$$

In practice, an iterative delayed constraint-generating algorithm is used to solve this type of problem. In the inner level (Benders' sub-problem), $f(x)$ or $f'(x)$, are solved using an initial $\hat{x}$, to generate optimality or feasibility cuts. Then the next iteration (5) is solved using all the extreme points($\mathcal{O}'$) or extreme rays($\mathcal{F}'$) that are generated by the inner level in previous iterations. Note that in a modern linear programming solver, solving the primal form of $f(x)$ is sufficient because the solver provides the dual values associated with every constraint.

In theory, if the sub-problem corresponding to the $\hat{x}$ ($f'(\hat{x})$), is feasible, an optimality cut should be generated. And if the sub-problem corresponding to the $\hat{x}$ is infeasible, $f'(\hat{x})$ is unbounded and a feasibility cut should be generated. An issue in the implementation of the iterative process is that there should be an upper limit on $f'(\hat{x})$, to prevent it from going unbounded and causing an error on the solver, which complicates the detection of feasibility cuts. For optimality cuts, the violation of a cut has a natural interpretation; it's the amount by which the variable $\hat{\phi}(x, \hat{\theta})$, contributes to the objective function. As such, for optimality cuts, we use the regular optimality tolerance used by the solver. For feasibility cuts, there is no such interpretation, and any scaling of feasibility cuts is arbitrary. Therefore, we consider a master solution $(\hat{x}, \hat{\phi})$ to be violated if and only if the corresponding cut-generating sub-problem is infeasible (according to the feasibility tolerances) regardless of whether the feasibility cut is violated enough or not [110]. So there needs to be a big enough upper limit on $f'(\hat{x})$, and whenever the sub-problem reaches the upper limit, a feasibility cut will be generated and added to $\mathcal{F}'$.

The auxiliary variable ϕ is an understimator of the optimal sub-problem objective value, so it is always less than the optimal value of the sub-problem in every iteration. When ϕ gets sufficiently close to the optimal value of the sub-problem, it can be assumed that the problem is converged, and an optimal solution is obtained.

5.3.2 Adaptive Robust UC with Reserve Constraint

The UC problem is a mixed-integer problem and is usually solved with MILP solvers after the linearization of nonlinear terms. To solve the UC problem with uncertainty, an adaptive robust formulation is employed in [111] and [112]. The formulation is robust, because it considers all of the possible realizations of the uncertain input, and makes sure that the chosen commitment status of the units, which is decided at the master level, will be feasible for any realization of the uncertain variable. The formulation is adaptive because the subproblem level is a function of the

uncertain variables and can adapt the master level decision variable, depending on the different realizations of the uncertain variable. A general representation of the UC problem with reserve constraint and uncertain wind power injection is provided in the following. It's similar to eq. (2.1) in some aspects, but the stochastic variables and the dual variables of each constraint are also highlighted here.

$$\min_{u,p(\omega)} \; suc(u_{t,i}) + gc(p_{i,t}) \tag{5.7}$$

$$u_{t,i} - u_{t-1,i} = v_{t,i} - w_{t,i} \qquad t \in \mathcal{T},\ i \in \mathcal{I} \tag{5.7a}$$

$$v_{i,t} + w_{i,t} \leq 1 \qquad t \in \mathcal{T},\ i \in \mathcal{I} \tag{5.7b}$$

$$\sum_{tt=t-UT_i+1}^{t} v_{tt,i} \leq u_{t,i} \qquad t \in \{UT_i, \ldots, T\} \tag{5.7c}$$

$$\sum_{tt=t-DT_i+1}^{t} w_{tt,i} \leq 1 - u_{t,i} \qquad t \in \{UT_i, \ldots, T\} \tag{5.7d}$$

$$p(\omega)_{t,i} \geq \underline{\mathcal{P}_i}.u_{t,i} \qquad t \in \mathcal{T},\ i \in \mathcal{I},\ \omega \in \Omega\ , \alpha \tag{5.7e}$$

$$p(\omega)_{t,i} + r(\omega)_{t,i} \leq \overline{\mathcal{P}_i}.u_{t,i} \qquad t \in \mathcal{T},\ i \in \mathcal{I},\ \omega \in \Omega,\ \beta \tag{5.7f}$$

$$p(\omega)_{t-1,i} - p(\omega)_{t,i} \leq \underline{\mathcal{R}_i} \qquad t \in \mathcal{T},\ i \in \mathcal{I},\ \omega \in \Omega,\ \gamma \tag{5.7g}$$

$$p(\omega)_{t,i} - p(\omega)_{t-1,i} \leq \overline{\mathcal{R}_i} \qquad t \in \mathcal{T},\ i \in \mathcal{I},\ \omega \in \Omega,\ \delta \tag{5.7h}$$

$$\sum^{i \in \mathcal{I}} \left(p(\omega)_{t,i}\right) + wg(\omega)_t = \mathcal{D}_t \qquad t \in \mathcal{T},\ \omega \in \Omega,\ \zeta \tag{5.7i}$$

$$wg(\omega)_t \leq \omega_t \qquad t \in \mathcal{T},\ \omega \in \Omega\ , \eta \tag{5.7j}$$

$$\sum_{ii \neq i}^{ii \in \mathcal{I}} \left(\overline{\mathcal{P}_i} - p(\omega)_{t,ii}\right) \geq p(\omega)_{t,i} \qquad t \in \mathcal{T}, i \in \mathcal{I}, \omega \in \Omega, \mu \tag{5.7k}$$

Just to restate, $suc(.)$ and $gc(.)$ are the start-up and generation cost functions in euros, respectively. u, v, and w are binary variables of commitment, start-up, and shut-down, respectively. $p(.)$ and r are the generation and reserve power variables in megawatts, respectively. t is the index for time intervals. i is the index of generators. $\overline{\mathcal{P}}$ and $\underline{\mathcal{P}}$ are maximum and minimum power output of generators, respectively. $\overline{\mathcal{R}}$ and $\underline{\mathcal{R}}$ are ramp-up and ramp-down limitation of generators, respectively. $\mathcal{D}$ is the demand. The aim is to solve eq. (5.7) subject to eq. (5.7a) to eq. (5.7d), which only depends on binary variables, and eq. (5.7e)-eq. (5.7k), which depend on both binary and real variables. $gc(.)$ is usually a quadratic cost function, which will be piecewise linearized to be utilized in a MILP problem. Equation (5.7a) and eq. (5.7b) represent the binary logic of the UC problem. Equation (5.7c) and Equation (5.7d) are the minimum up-time and minimum down-time constraints of the units. Equation (5.7e) is the minimum power generation constraint, with dual multiplier α. Equation (5.7f) is the maximum power generation constraint with dual multiplier β and states that the summation of power generation and power reserve of every online unit, should be less than the maximum output of the unit. Equation (5.7g) and eq. (5.7h) are ramp-down and ramp-up constraints, with dual multipliers γ and δ respectively. Equation (5.7i) is the power balance equation with dual multiplier ζ. Equation (5.7j) with the dual multiplier, η makes

sure that the scheduled wind power is always equal to or less than the uncertain forecasted wind. Equation (5.7k) is the current reserve constraint with dual multiplier μ and makes sure that in case of any contingency, there is enough headroom to compensate for the lost generation. These dual variables will be later used when the dual form of the problem is defined.

Note that all the decision variables from eq. (5.7e) to eq. (5.7k) are a function of uncertain wind power realization. In practice, an iterative delayed constraint generating Benders' decomposition algorithm is used to solve this problem [113]. The problem is broken to a master problem minimization subjected to eq. (5.7a) to eq. (5.7d), and a subproblem with max-min form subjected to eq. (5.7e) to eq. (5.7k).

$$\min_{u} \Big(suc(u_{t,i}) + \max_{\omega \in \Omega} \min_{p} gc(p_{i,t}) \Big) \tag{5.8}$$

The minimization on the master level is subjected to eq. (5.7a) to eq. (5.7d), and the subproblem level minimization is subjected to eq. (5.7e) to eq. (5.7k). The subproblem minimization problem determines the ED cost for a fixed commitment $\hat{u}$, and then it's maximized over the uncertainty set Ω. Here the concept of duality in linear problems can be used. As the strong duality suggests, *the dual has an optimal solution if and only if the primal does, and the solutions are equal*. Taking the dual of subproblem converts the max-min form into a maximization problem. Considering the decomposed form of the problem, the feasible region of subproblem maximization is independent of u. So the subproblem maximization can be described as a set of extreme points and extreme rays of the solution region. Let $\mathcal{O}$ be the complete set of possible extreme points, and $\mathcal{F}$ be the complete set of possible extreme rays. These properties will later be used to define the decomposed master problem. In the iterative solution process, the binary variable, $\hat{u}_{t,i}$, is obtained from the masters' problem, hence it's fixed. With that in mind, and defining the auxiliary variable ϕ, as an understimator of optimal subproblem objective value, the dual form of the subproblem is defined as follows,

$$\phi \geq \max_{p} \begin{pmatrix} \sum_{t\in\mathcal{T}} \sum_{i\in\mathcal{I}} \alpha_{t,i} (\underline{\mathcal{P}}_i . \hat{u}_{t,i}) \\ - \sum_{t\in\mathcal{T}} \sum_{i\in\mathcal{I}} \beta_{t,i} (\overline{\mathcal{P}}_i . \hat{u}_{t,i}) \\ - \sum_{t\in\mathcal{T}} \sum_{i\in\mathcal{I}} (\gamma_{t,i} . \underline{\mathcal{R}}_i + \delta_{t,i} . \overline{\mathcal{R}}_i) \\ - \sum_{t\in\mathcal{T}} (\zeta_t . \mathcal{D}_t + \eta_t . \omega_t) \\ - \sum_{t\in\mathcal{T}} \sum_{i\in\mathcal{I}} \mu_{t,i} \Big(\sum_{ii\neq i}^{ii\in\mathcal{I}} (\overline{\mathcal{P}}_i . \hat{u}_{t,i}) \Big) \end{pmatrix} \tag{5.9}$$

$$C_i - \alpha_{t,i} + \beta_{t,i} + \gamma_{t,i} + \delta_{t,i} + \zeta_t + \eta_t + \sum_{ii}^{ii\in\mathcal{I}} \mu_{t,ii} \geq 0 \quad t \in \mathcal{T},\ i \in \mathcal{I} \tag{5.9a}$$

$$\zeta_t + \eta_t \geq 0 \quad t \in \mathcal{T} \tag{5.9b}$$

$$\alpha, \beta, \gamma, \delta, \eta, \mu \geq 0 \text{ and } \zeta \text{ is free} \tag{5.9c}$$

The dual form is eq. (5.9) subject to eq. (5.9a) to eq. (5.9c). ζ is a free variable, because eq. (5.7i) is an equality. To find out more about writing a standard form of a problem, and taking the dual, have a look at [109]. The dual variables of each constraint in eq. (5.7) have appeared in the dual form. In the maximization objective function in eq. (5.9), all the terms are linear, except the term $\eta_t \omega_t$, which is nonlinear because a dual variable (η) is multiplied by the stochastic variable (ω). An outer approximation approach from [114] is employed to cope with this nonlinearity. The objective function of the dual subproblem is a function of all dual variables and fixed $\hat{u}_{t,i}$ from the master problem in the previous iteration. Let's define the set of dual variables as Γ and the dual objective solution as $f(\hat{u}_{t,i}, \hat{\Gamma})$. Then the master problem is defined as follows,

$$\begin{aligned} \min_{u} \quad & suc(u_{t,i}) + \phi, \\ \textbf{s.t.} \quad & (5.7a) \text{ to } (5.7d), \\ & \phi \geq f(\hat{u}_{t,i}, \hat{\Gamma}) \quad \forall \Gamma \in \mathcal{O} \\ & 0 \geq f(\hat{u}_{t,i}, \hat{\Gamma}) \quad \forall \Gamma \in \mathcal{F} \end{aligned} \tag{5.10}$$

The iterative solution process starts with empty sets of $\mathcal{O}$ and $\mathcal{F}$. Then if the subproblem solution corresponding to $\hat{u}_{t,i}$ ($f(\hat{u}_{t,i}, \hat{\Gamma})$), is feasible, an optimality cut is generated and added to $\mathcal{O}'$. And if the subproblem solution corresponding to the $\hat{u}_{t,i}$ is infeasible, $f(\hat{u}_{t,i}, \hat{\Gamma})$ is unbounded and a feasibility cut is generated and added to $\mathcal{F}'$. The iterations continue until ϕ is converged enough. The iterative algorithm is presented in algorithm 1. The UC problem is solved for different levels of the reserve requirement. The optimal commitment variables are then used to solve the ED problem for various stochastic wind scenarios to build an initial dataset, which will be implemented in the SFR model.

Algorithm 1 Iterative UC with reserve

Input: System specifications, wind uncertainty set, power demand
Output: ϵ-optimal solution

1: $j = 0$
2: **while** $|\phi^j(\hat{u}^j_{t,i}, \hat{\Gamma}^j) - \phi^j(\hat{u}^j_{t,i}, \hat{\Gamma}^{j-1})| < \epsilon$ **do**
3: Solve master, minimizing $suc(u^j_{t,i}) + \phi^j(u^j_{t,i}, \hat{\Gamma}^{j-1})$ to get $\hat{u}^j_{t,i}$
4: Solve subproblem using outer approximation, maximizing $f(\hat{u}^j_{t,i}, \Gamma^j)$ to get $\hat{\Gamma}^j$
5: If $f(\hat{u}^j_{t,i}, \hat{\Gamma}^j)$ is bounded $\rightarrow \mathcal{O}' \cup \{\hat{\Gamma}_j\}$
6: If $f(\hat{u}^j_{t,i}, \hat{\Gamma}^j)$ is unbounded $\rightarrow \mathcal{F}' \cup \{\hat{\Gamma}_j\}$
7: $j = j + 1$
8: **end while**

5.3.3 SFR Model

The SFR model is previously explained in section 3.2.1 and fig. 3.2. Since frequency can be considered uniform, equivalent normalized system inertia $\widetilde{\mathcal{H}}$ can be defined as follows,

$$\widetilde{\mathcal{H}}_t = \sum^{i\in\mathcal{I}} \frac{\mathcal{H}_i \mathcal{M}_i^{base} u_{t,i}}{\mathcal{S}^{base}} \tag{5.11}$$

Where $\mathcal{M}$ and $\mathcal{S}$ are base power of the units and base power of the system in megawatts, respectively. Some details are mentioned in section 3.2.1 and the complete model is explained in [1].

In practice, the UFLS scheme is designed to stabilize the system after large outages. For the purpose of building a data set to train the LR model, the UFLS scheme should be deactivated so the results capture the free frequency responses, including the ones that lead to instability or unacceptable low-frequency nadir and steady-state frequency. Note however that the UFLS scheme will be considered to obtain the expected amount of UFLS when comparing the new reserve constraints with the conventional one in section 5.4.

5.3.4 Logistic Regression

Regression methods are used for data analysis, concerned with describing the relationship between a response variable and one or more explanatory variables. Sometimes the output variable needs to be discrete, taking one or more possible values. In these instances, logistic regression is usually used. Consider a collection of m independent variables denoted by the vector $\xi^{'} = (\xi_1, \xi_2, \ldots, \xi_m)$ related to a dichotomous dependent variable υ, where υ is typically labeled as 1 or 0 for its two possible categories. Considering that for a $(0, 1)$ random variable, the expected value of υ is equal to the probability of $\upsilon = 1$ (i.e., $\pi(\upsilon = 1)$), and is defined here,

$$\pi(\upsilon = 1) = \frac{1}{1 + e^{-(c_0 + c_1\xi_1 + c_2\xi_2 + \cdots + c_m\xi_m)}} \tag{5.12}$$

The regression coefficients c_0 to c_m in the logistic model eq. (5.12) provide important information about the relationships of the independent variables in the model to the dichotomous dependent variable. For the logistic model, these coefficients are used to estimate the odds ratio. Odds are defined as the ratio of the probability that some event will occur divided by the probability that the same event will not occur. Thus the odds for the event $\upsilon = 1$ is,

$$odds(\upsilon = 1) = \frac{\pi(\upsilon = 1)}{1 - \pi(\upsilon = 1)} \tag{5.13}$$

Generally the conditional probability that the outcome presents is denoted by $\pi(\upsilon)$. The logit transformation of the probability $\pi(\upsilon = 1)$ is defined as natural logarithm of the odds of event $\upsilon = 1$, and considering eq. (5.12) is defined as,

$$\begin{aligned} logit\big(\pi(\upsilon = 1)\big) &= ln\Big(\frac{\pi(\upsilon = 1)}{1 - \pi(\upsilon = 1)}\Big) \\ &= c_0 + c_1\xi_1 + c_2\xi_2 + \cdots + c_m\xi_m \end{aligned} \tag{5.14}$$

This is the *logit form* of the model and is given by a linear function [115]. The logit transformation is primarily applied to convert a variable that is bounded by 0 and 1 (i.e., probabilities) to a variable with no bounds [116]. When $logit\big(\pi(\upsilon = 1)\big)$ goes toward $+\infty$, the probability of event $\upsilon = 1$ gets closer to 1, and when $logit\big(\pi(\upsilon = 1)\big)$ goes toward $-\infty$, the probability of event $\upsilon = 1$ gets closer to 0. Usually $logit\big(\pi(\upsilon = 1)\big) = 0$ is considered as a cut-point, that separates those events with the probability of more than 0.5 on the positive side, and those events with the probability of less than 0.5 on the negative side. Depending on the required accuracy for the model, different cut-points can be chosen.

As the frequency response of the system after contingencies is highly nonlinear, different approaches are employed in the literature to somehow linearize and include them in the UC problem. Some of these approaches are mathematically complicated and often tremendously burdensome for the solver. The argument here is that instead of linearizing the complex nonlinear equations, the output of developed SFR models can be analyzed to drive a linear constraint. To do so, the frequency response after each contingency can be marked as acceptable or unacceptable, depending on whether it violates the predefined limits or not. Then logistic regression is employed here to analyze the data and separate acceptable and unacceptable results with a trained line. This line is added later to the UC problem as a constraint by replacing the current reserve constraint eq. (5.7k). Such constraint can improve the frequency response quality and reduce the amount of load shedding due to unexpected outages, as it takes into account the expected dynamic behavior of the system.

As it's going to be further discussed in the results section, a training dataset consisting of either synthetic or historic UC solutions is created to train the LR model. The independent variables of the LR model are assigned for every possible generator outage n in the training dataset. The independent variables that are defined should have a good correlation with the frequency response metrics after outage n. In this chapter, the defined independent variables are the weighted summation of online inertia ($\xi_{1,n}$), the summation of inverse droop of the online units ($\xi_{2,n}$), lost power ($\xi_{3,n}$), lost power divided by the corresponding demand of that hour ($\xi_{4,n}$), and remaining of the reserve power after generator outages ($\xi_{5,n}$). Then every possible generator outage n in the training dataset is simulated with the SFR model to obtain a frequency response for each outage. Depending on the results of the SFR model, outage n will be tagged as 1 (acceptable) if the frequency response is within tolerable boundaries or 0 (unacceptable) if it's not. These binary tags will be employed as dependent variables of each outage for the LR model (υ_n). Now that both independent and dependent variables of the LR model are formed, the training process can be performed to obtain coefficients c_0 to c_5. The process is shown in fig. 5.2 and explained again later in the results section for the case study. The general form of the trained constraint estimated by the LR model is presented as follows,

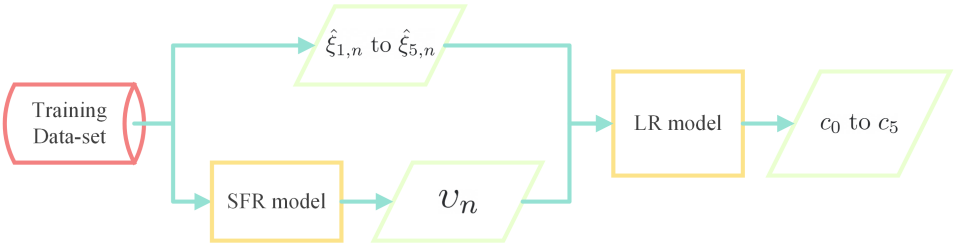

Figure 5.2: Flowchart of calculating logistic regression coefficients.

$$
\begin{aligned}
& c_0 + c_1\Big(\sum_{ii\neq i}^{ii\in\mathcal{I}} \mathcal{H}_{ii}\mathcal{M}_{ii}^{base}u_{t,ii}\Big)+ \\
& c_2\Big(\sum_{ii\neq i}^{ii\in\mathcal{I}} \mathcal{K}_{ii}u_{t,ii}\Big) + c_3 p_{t,i} + \frac{c_4}{\mathcal{D}_t}p_{t,i}+ \\
& c_5\Big(\sum_{ii\neq i}^{ii\in\mathcal{I}} (\overline{\mathcal{P}}_{ii}u_{t,ii} - p_{t,ii})\Big) \geq \psi \quad t\in\mathcal{T},\ i\in\mathcal{I},\ \rho
\end{aligned}
\tag{5.15}
$$

Where $\mathcal{K}$ is the normalized gain of the turbine-governor model and ψ is the regression cut-point. Setting the value of the cut-point to ψ classifies the events with the probability of more than $e^{\psi}/(1+e^{\psi})$ in one class and the rest of the events in another class. For example, $\psi = 0$ classifies the events with the probability of more than 0.5 on one side, and the rest on the other side. This constraint (eq. (5.15)) enables the UC problem to also take into account the inertia and time constants of the system. The purpose is to improve the quality of frequency response with these measures. To obtain c_0 to c_5, the size and coherency of the training set should be good enough to describe the system. Although a small training data set can be classified with high precision, it might be insufficient to reflect the behavior of the system. Figure 5.3 shows a hypothetical example of the distribution of two variables. According to the distribution in fig. 5.3.A all the lines, L1 to L3, can perfectly separate the two variables. But with a bigger size distribution sample, fig. 5.3.B shows that L2 is a better candidate.

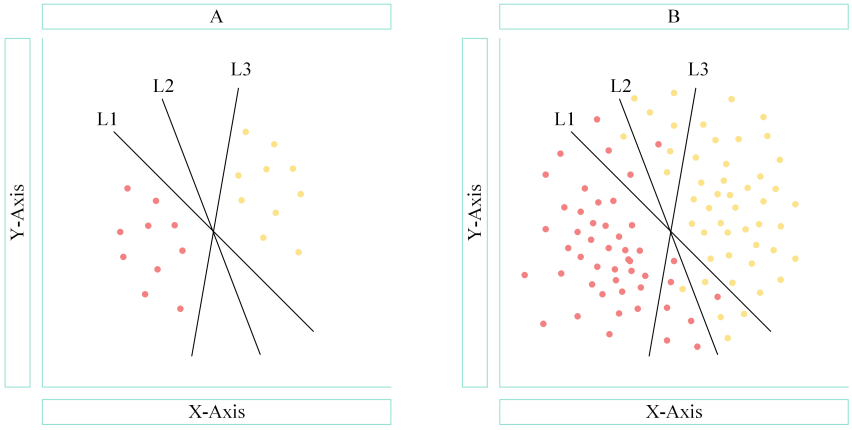

Figure 5.3: A hypothetical example to show the importance of the size of the training data set

5.3.5 Adaptive Robust UC with LR constraint

The general formulation is similar to eq. (5.7), but reserve constraint in eq. (5.7k) is replaced by the LR constraint in eq. (5.15). The subproblem dual with the new constraint will become as follows,

$$\phi \geq \max_{p} \left(\begin{array}{l} \sum_{t\in\mathcal{T}} \sum_{i\in\mathcal{I}} \alpha_{t,i}(\underline{\mathcal{P}}_i.\hat{u}_{t,i}) \\ -\sum_{t\in\mathcal{T}} \sum_{i\in\mathcal{I}} \beta_{t,i}(\overline{\mathcal{P}}_i.\hat{u}_{t,i}) \\ -\sum_{t\in\mathcal{T}} \sum_{i\in\mathcal{I}} (\gamma_{t,i}.\underline{\mathcal{R}}_i + \delta_{t,i}.\overline{\mathcal{R}}_i) \\ -\sum_{t\in\mathcal{T}} (\zeta_t.\mathcal{D}_t + \eta_t.\omega_t) \\ -\sum_{t\in\mathcal{T}} \sum_{i\in\mathcal{I}} \rho_{t,i}\Big(c_0 \\ \quad + c_1\big(\sum_{ii\in\mathcal{I}, ii\neq i} \mathcal{H}_{ii}\mathcal{M}^{base}_{ii}\hat{u}_{t,ii}\big) \\ \quad + c_2\big(\sum_{ii\in\mathcal{I}, ii\neq i} \mathcal{K}_{ii}\hat{u}_{t,ii}\big) \\ \quad + c_5\big(\sum_{ii\in\mathcal{I}, ii\neq i} (\overline{\mathcal{P}}_{ii}\hat{u}_{t,ii})\big) - \psi\Big) \end{array} \right) \tag{5.16}$$

$$C_i - \alpha_{t,i} + \beta_{t,i} + \gamma_{t,i} + \delta_{t,i} + \zeta_t + \eta_t + (c_3 + \frac{c_4}{\mathcal{D}_t})\rho_{t,i} + c_5 \sum_{ii\in\mathcal{I}, ii\neq i} \rho_{t,ii} \geq 0 \quad t \in \mathcal{T},\ i \in \mathcal{I} \tag{5.16a}$$

$$\zeta_t + \eta_t \geq 0 \quad t \in \mathcal{T} \tag{5.16b}$$

$$\alpha, \beta, \gamma, \delta, \eta, \rho \geq 0 \text{ and } \zeta \text{ is free} \tag{5.16c}$$

Where C is the cost coefficient of the generators. As the objective function in the primal form and all the constraints that only involve binary variables are the same, the master problem remains the same as section 5.3.2. Considering that the eq. (5.15) is added to the formulation in eq. (5.7), the dual form of the subproblem should be adjusted accordingly. Which eventually will have the form of eq. (5.16), subjected to eqs. (5.16a) to (5.16c). The iterative solution procedure here is the same as algorithm 1. A flowchart of the different steps of the proposed method is presented in fig. 5.4.

5.4 Results

5.4.1 Case study and inputs

Simulations for the proposed methodology are carried out on the real power system of La Palma island, one of Spain's Canary Islands. The yearly demand in 2018 is reported as about 277.8 GWh (average hourly demand of 31.7 MWh), supplied by eleven Diesel generators predominantly. According to [117], the installed capacity of the La Palma island power system mounts to 117.7 MW, where about 6% of the installed capacity belongs to wind power generation. RES covers about 10% of the yearly demand. The capacity of the generators is shown in table 2.1. The input data for solving the UC problem is obtained from real data. Different scenarios of forecasted wind generation data of a sample day are chosen, which also provide the upper bound and the lower bound of the wind availability for the robust formulation. Wind data with 10 scenarios is shown in fig. 5.5. The scenarios are from [118] and are scaled for La Palma island installed wind capacity.

An initial data set is required to train the LR model. The training data set should be able to represent the system, even in extreme circumstances, so it should include incidents with bad and unstable frequency responses too. Here it's decided to consider different reserve levels and different probable wind scenarios, to provide a wide range of plausible data to train the LR model, so it can reliably distinguish acceptable and unacceptable results. To achieve such a training data set, the conventional day-ahead robust UC is solved for ascending reserve requirements levels, starting from zero requirements until the problem becomes infeasible. By doing so a wide range of plausible UC solutions will be obtained, including generator outages that lead to tolerable frequency responses, poor frequency responses, and even unstable responses. In the conventional UC, the reserve requirement is typically the largest generation source under moderate RES penetration. A multiplier is defined here for the reserve requirement starting from 0, with 0.1 ascending steps, until 1.5, which is the point that the problem becomes infeasible in this case. The OCT commitment schedule and the corresponding frequency response of every single outage for a sample hour are shown in fig. 5.6, for minimum reserve level (reserve level multiplier= 0) and maximum feasible reserve level (reserve level multiplier= 1.4). As it can be seen in fig. 5.6 when the reserve requirement is low, fewer units are committed but in case of any outage, the frequency response becomes unstable. On the other hand, when the reserve requirement is high, the number of online units is more and they have more headroom. In this case, if a unit goes out, the frequency response is good. Then the ED is solved for 10 probable wind scenarios, using the robust UC

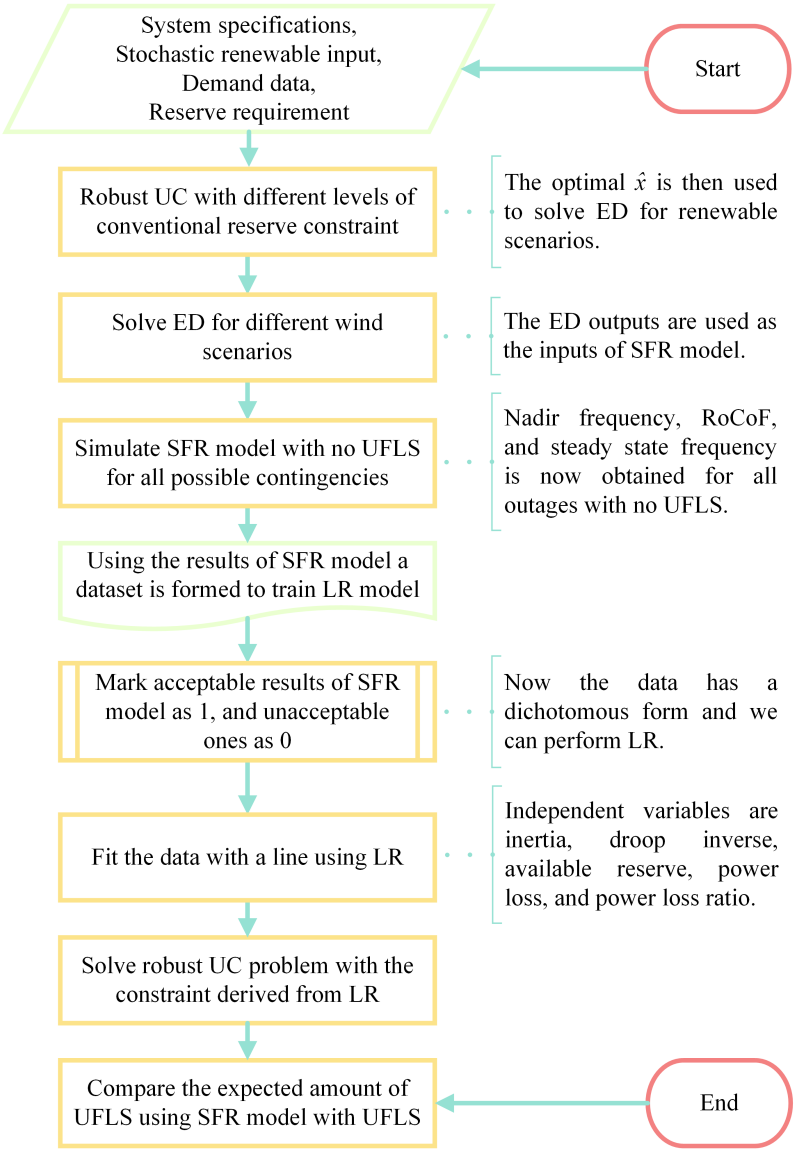

Figure 5.4: Flowchart of the proposed method.

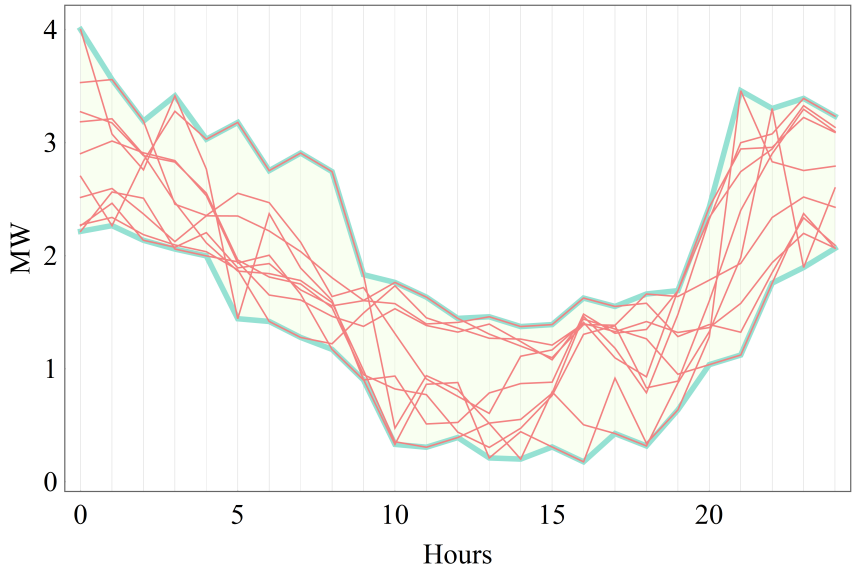

Figure 5.5: Wind data uncertainty set

solution for each reserve requirement level. At this stage, independent variables for the LR model can be picked up from ED results. Every possible generator outage n in the obtained ED solution is simulated with the SFR model, resulting in the corresponding frequency responses, to form the LR training data set. Considering the solved hourly RUC and then for each of them hourly EDs of 10 wind scenarios, there will be around 20000 possible single outages in total (every possible outage in every hour), building up the diverse training data set. The first OCT with a reserve level of zero is very fast. The corresponding ED problem receives fixed binary values from OCT, hence it's a linear problem with no integer values involved, so it's also very fast even when the quadratic cost function is used. As all the wind scenarios (fig. 5.5) are within the upper bound and lower bound of the OCT, it's certain that the ED for any scenario is feasible. To reduce solution time for higher levels of the reserve, the lower bound of the objective function can be set as the objective function of the previous level and a feasible binary solution can be attained from the previous level to give the current level a warm start. Obtained results confirm that other system characteristics, like online inertia, lost power, lost power percentage, and the droop of the turbine-governor system are more correlated with the quality of the frequency response, compared to the amount of reserve. The reason is that in systems with low inertia (like islands) frequency drops so fast after outages that the UFLS scheme is activated, although there is enough headroom in the remaining units (enough reserve). Table 5.2 shows Pearson's correlation between mentioned characteristics and frequency response metrics, around 20000 single outages that are simulated by the SFR model. For our case study, the whole process of building up the training data set and carrying out the dynamic simulations takes around 1 hour. The SFR simulations are done by MATLAB Simulink. As expected, the ratio of lost generation to hourly demand has the best correlation with frequency metrics, as the big outages relative to the whole generation tend to disturb frequency considerably. Interestingly enough, the sum of the available reserves has a weaker correlation with frequency metrics, compared to the others. Meaning that fulfilling reserve criteria do not guar-

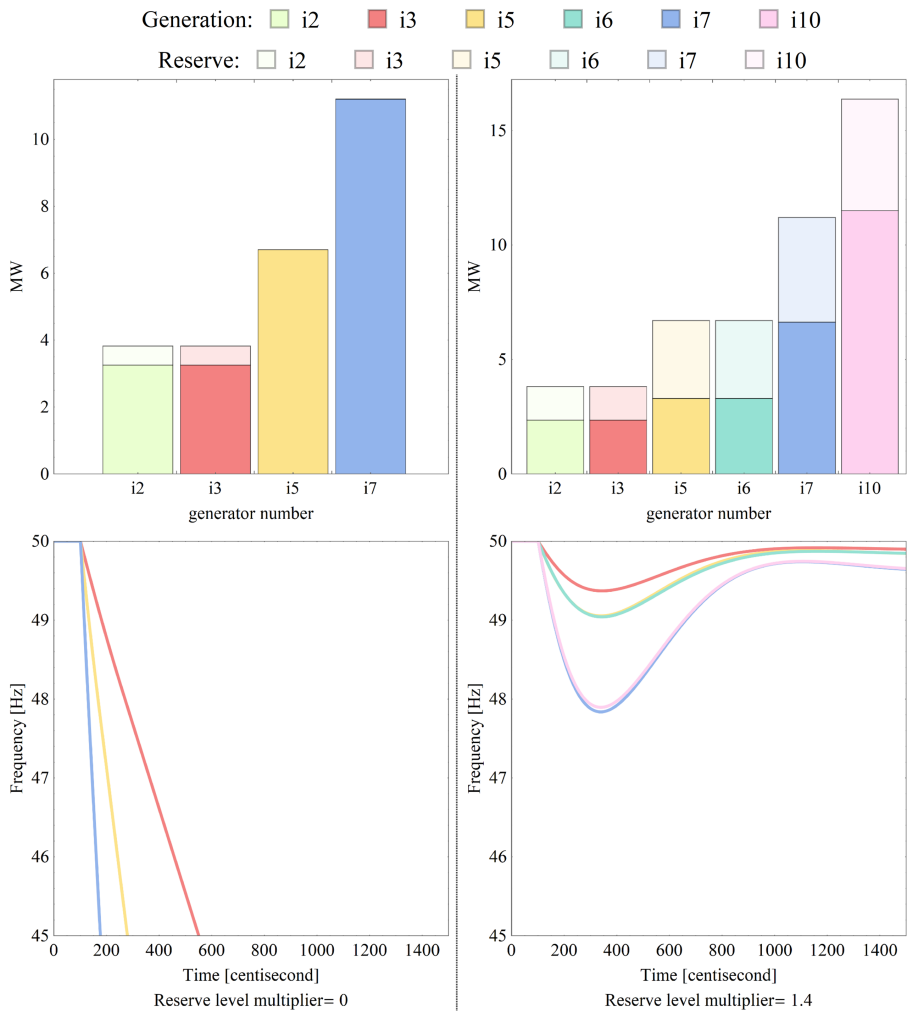

Figure 5.6: Schedule generation and reserve for different reserve levels and their corresponding frequency response after single outages for a sample hour

Table 5.2: Pearson's correlation between parameters

	f^{nadir}	f^{qss}	RoCoF
$\sum \mathcal{H}$	0.568	0.558	0.668
$\sum \mathcal{K}$	0.286	0.283	0.319
p^{loss}	-0.561	-0.532	-0.876
$p^{loss}/\mathcal{D}$	-0.617	-0.588	-0.965
$\sum r$	0.506	0.516	0.269

antee the quality of frequency response in small power systems with low inertia, as the remaining units are not fast enough to compensate for the power mismatch, while the frequency is dropping fast due to lack of inertia. So other parameters like total available inertia and power loss ratio are better representatives of the system dynamics.

From the results of the SFR model for every single outage, it's possible now to determine acceptable and unacceptable outages. At this stage generator outages n, which are followed by bad frequency responses are tagged with 1, and the outages that are followed by tolerable frequency outages are tagged with 0. This forms the dependent variable υ_n in the LR model. For the purpose of this chapter, any generator outage incident which leads to frequency nadir less than 47.5 Hz, or a RoCoF higher than 1.5 Hz/s, or steady-state frequency less than 49.6 Hz, is considered an unacceptable incident and is tagged with 0. Other incidents are considered acceptable and are tagged with 1.

Independent variables that are chosen should have a good correlation with the frequency response metrics and have the ability to be used in the linear constraint. For this study, the presented parameters in table 5.2 are defined as independent variables. Now that both independent variables and their associated dependent variables are acquired, the LR model can be trained to calculate the coefficients of eq. (5.15). The LR coefficients for the case study of La Palma island are presented in table 5.3. These coefficients can be implemented to eq. (5.15), with an adjustable

Table 5.3: Logistic regression coefficients

Independent variable		LR coefficient	
–	–	c_0	26.577
ξ_1	$\sum_{\substack{ii\in\mathcal{I}\\ii\neq i}} \mathcal{H}_{ii}\mathcal{M}_{ii}^{base}u_{t,ii}$	c_1	-0.366
ξ_2	$\sum_{\substack{ii\in\mathcal{I}\\ii\neq i}} \mathcal{K}_{ii}u_{t,ii}$	c_2	0.102
ξ_3	$p_{t,i}$	c_3	1.484
ξ_4	$p_{t,i}/d_t$	c_4	-173.995
ξ_5	$\sum_{\substack{ii\in\mathcal{I}\\ii\neq i}} (\overline{\mathcal{P}}_{ii}u_{t,ii} - p_{t,ii})$	c_5	2.356

cut-point ψ to set up a new constraint. As discussed in section 5.3.4, the logit form is a transformation of probabilities. In this case, incidents that are more probable to be acceptable should have a positive logit and a probability close to 1. On the other hand, incidents that are more probable to be unacceptable should have a negative logit and a probability close to 0. There will also be some errors, mainly around 0.5 probability, meaning that some acceptable incidents might end up possessing a negative logit value and vice versa. Depending on the preferred outcome, a proper cut-point can be chosen to create a more conservative or less conservative constraint. Figure 5.7 shows how accurately the applied logistic regression can separate acceptable and unacceptable results. Acceptable results are in red and unacceptable ones are in yellow.

Depending on the required conservativeness a cut-point is chosen. For example $\psi = 0$ corresponds to $\pi(\upsilon = 1) = 0.5$. Putting $\psi = 0$, means all the incidents that their probability of being unacceptable is more than 0.5, will be eliminated, hence it's very conservative. A less conservative

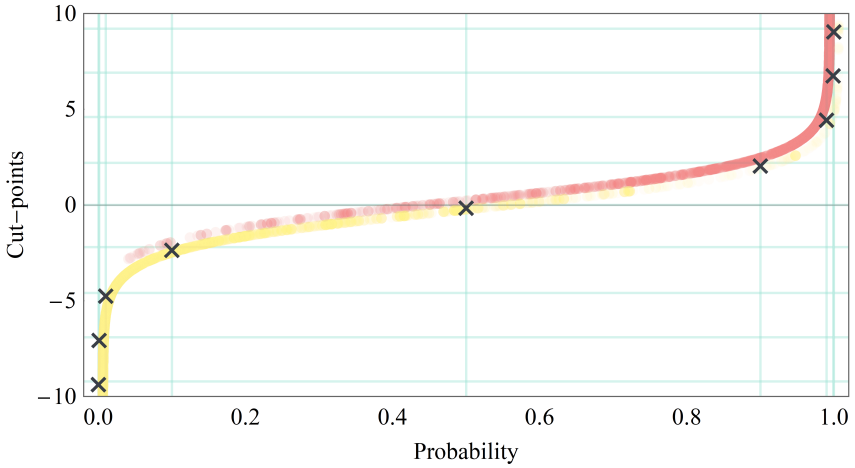

Figure 5.7: Logistic regression approximation

approach is to only eliminate the instances with the probability of being unacceptable more than 0.9 ($\pi(\upsilon = 1) \leq 0.1$). Then ψ should be set equal to -2.12 (considering eq. (5.14)). Some probabilities and their corresponding cut-points are shown with the cross sign in fig. 5.7.

In fig. 5.8, it's shown how different independent variables, ξ_1 to ξ_5 (as defined in table 5.3), are described by the logistic regression approximation. Those incidents that are marked as acceptable before are the red dots, and unacceptable incidents are the yellow dots. There are some errors, especially close to the $logit(\pi = 1)$ line, but the overall accuracy is justifiable. The summation of online inertia, ξ_1, is depicted in the fig. 5.8.I. Acceptable results are more concentrated on the top side which are the incidents with higher online inertia, and as the online inertia drops, the dots move towards unacceptable results. A similar conclusion can be drawn for the summation of the droops of online turbine-governor systems, ξ_2, shown in fig. 5.8.II. The amount of lost generation, ξ_3, is depicted in fig. 5.8.III. As expected, larger outages tend to result in unacceptable incidents and as the figure goes toward smaller outages, the concentration of acceptable incidents grows. The same conclusion is derived from fig. 5.8.IV, which shows the ratio of lost generation to hourly demand, ξ_4. The available reserve is depicted in fig. 5.8.V. Generally incidents with a higher amount of online reserve tend to lead to better results, but still there are a considerable number of incidents that lead to unacceptable results, although they have a relatively high available reserve. This confirms that the available reserve is not the best indicator to ensure the quality of dynamic response after outages. The goal is to improve the quality of frequency response by including all of these independent variables, each of them weighted carefully with logistic regression coefficients.

5.4.2 Comparison of different methods

Simulations are carried out for three different methods:

Conventional approach: the conventional formulation of robust UC, that the frequency response after an outage is only guaranteed by reserve criteria. Reserve requirement is the biggest online generation infeed.

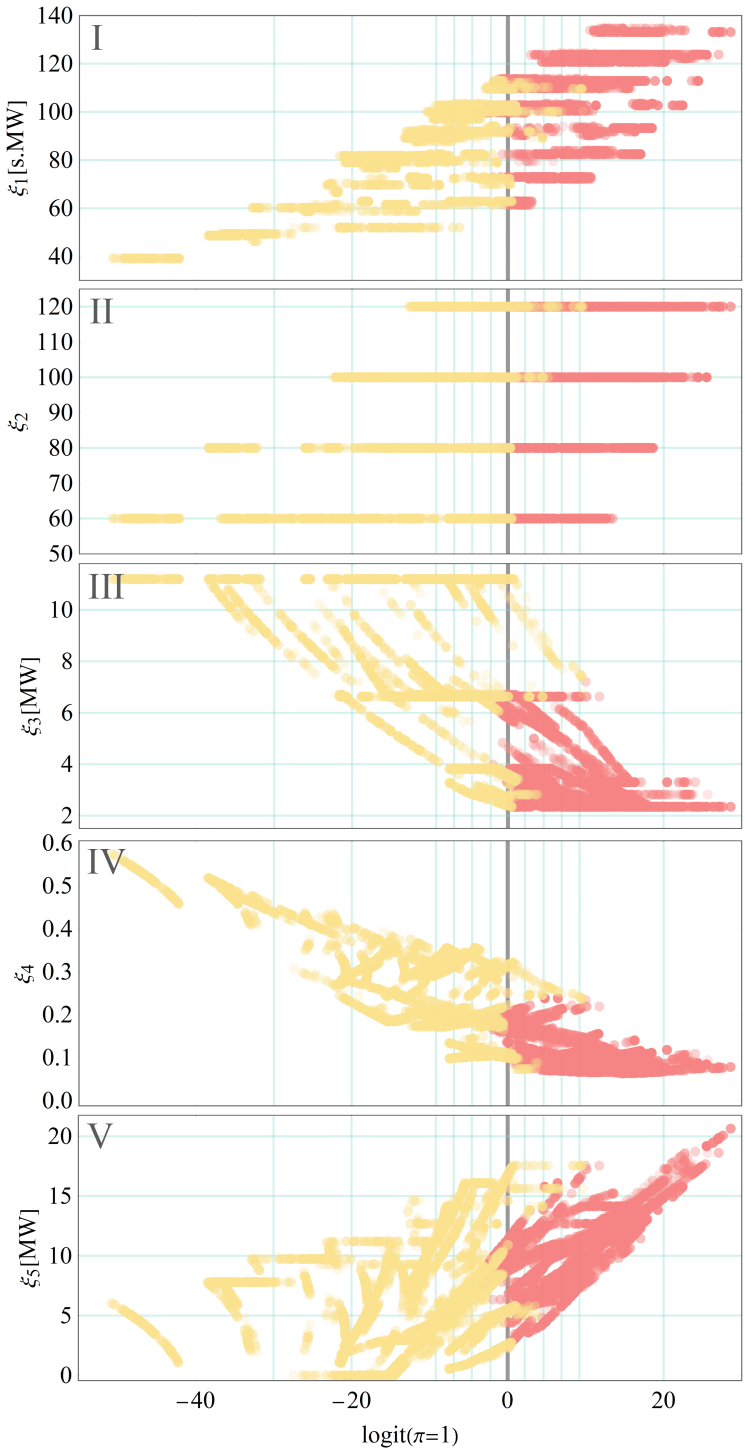

Figure 5.8: Logit transformation - variables

LR: the proposed logistic regression method. Reserve criteria are substituted with a constraint that is trained by the LR model. Different cut-points (ψ) are considered to assess the effectiveness of the proposed method, when the LR constraint is looser (smaller ψ) or tighter (bigger ψ).

OCT: To also compare the proposed method with other recent data-driven methods in the literature, optimal classification trees are implemented to train a constraint, as introduced in [102]. The outputs of the SFR model are classified into acceptable and unacceptable incidents, using the MILP solution method of [119]. As solving the optimization problem for classification becomes very hard with a big set of inputs and a high depth of trees, only the biggest hourly outage of a limited number of scenarios is fed to the OCT problem as input, with the maximal depth of one and two.

RoCoF: The RoCoF estimation from the swing equation is linear and can be directly used in MILP formulation. Different critical RoCoF are considered to make comparison easier. More detail can be found in [96] and [98]. The added constraint to the conventional OCT is as follows,

$$2\Big(\sum_{ii\neq i}^{ii\in\mathcal{I}} \mathcal{H}_{ii}\mathcal{M}_{ii}^{base}u_{t,ii}\Big) \times \Delta f_{crit}^{'} \geq p_{t,i} \quad t\in\mathcal{T},\ i\in\mathcal{I} \tag{5.17}$$

Where $\Delta f_{crit}^{'}$ is critical rate of change of frequency. A comparison of frequency response indicators for the conventional approach, LR, and OCT is presented in table 5.4.

Table 5.4: Results of the simulations on La Palma island

	HQFR (%)	HQFR (%)	average f^{qss}	average f^{nadir}	average RoCoF	average UFLS	operation cost	run-time (s)
Conventional approach	67.6%	32.4%	49.61 Hz	48.29 Hz	-1.31 Hz/s	2.30 MW	140.61 k€	$1,422''$
LR with $\psi = 2.12$	81.8%	18.2%	49.81 Hz	48.81 Hz	-1.00 Hz/s	1.14 MW (-50.5%)	145.26 k€ (+3.3%)	$1,819''$
LR with $\psi = 0$	81.3%	18.7%	49.82 Hz	48.77 Hz	-1.03 Hz/s	1.23 MW (-46.5%)	143.68 k€ (+2.1%)	$2,092''$
LR with $\psi = -2.12$	78.9%	21.1%	49.81 Hz	48.68 Hz	-1.09 Hz/s	1.47 MW (-36.1%)	142.90 k€(+2.3%)	$2,345''$
LR with $\psi = -4.95$	78.2%	21.8%	49.74 Hz	48.57 Hz	-1.12 Hz/s	1.75 MW (-23.9%)	141.32 k€ (+0.5%)	$1,965''$
LR with $\psi = -5$	73.4%	26.6%	49.73 Hz	48.48 Hz	-1.18 Hz/s	2.03 MW (-11.7%)	140.78 k€ (+0.1%)	$1,411''$
LR with $\psi = -6.91$	76.8%	23.2%	49.66 Hz	48.52 Hz	-1.13 Hz/s	2.06 MW (-10.4%)	139.83 k€ (-0.6%)	$1,015''$
LR with $\psi = -9.21$	69.8%	30.2%	49.26 Hz	48.09 Hz	-1.24 Hz/s	2.20 MW (-4.3%)	138.53 k€ (-1.5%)	$794''$
LR with $\psi = -10$	64.2%	35.8%	47.97 Hz	46.96 Hz	-1.28 Hz/s	2.44 MW (+6.1%)	136.86 k€ (-2.7%)	$847''$
LR with $\psi = -11.51$	61.9%	38.1%	47.91 Hz	46.85 Hz	-1.36 Hz/s	2.61MW(+13.5%)	136.67 k€ (-2.8%)	$761''$
OCT, d=1, N=1001	79.2%	20.8%	49.80 Hz	48.75 Hz	-1.05 Hz/s	1.31 MW (-43.0%)	144.33 k€ (+2.6%)	$1,750''$
OCT, d=2, N=1001	79.1%	19.9%	49.81 Hz	48.77 Hz	-1.04 Hz/s	1.29 MW (-43.9%)	145.09 k€ (+3.2%)	$3,144''$
OCT, d=1, N=2800	79.2%	20.8%	49.80 Hz	48.76 Hz	-1.05 Hz/s	1.30 MW (-43.5%)	144.12 k€ (+2.5%)	$1,807''$
RoCoF ($\Delta f_{crit} = 1.5$)	88.4%	11.6%	49.80 Hz	48.81 Hz	-0.91 Hz/s	1.17 MW (-49.1%)	151.41k€ (+7.1%)	$1,104''$
RoCoF ($\Delta f_{crit} = 2$)	75.3%	24.7%	49.79Hz	48.60Hz	-1.16Hz/s	1.41 MW (-36.8%)	144.40k€ (+2.7%)	$1,984''$
RoCoF ($\Delta f_{crit} = 2.5$)	69.3%	30.7%	49.78Hz	48.42Hz	-1.26Hz/s	2.01 MW (-12.6%)	142.10k€ (+1.1%)	$1,620''$

Frequency-response quality indicators are the average amount of UFLS which is obtained from SFR with UFLS active, average frequency nadir, average RoCoF, and average quasi-steady-state frequency, which is obtained from SFR with UFLS deactivated. The changes in average UFLS and operation costs relative to the conventional approach are presented in percentage too. To better compare the overall frequency response quality of all presented methods, HQFR and HQFR are defined in percentage. HQFR is the percentage of incidents with low-quality frequency response, which are incidents with RoCoF higher than 1.5 Hz/s or frequency nadir lower than 47.5 Hz or quasi-steady-state frequency lower than 49.6 Hz. The rest of the incidents are counted as HQFR, or High-quality frequency response. Cut-points beyond $\psi = 2.12$ make the problem infeasible, so $\psi = 2.12$ is presented in the table as the most conservative cut-point that is feasible. The results assert that more conservative approaches lead to higher operation costs. But depending on the chosen cut-point, the proposed approach can sometimes lead to better frequency response quality, while keeping the operation costs relatively low. As it can be seen in table 5.4, more conservative cut-points lead to less percentage of HQFR. Each column in the table is compared with the conventional approach. The ones that perform better than the conventional approach are underlined with red lines, and the ones that perform worse are underlined with yellow lines. The results also show that the proposed approach can guarantee a better frequency response quality if a proper cut-point is chosen. Depending on the required level of cautiousness, the operator can choose a cut-point. For the La Palma island, a probability assurance of $\psi = -6.91$ seems appealing, because both frequency response quality and operation cost are improved.

To better compare and choose the best ψ, all the simulated cases of La Palma island are compared with the conventional approach (highlighted with a yellow cross) in fig. 5.9. Although the

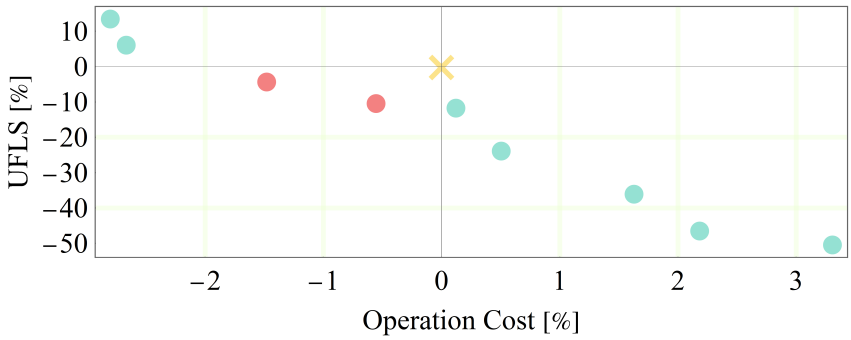

Figure 5.9: Average UFLS and operation cost in percentage

operation costs go higher by choosing ψ closer to zero, the average UFLS is decreased considerably. Also, there are cases that lead to improvement in both operation cost and average UFLS, which are highlighted in red.

The results for OCT in table 5.4 show improvements in the quality of frequency response compared to the conventional approach and LR with some cut-points. d is the depth of the tree structure. OCT with $d = 1$ leads to one set of constraints (so the size of the UC problem will remain the same), and OCT with $d = 2$ leads to two sets of constraints. Although OCT is very accurate in classifying the inputs, the run-time of the optimization problem relies heavily on the number of inputs and the depth of the tree structure. For that reason making the training set

smaller was necessary. Solving OCT with a full set of training set (around 20000 points) can take many days. So only the biggest hourly outages of some scenarios are considered (like in [102]), creating two training data-sets, one smaller with 1001 points, and one bigger with 2800 points. A comparison between the accuracy of representing the data set and solution run-time is presented in table 5.5. The downside of a small training set for this practice is that more unacceptable inci-

Table 5.5: Comparison of the training process

method	N	inaccuracy	run-time
LR	19860	3.71%	00'03"
OCT, $d = 1$	1001	1.15%	00'32"
OCT, $d = 2$	1001	0.1%	28'07"
OCT, $d = 1$	2800	2.07%	42'06"

dents might be flagged as acceptable and vice versa. As it can be seen in table 5.5, the advantage of OCT compared to LR is the superior accuracy in classifying the training set and the OCT disadvantage compared to LR is the computational burden of the training process, which effectively limits the size of the training set. Also, tuning the initial values in the OCT optimization problem is hard, and time-consuming. More discussion about this can be found in [119].

Simulations are also carried out for OCT with reserve constraint, plus the linear RoCoF constraint, considering different critical values for RoCoF. The problem is infeasible for Δf_{crit} below 1.5 Hz/s. This criterion keeps the RoCoF of any outage, under the defined Δf_{crit}. Yet it cannot prevent some of the unacceptable f^{qss} and f_{nadir} from happening. Also, the operation cost is considerably higher, because so many units should be online at the same time to keep RoCoF within boundaries after outages. Higher Δf_{crit} results are less conservative, but as expected they will cost more than the conventional approach. As it can be concluded from the results, even for the most restricted criteria, the percentage of HQFR is impossible to be zero for La Palma island. There is no feasible solution that can guarantee only HQFR incidents. Simply starting up more units would not solve the issue, as the units should maintain the minimum power output constraint, which effectively limits the maximum number of online units. For all the simulations in this chapter, a computer with Intel core i7-8700 CPU and 32 GB installed RAM is used. All of the MILP problems (OCT and OCT), and ED which are quadratic, are solved by CPLEX solver in GAMS. The run-time of each respective method is presented in table 5.4 as well. Different things might affect the solution-time of an MILP problem, including: tightness of the solution domain, compactness of the problem (problem size), lower bound of the objective function that the solver finds, number of feasible cuts, optimality gap, and etc.

It's also interesting to see and compare the dynamic frequency responses obtained from the SFR model. In fig. 5.10 and fig. 5.11 the frequency response for a period of 15 seconds after outages are presented, for every single outage of online units in a random hour. In fig. 5.10 the UFLS scheme is activated, and fig. 5.11 shows frequency responses without UFLS. The simulations for the conventional approach are in yellow, the most conservative case with $\psi = 2.12$ in red, and one of the preferred cases with $\psi = -6.91$ in green. The moments that the UFLS scheme has operated are also highlighted with dashes. The better performance of the conservative case is no-

ticeable. Also, the case with $\psi = -6.91$ outperforms the conventional approach. The minimum allowed frequency nadir is shown with the gray line in fig. 5.11.

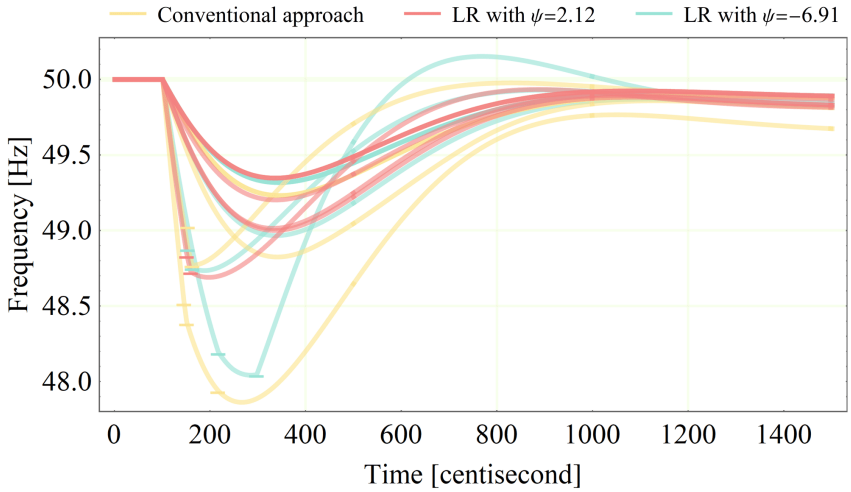

Figure 5.10: Frequency response after outages for a random hour with UFLS.

5.5 Conclusion

This chapter proposes a novel procedure to schedule short-term UC in island power systems. Island power systems usually suffer from a lack of inertia and frequency response capacity, complicating containing frequency within an acceptable range during large disturbances.

The proposed method uses an initial data set to train a linear constraint that takes into account the dynamic response of the system. For the purpose of training this constraint, logistic regression is employed to avoid incidents with undesirable frequency responses as much as possible. Then the logistic regression constraint is included in an adaptive robust formulation. Results show that by choosing a proper cut-point, the proposed method improves the frequency response, as well as the operation costs. The chosen value for the best cut-point depends on the expectations of the operator and the system under study. As training data with the LR model is very fast, the size of the training set is not an issue. A complete training data set can better represent the system, leading to a more reliable frequency constraint. The proposed approach is compared with OCT as a method to classify the training set and also with linear RoCoF constraint. In both cases, the proposed method is more cost-efficient. The operator can use the proposed constraint in the UC problem to improve the frequency response of the system after outages.

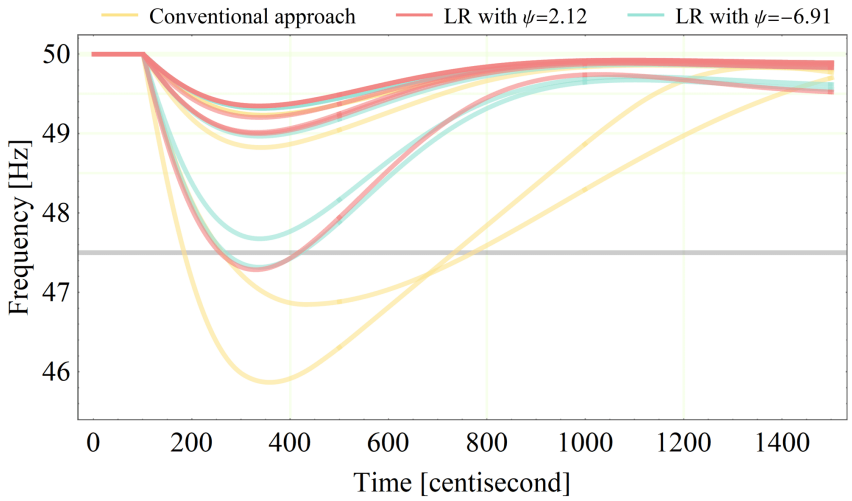

Figure 5.11: Frequency response after outages for a random hour without UFLS.

6 Comparing Analytical and ML based Frequency Nadir in UC Problem

In this chapter first, a synthetic training dataset is generated. Then some classic ML methods are applied to predict the frequency nadir. Our results show that the UC problem with a ML-based frequency nadir constraint is solved considerably faster than the analytical formulation, while still achieving an acceptable frequency response quality after outages. Scheduling the units while making sure that the frequency stability is maintained is essential in systems that are facing inertia scarcity. The methodology and findings of this paper are submitted for publication. A preprint can be found in [120].

Small island power systems typically suffer from inertia scarcity and are therefore more prone to frequency volatility. For that reason, when integrating RES in such systems, it can be very challenging to maintain frequency stability in case of contingencies. To address this issue, researchers have included frequency dynamics in short-term scheduling processes like UC to form a FCUC, in [95], [96], [97], and etc.

6.1 Framework

The standard (non-FCUC) problem can be formulated as a MILP problem, which can be solved efficiently using standard solvers. Unfortunately, the frequency dynamics of a power system are highly nonlinear and non-convex, complicating how the UC problem can still be formulated as a MILP problem. There is valuable research work in the literature, addressing this very issue ([99], [100], [101], and [121]). Frequency dynamics after outages are usually described by the RoCoF, frequency nadir, and steady-state frequency. RoCoF and steady-state frequency can be formulated linearly, but frequency nadir cannot. In previously mentioned studies, the non-linear constraint on the frequency nadir (derived from the well-known swing equation) has been simplified or approximated so that it still can be used in the MILP formulation of UC problem. These formulations are based on simplifying assumptions and usually are computationally demanding. More recently, data-driven approaches are being introduced to more accurately model the frequency

dynamics in the UC problem, instead of relying on analytical methods ([102], [103], [104], [122]). These methods try to estimate the dynamics of the system accurately while keeping the solution time of UC reasonably low. Both analytical and data-driven methods are reviewed thoroughly in chapter 5.

In [121], the frequency nadir is approximated as a piece-wise linear function to good (and in principle, arbitrary) precision, and the resulting constraint is then reformulated as a MILP using separable programming. A common assumption in [95], [96], [97], [101], [121], and many other similar works, is that the provision of reserve increases linearly in time, and all units will deliver their available reserve within a given fixed time. This assumption is the key to calculating the frequency nadir as a function of other variables. The proposed method in [121] is presented in this chapter, as an analytical method, for the sake of comparison.

Continuing the line of research of the data-driven approaches as used in the previous chapter 5, this chapter generates a synthetic training dataset, and then applies ML methods to the dataset to derive a linear constraint that approximates the original non-linear frequency nadir constraint for all scenarios in the dataset. A synthetic data set is proposed here to reduce the computational burden of generating the data set by simulation of UC (for instance see chapter chapter 5). To evaluate the effectiveness of the ML methods, the weekly FCUC of the La Palma island power system is solved for seasonal sample weeks. The results are compared to one of the recent FCUC formulations that employ a MILP formulation based on an analytical expression of the frequency nadir [121]. The contributions and highlights of this chapter are as follows,

- A novel synthetic data generation algorithm is presented that includes feasible operating points. These operating points are sorted by their quadratic generation cost function. Operating points that are cost-efficient are added to the training dataset. Such a dataset is only composed of operating points that are close to the optimal solution of the UC problem, as they are feasible and cheaper. Compared to the proposed datasets in the literature, the data generation algorithm here covers all the feasible generator operating points that are likely to be picked by the solver. An advantage of this dataset is that it's not sensitive to the daily demand and RES forecast. So once it's generated, the models that are obtained from it can be used throughout the year.

- The training dataset is passed through different ML methods to train a linear constraint that can classify tolerable and intolerable frequency nadirs after any outage. This linear constraint can be directly employed in the UC problem as the frequency nadir constraint.

- The performance of the ML methods is compared to the analytical method of predicting frequency nadir, showing that the UC is solved considerably faster, whilst still achieving an acceptable frequency response quality after outages ($N-1$ security criteria). It should be noted that reducing computation times is critical when modeling uncertainties in stochastic or robust UC problems.

The rest of this chapter is organized as follows: the underlying methodologies used in this chapter are presented in section 6.2. Meanwhile, the simulation results and corresponding comparisons are discussed in section 6.3. Finally, the conclusions are drawn in section 6.4.

6.2 Methodology

In this section, a general UC formulation is presented. To incorporate the frequency dynamics in the UC problem, rate of change of frequency (in section 6.2.3), steady-state frequency (in section 6.2.4), and frequency nadir (in section 6.2.5) constraints are formulated. Frequency nadir is incorporated with both analytical (in section 6.2.5) and ML based (in section 6.2.5) methods. Finally, in section 2.6, the two options (analytic and ML modeling of frequency nadir) are compared in practice using the FCUC results.

6.2.1 UC Formulation

The UC problem is a mixed-integer problem and is usually solved with MILP solvers after linearization of non-linear terms, introducing additional integer or binary auxiliary variables where need be to handle non-linearities. The general form of the UC problem that is used in this chapter is similar to what is defined in chapter 2. The objective function is 2.1, subjected to the same constraint. The only difference is that the reserve constraint is combined with the maximum capacity constraint as follows,

$$p_{t,i} + r_{t,i} \leq \overline{\mathcal{P}}_i u_{t,i} \quad t \in \mathcal{T},\ i \in \mathcal{I} \tag{6.1}$$

And the power balance equality is defined as,

$$\sum_{i \in \mathcal{I}} (p_{t,i}) + wg_t + sg_t = \mathcal{D}_t \quad t \in \mathcal{T} \tag{6.2}$$

where wg and sg are wind and solar generation variables, respectively and $\mathcal{D}$ is the demand.

6.2.2 Frequency Dynamics

The dynamics of the generator rotor are usually described by the swing equation,

$$\frac{2H}{f_0}\frac{d\Delta f(t)}{dt} + D\mathcal{D}_t \Delta f(t) = P_m - P_e \tag{6.3}$$

Where f_0 is the nominal frequency. D is the load damping factor. $f(t)$ is the frequency. P_m and P_e are mechanical and electrical powers in megawatts, respectively. This is a first-order differential equation. When an outage happens, there will be a power mismatch between the mechanical output of the units and the electrical demand, which is equal to the amount of lost power.

$$P_\ell := P_m - Pe \tag{6.4}$$

The available inertia after the outage of unit ℓ can be defined as,

$$\mathcal{H}_\ell := \sum_{i \in \mathcal{I}, i \neq \ell} (H_i \mathcal{M}_i u_{t,i}) \tag{6.5}$$

Considering the swing equation and the operating point of the system before the outage, the frequency response of the system after the outage can be calculated. The frequency response is reflected in metrics like RoCoF, steady state frequency, and frequency nadir.

6.2.3 Rate of Change of Frequency Modelling

The RoCoF after the outage can be driven from eq. (6.3) (see also chapter 5). The amount of inertia after the outage should be able to prevent exceeding critical RoCoF,

$$\mathcal{H}_\ell \geq \frac{P_\ell f_0}{2\Delta f'_{crit}} \quad t \in \mathcal{T},\ \forall \ell \tag{6.6}$$

Where $\Delta f'_{crit}$ is the critical rate of change of frequency. This equation is linear and can be directly added to the MILP for the UC problem.

6.2.4 Steady State Frequency Modelling

For the steady state frequency after an outage, it is assumed that frequency is converged and there has been enough time for units to deliver their reserve power. To make sure that the steady state frequency is not violated, this constraint can be derived from the swing equation,

$$\sum_{i \in \mathcal{I}, i \neq \ell} r_{t,i} \geq P_\ell - D\mathcal{D}_t \Delta f^{ss}_{crit} \quad t \in \mathcal{T},\ \forall \ell \tag{6.7}$$

Where Δf^{ss}_{crit} is the critical steady state frequency. This equation is also linear and can be directly added to the MILP. Note that this equation holds as long as generators do not hit their maximum output power.

6.2.5 Frequency Nadir Modelling

The inclusion of frequency nadir into the MILP is more complicated, as it is non-convex. Traditionally researchers have proposed analytical methods to calculate frequency nadir from the swing equation, and then implement a MILP approximation of it to the UC problem, which is discussed in section 6.2.5. More recently the use of ML is gaining popularity to model these more complicated situations. The proposed method of this study to estimate frequency nadir is presented in section 6.2.5.

Frequency nadir: analytical modelling

After the outage happens the frequency starts to decrease. As a response, the remaining units start ramping up, if they have any available reserve. Here, and in [95, 96, 97, 101, 121] it is assumed that the reserve power of all units is delivered linearly and will reach its maximum output power in T_g seconds. Note that g here is not and index. T_g is a constant number which is the same for all

generators. This is a key assumption to finding an analytical expression for the frequency nadir and relates to the minimum response requirement as imposed by grid codes.

$$r_{t,i}(\tau) = \begin{cases} \frac{r_{t,i}\tau}{T_g} & \text{if } t \leq T_g \\ r_{t,i} & \text{if } t > T_g \end{cases} \tag{6.8}$$

It is also assumed that frequency nadir happens before T_g. Let's also define the amount of remaining reserve after the outage of unit ℓ as,

$$\mathcal{R}_\ell = \sum_{i \in \mathcal{I}, i \neq \ell} r_{t,i} \tag{6.9}$$

With these assumptions, the frequency nadir constraint is as follows,

$$\mathcal{H}_\ell \mathcal{R}_\ell - \frac{f_0 T_g P_\ell^2}{4\Delta f_{crit}^{nadir}} + \frac{D\mathcal{D}_t T_g P_\ell f_0}{4} \geq 0 \quad t \in \mathcal{T},\ \forall \ell \tag{6.10}$$

Where Δf_{crit}^{nadir} is the critical frequency nadir. This constraint cannot be added to the MILP formulation of UC, because it is non-convex, due to the product of inertia and reserve. In [121], auxiliary variables and separable programming are introduced to linearize these terms. The following constraints are used to linearize the square of lost power,

$$P_\ell = \sum_{j=0}^{J} a_j \lambda_j \tag{6.11a}$$

$$P_\ell^2 \approx \sum_{j=0}^{J} (a_j)^2 \lambda_j \tag{6.11b}$$

$$\sum_{j=0}^{J} \lambda_j = 1 \tag{6.11c}$$

$$\sum_{j=1}^{J} \gamma_j = 1 \tag{6.11d}$$

$$\lambda_0 \leq \gamma_1 \tag{6.11e}$$

$$\lambda_j \leq \gamma_j + \gamma_{j+1} \qquad j \in \{1, ..., J-1\} \tag{6.11f}$$

$$\lambda_J \leq \gamma_J \tag{6.11g}$$

Here, the a_j are fixed constants that control the approximation. To linearize the production of inertia and reserve in the same manner, first, a change in variables should be applied,

$$\mathcal{H}_i \alpha \mathcal{R}_\ell \beta = {z_1}^2 - {z_2}^2 \tag{6.12a}$$

$$\frac{z_1 + z_2}{\alpha} = \mathcal{H}_i \tag{6.12b}$$

$$\frac{z_1 - z_2}{\beta} = \mathcal{R}_\ell \tag{6.12c}$$

Now the new variables z_1 and z_2 can be used instead of inertia and reserve and their square form can be linearized similar to P_ℓ^2.

Frequency Nadir: ML based modelling

ML methods entail different components: (I) Data, which is a collection of data points that are characterized by features, (II) Model, which consists of feasible hypothesis maps from feature space to label space, (III) Loss function to measure the quality of the model, (IV) and a process of model validation to assess its performance. Each of these topics is discussed in the following.

Data Generation: A proper set of data is needed from which to learn the frequency nadir. The training dataset comprises features $x \in \mathcal{X}$ and labels $y \in \mathcal{Y}$. In the case of implementing frequency nadir in the UC problem, features are extracted from operating points, and labels are obtained from the frequency nadir measurements after outages. These measurements can be obtained by solving high-order differential swing equations, or by using SFR models. Assigned labels can be numeric (for example the frequency nadir measurement in Hz) or categorical (for example a binary label of whether the obtained frequency nadir is tolerable or not). The features should be chosen wisely so they represent a reasonable amount of information about their labels. On the other hand, an unnecessarily large number of features can be detrimental in both computational and statistical aspects. Computationally, choosing a large feature vector increases the dimensions of the problem, so more resources are needed for the calculations. Statistically, using a higher number of features makes the model more susceptible to overfitting. It is beneficial to only use features with the most relevant information to predict the label y [123]. In this chapter y is binary, so the proposed ML methods are binary classifications. In the literature, different methods are introduced to reduce the size of the feature vector. For the purpose of this chapter, features must be accessible throughout the UC optimization process. Therefore, the variables that are correlated most with the label will be picked as the features. As will be shown later in section 6.3, the selected features for predicting frequency nadir adequacy are available inertia after an outage ($\mathcal{H}_\ell$), the weighted gain of the turbine-governor model ($\mathcal{K}_\ell$), the amount of lost generation (P_ℓ), and the amount of available reserve ($\mathcal{R}_\ell$).

To have a complete dataset, one approach is to consider every combination of possible generation outputs of the units. But many of these combinations are infeasible as they do not satisfy all UC constraints (power balance, reserve constraint, or maximum RoCoF), or are unappealing as the optimization problem will favor cheaper combinations. In this chapter, a data generation method is used, to only generate feasible control points that are cost-effective, hence more probable to be close to the solution of the UC optimization problem. The process is listed in algorithm 2. The first vectors of the power output of each generation are defined. The number of power steps depends on the level of accuracy that is required. Then a vector of all possible combinations of generator productions is produced. Among the combinations, those that are violating the UC constraints or are not within the hourly net demand range will be removed. The remaining combinations will be sorted based on the total values of the quadratic cost function of their respective generator outputs. Expensive combinations, that can safely be assumed that UC opti-

Algorithm 2 Synthetic Data Generation

Input: for each generator $i \in \{1, \dots, I\}$, a vector of power levels $(p_i^1, p_i^2, \dots, p_i^{K_i})$ where $p_i^1 = \underline{\mathcal{P}}_i$ and $p_i^{K_i} = \overline{\mathcal{P}}_i$,
lower and upper bounds for total generation: $\underline{\mathcal{D}}$, $\overline{\mathcal{D}}$
Output: All feasible and cheap combinations

for $(k_1, \dots, k_I) \in \bigtimes_{i=1}^{I} \{0, \dots, K_i\}$ **do** ▷ Combinations of power levels
  for $i \in \{1, \dots, I\}$ **do**
    $u_i \coloneqq 0$ if $k_i = 0$ else 1 ▷ Unit i status
  end for
  $R \coloneqq \sum_{i=1}^{I} (p_i^{K_i} u_i - p_i^{k_i})$ ▷ Total reserve
  $G \coloneqq \sum_{i=1}^{I} p_i^{k_i}$ ▷ Total generation
  $H \coloneqq \sum_{i=1}^{I} (H_i \mathcal{M}_i u_i)$ ▷ Total inertia
  if $G \in [\underline{\mathcal{D}}, \overline{\mathcal{D}}]$ and $R \geq \max_{i=1}^{I} p_i^{K_i}$ and $H \geq \frac{p_i^{k_i} f_0}{2\Delta f'_{crit}}$ **then**
    $FC \leftarrow FC \cup (p_1^{k_1}, \dots, p_I^{k_I})$ ▷ Combination is feasible
  end if
end for
Sort FC by the quadratic generation cost function
Keep a reasonable number of cheaper combinations and remove the rest

mization problem will not elect, will also be removed. The obtained dataset only includes feasible and cheaper solutions. These solutions are expected to be around the optimal solution of the UC problem. In addition, considering solutions around the optimal one accounts for deviations from the planned generation schedule during real-time operation. This dataset can be used as the training dataset for the intended ML methods.

Labelling the Data: The SFR model which is previously introduced in section 3.2.1 is used to label the data. Gain k_i is an important parameter in indicating the frequency response of unit i. Since it is important in the learning process of the ML model to have features that are able to represent the frequency dynamics after the outage, a weighted gain after the outage is defined here, which will later be used as a feature for the training dataset.

$$\mathcal{K}_\ell = \sum_{i \in \mathcal{I}, i \neq l} (k_i \mathcal{M}_i u_{t,i}) \tag{6.13}$$

Since the primary spinning reserve is finite, power output limitations $\Delta p_{i,min}$ and $\Delta p_{i,max}$ are forced, so the units can only participate as much as their available reserve. Moreover, the ramp-up speed of the units should be limited to the maximum ramping capacity of each respective unit. The complete model is explained in [1].

Learning the Model: Considering the features $x \in \mathcal{X}$ and labels $y \in \{-1, +1\}$, with $+1$ for acceptable data points and -1 for unacceptable data points.

The purpose of the ML model is to learn a decision function $f_\theta(x)$ which is positive when the label is $+1$ and negative when the label is -1, whilst minimizing misclassifications. Here, θ parametrizes the class of decision functions considered. For the purpose of this chapter, the label indicates whether the resulting frequency of nadir after an outage is tolerable or not. As the classifier is going to be implemented in the UC problem to be solved with MILP solvers, only decision functions of the following form are considered (with $\Theta := (\theta_1, \ldots, \theta_M)$):

$$f_\theta(x) := \Theta^\intercal x + \theta_0 \tag{6.14}$$

Once θ_0 and Θ have been trained from the data, eq. (6.14) can be directly added to the MILP formulation, simply by adding the following constraint:

$$\Theta^\intercal x + \theta_0 \geq 0 \tag{6.15}$$

Loss Function: The loss value $\ell(f_\theta(x), y)$ is the discrepancy between the true label y and the sign of the decision function $f_\theta(x)$. The loss function measures how well the model predicts the actual outcome. We will find a classifier that minimizes the empirical risk (defined as the average loss value across the training data) plus a regularization term (if need be),

$$L_\theta := \frac{1}{N}\sum_{n=1}^{N} \ell(f_\theta(x_n), y_n) + \frac{1}{C}\sum_{m=1}^{M} \theta_m^2 \tag{6.16}$$

where we assume the training data has N samples. C represents a regularization parameter. With smaller C regularization is more effective, hence the model will be less prone to overfitting. With a larger C the number of misclassifications on the training data might reduce, but at the cost of overfitting.

Different ML methods use different loss functions. For the purpose of this chapter two ML methods suitable for binary classification are applied to the training dataset, namely LR and support vector machine (SVM). LR uses the log loss, without regularization ($C = \infty$):

$$\ell(f_\theta(x), y) := -(1+y)\log\left(\frac{1}{1+e^{-f_\theta(x)}}\right) - (1-y)\log\left(\frac{e^{-f_\theta(x)}}{1+e^{-f_\theta(x)}}\right) \tag{6.17}$$

The SVM model in this chapter uses the regularized hinge loss function:

$$\ell(f_\theta(x), y) := \max\big(0, 1 - y f_\theta(x)\big) \tag{6.18}$$

Validation: A standard way of validating the ML models is by cross-validation. Cross-validation is a statistical method of evaluating and comparing learning models by dividing the training dataset into two segments; one is used to learn the model and the other is used to validate the model. Cross-validation is used to check the quality of ML models in section 6.3.

6.2.6 Evaluating the Methods

A good method is able to ensure the frequency dynamics after outages while keeping the operation cost low, and with a formulation that is computationally affordable. In the results, the proposed ML method of including frequency nadir in UC is compared with the analytical method and a base case (no frequency nadir constraint). To evaluate each of the methods, UC operation cost (as a representative of the costs), the amount of UFLS (as a representative of frequency dynamic quality), average frequency nadir after an outage (as a representative of frequency dynamic quality), and the solution time of each method (as a representative of computational burden) are compared. A flowchart of the methodology is presented in fig. 6.1.

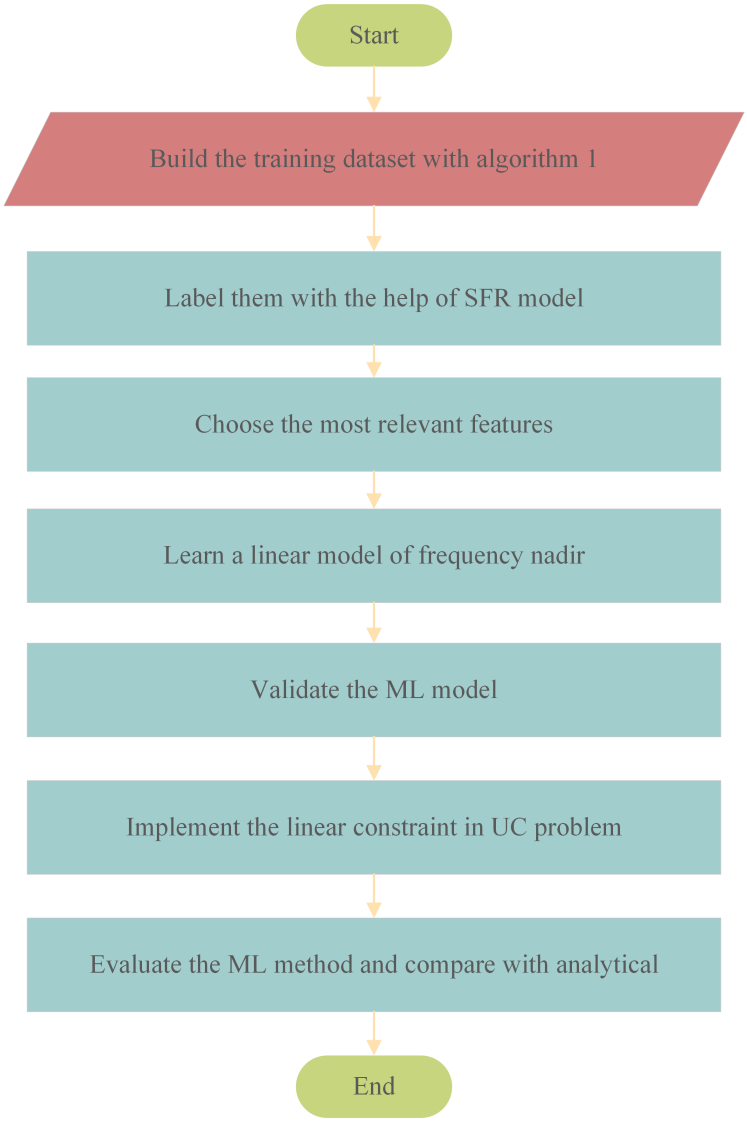

Figure 6.1: Flowchart of the machine learning based methods

6.3 Results

6.3.1 Case study

Simulations and comparisons of the methods are carried out on the real power system of La Palma island, one of Spain's Canary Islands. The yearly demand in 2018 is reported as about 277.8 GWh (average hourly demand of 31.7 MWh), supplied by eleven Diesel generators pre-dominantly. According to [117], the installed capacity of the La Palma island power system mounts to 117.7 MW, where about 6% of the installed capacity belongs to wind power generation. RES covers about 10% of the yearly demand. The input data of the demand and availability of the RES to solve the UC problem is obtained from the most recent real data. The weekly demand of each sampling week is shown in fig. 6.2, and weekly available RES is shown in fig. 6.3. Note that data of weekly demand and RES for the simulations in this chapter, is different from what is used in the previous chapters. To compare the methods, weekly UC is solved for sample weeks of different seasons. Doing

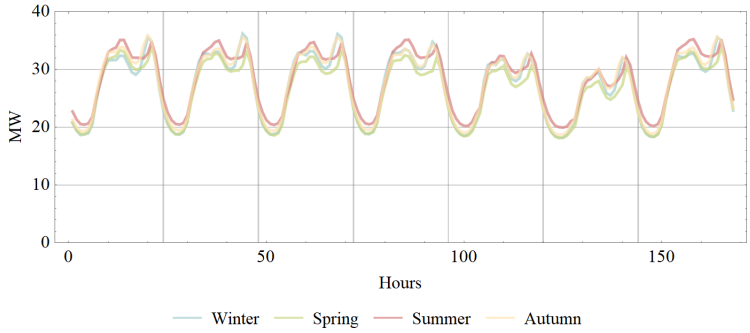

Figure 6.2: Weekly demand for each season

so reveals any temporal dependency of the ML approaches to the training dataset. All the codes, input data, and results of this chapter can be found at https://doi.org/10.5281/zenodo.7082627.

6.3.2 Training Dataset

Algorithm 2 is used to build a training dataset for La Palma island. Steps of 0.5 MW are used to define the vector of power levels. Then all possible combinations of operation points are generated. Among all the combinations, those that are either bigger than the annual thermal generation peak or smaller than the annual thermal generation minimum are excluded. Considering the historical data, thermal generation in La Palma island is between $\overline{\mathcal{D}} = 36$ MW and $\underline{\mathcal{D}} = 16$ MW, throughout the year. The training dataset should only include those operation points that are between maximum and minimum thermal generation. This training dataset is built to train the frequency nadir constraint. There is therefore no point to include any operation points that are violating other UC constraints, as they are not feasible. Notwithstanding this point, the operating points that are unable to provide enough reserve or cannot maintain minimum RoCoF constraints should be excluded as well. Amongst the remaining data points, those that are far from the optimal solution of the UC because of their incurred costs will never be selected as an optimal solution and therefore there is no point in keeping them either.

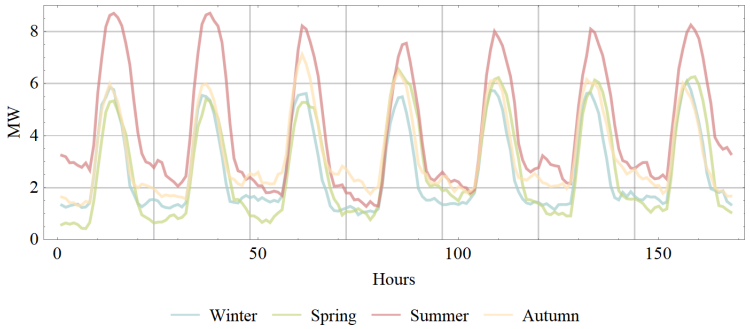

Figure 6.3: Weekly available RES for each season

The remaining operating points are then sorted by the total value of their respective quadratic generation cost functions, and for every thermal generation level, those that are cheaper are kept. For the purpose of this chapter, 500 operating points are kept for every thermal generation level. This final set of data points is considered feasible data points and will be used as the training dataset for the frequency nadir constraint. All points should be labeled with the SFR model, as explained in section 6.2.5. To this end, all the data points are fed into the SFR model and the frequency dynamics of every single generator outage will be obtained. The number of possible outages for the training dataset exceeds 90,000. The criterion here is to label any outage frequency nadir deviation more than 3.5 Hz as unacceptable (labeled with -1), and other outages as acceptable (labeled with 1). A summary of building and labeling the training dataset is presented in table 6.1. The process of building the training dataset can be updated annually.

		run time
generating data	$19,500$ operation points	$2,811''$
labelling data	$90,001$ single outages	$38,400''$

Table 6.1: Summary of building and labeling the training dataset

It is important to define relevant features for the data points, that can represent the frequency nadir. Pearson correlation between frequency nadir and the chosen features for this study are shown in table 6.2. It is also stated how each of the features represents different operating points. It's interesting to mention that weighted inertia after an outage ($\mathcal{H}_\ell$) and weighted gain after an

feature	x_1	x_2	x_3	x_4
value	$\mathcal{H}_\ell$	$\mathcal{K}_\ell$	P_ℓ	$\mathcal{R}_\ell$
correlation	0.45	0.47	-0.81	0.41

Table 6.2: Pearson correlation of chosen features and frequency nadir

outage ($\mathcal{K}_\ell$) are more correlated with frequency nadir, in comparison with available reserve ($\mathcal{R}_\ell$). Traditionally available reserve constraint has been the only criteria in the UC problem to ensure the frequency stability after outages. Observations like what table 6.2 shows, confirm that other

than the available reserve, more frequency mdynamic related terms like available inertia and gain (which is inverse of the droop of the unit) should be taken into account too.

6.3.3 Learning and Validating the Model

Using different ML methods on the training dataset which consists of features in table 6.2 and the labels from the SFR model, results in the learned decision function to be used in the UC problem. Different ML methods that are applied to the training dataset, their obtained decision function, and their corresponding training times and cross-validations are summarized in table 6.3. For cross-validation purposes, the training dataset is randomly divided into a temporary test set, including 30% of the whole data, and the model is trained with the rest of the data. The percentage in the table is the accuracy of the model in predicting the labels of the test set. As it can be seen

	θ_0	θ_1	θ_2	θ_3	θ_4	training time	cross validation
LR	1	0.084	−0.013	0.626	−0.115	0.4″	96.7%
SVM, C=1	1	0.059	−0.012	0.806	−0.154	58.7″	96.5%
SVM, C=0.1	1	0.062	−0.012	0.718	−0.129	92.6″	96.6%
SVM, C=10	1	0.058	−0.012	0.795	−0.152	61.5″	96.5%

Table 6.3: Learning process and results of ML methods.

in table 6.3, training for the LR method is very fast. The SVM method can train the model in order of minutes. For LR and SVM, the scikit-learn package in Python is used [124]. The learning process is presented in fig. 6.4.

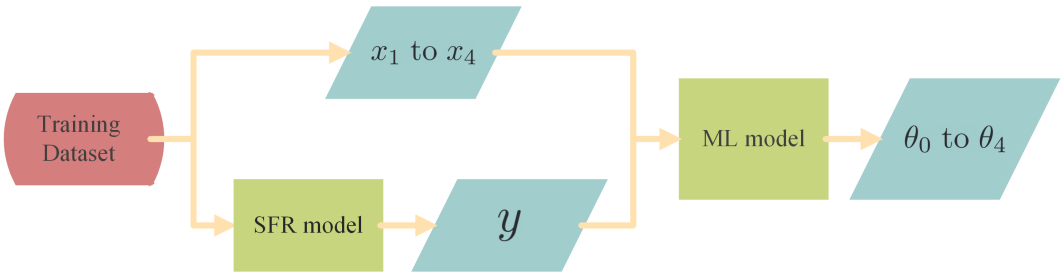

Figure 6.4: The machine learning process.

6.3.4 Evaluating the Methods

In the analytical method, the frequency nadir for each outage is estimated by a close approximation of eq. (6.10). In fig. 6.5 the frequency nadir calculated by eq. (6.10), its approximation by separable programming approach is compared, for all the outages in a sample day. This figure confirms that the linearized approximation of frequency nadir is very accurate. The maximum error of approximation is only 0.15 Hz. In fig. 6.6 the difference between the frequency nadir from the SFR model and the frequency nadir approximation by separable programming is shown on a histogram for a sample week. As shown in fig. 6.6, the analytical method is underestimating the frequency drop, compared to what is obtained from the SFR model. The main reason for this is

the underlying assumption in eq. (6.8). Equation (6.8) assumes that all the units will deliver their available reserve linearly in T_g seconds, regardless of their actual response speed.

All ML methods of learning frequency nadir that is presented in table 6.3 and the analytical method, which is explained in section 6.2.5, are applied to the UC problem. For the ML methods, the set of constraints that are defined in eq. (6.15) is added as the frequency constraint. However, for the analytical method, all the equations that are defined in section 6.2.5 to approximate the frequency nadir equation, should be added to the UC problem. Weekly UC is solved for sample weeks of winter, spring, summer, and autumn. Input demand and available RES are obtained from historical data and are shown in fig. 6.2 and fig. 6.3. In table 6.4 all the methods are compared. Some indicators are presented in table 6.4 to compare the performance of each method.

	operation cost(k€)	UFLS/outage (MW)	$f^{nadir}/outage(Hz)$	run-time
base case	824.08	1.682	-1.298	$317''$
LR	829.38	1.182	-1.146	$302''$
SVM, C=1	829.41	1.130	-1.127	$295''$
SVM, C=0.1	829.72	1.182	-1.140	$261''$
SVM, C=10	829.52	1.230	-1.151	$277''$
analytical	829.60	1.355	-1.167	$25,506''$

Table 6.4: Average weekly UC results for different methods.

The ultimate purpose is to minimize the operation cost and the UFLS, with a formulation that is computationally affordable. The operation cost in table 6.4, indicates the weekly expenditure on electricity generation. UFLS/outage indicates the average amount of load shedding after single outages. This is a good indicator of the quality of frequency response after the outage. Methods that have smaller load shedding per outage, are better able to prevent severe outages.

A histogram of the UFLS activation for different methods is presented in fig. 6.7. Figure 6.7 shows that the LR and SVM methods have been able to prevent the activation of UFLS more than the others. Also, they've considerably decreased the number of incidents with a big amount of UFLS activation.

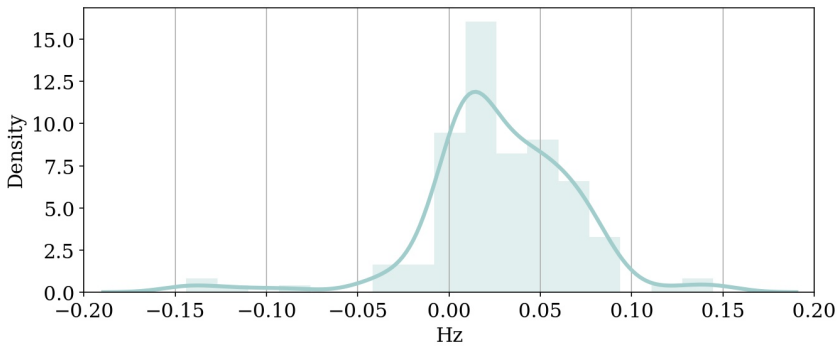

Figure 6.5: Histogram of the difference between frequency nadir by eq. (9) and its approximation by separable programming for a sample week.

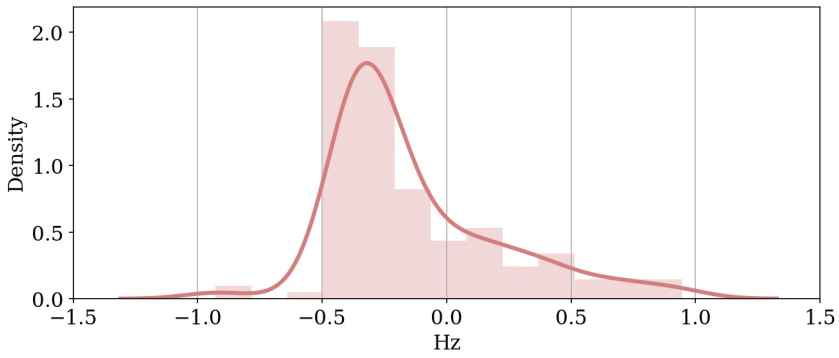

Figure 6.6: Histogram of the difference between the frequency nadir from the SFR model and the frequency nadir approximation by separable programming for a sample week.

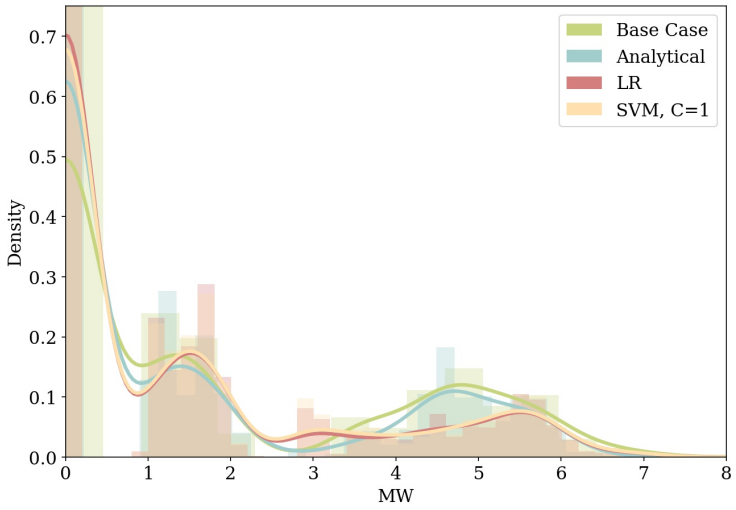

Figure 6.7: Histogram of UFLS for different methods.

The average run-time of weekly UC is presented in table 6.4 as an indicator of the computational efficiency of the methods. Furthermore, the average frequency nadir after outages is presented in the table. This shows how each method manages to restrict the severity of frequency nadir. There is a considerable difference in the run-time of ML-based methods with the analytical method. The studied ML base methods in this chapter, only introduce one constraint for the outage of each generator and each time interval to represent frequency nadir constraint in UC. But to represent frequency nadir analytically, an approximation of eq. (6.10) suitable for MILP must be formulated. To handle the non-convexity of eq. (6.10), a full set of constraints and very many additional auxiliary binary variables (see eq. (6.11)) must be introduced, adding substantial computational complexity. As the UC problem is usually solved weekly and daily for short-term scheduling, it's important to keep the solution time as low as possible. The results in table 6.4 confirm that the ML-based methods are much faster than the analytical method.

Among the ML-based methods, LR has led to the lowest operation cost, while keeping the load shedding low. The SVM method with $C = 10$ has the highest amount of load shedding per outage, among the ML-based methods. As expected, the SVM with big C tends to overfit. Another interesting point to mention is that although the ML-based methods are prone to misclassifying some of the incidents, the amount of average load shedding is lower than the analytical approach. The reason is that the analytical method's prediction of frequency nadir, is based on the assumption in eq. (6.8) and then it is approximated by a piecewise linear function. It is therefore seen that both analytical and ML-based methods have their own sources of error. On the other hand, analytical methods are independent of any training dataset. This is a big advantage because the training dataset depends on the inputs of the UC problem and the topology of the system. Once the topology of the system changes (e.g. a new generator is installed) or the inputs change radically (e.g. the annual demand or availability of RES changes), the training dataset and the ML model should be updated. Another downside of ML methods is the lack of trust in the ML methods, due to their black-box nature. A summary is presented in table 6.5 that compares ML-based methods with analytical ones.

	ML based	analytical
advantages	-it can be solved in a timely manner -it doesn't increase the size of the problem too much -it can be used in more complicated formulations of UC, like robust and stochastic models	-it's independent of training data -it's directly obtained from the physics of frequency dynamics in power systems
disadvantages	-it depends on training dataset which should be updated once in a while -labelling the dataset can be hard -operators might be skeptical about ML-based methods	-it imposes a lot of new constraint and variables to UC problem -UC solution time is high -implementing it in robust and stochastic models of UC is challenging
source of error	-misclassification of the model when it's applied to real inputs -inaccuracies in labeling -ill-defined dataset	-fixed time reserve response assumption -approximate due to piecewise linearization

Table 6.5: Comparison of ML-based and analytical methods

6.4 Conclusion

This chapter uses LR and SVM to classify outages with tolerable and intolerable frequency nadir. We compared these ML-based methods against a piecewise linear approximation of the frequency nadir that uses separable programming. Both the ML-based and the analytical approaches were then tested on the same test system (La Palma Island in Spain) for purposes of solving frequency-constrained UC problems as MILP. The piecewise linearized formulation of frequency nadir is computationally much more demanding. The results of the comparison study show that our ML-based methods are as accurate as the piecewise linear formulation, without the added computational burden, in preventing the outages that exceed critical frequency nadir. This is important in

building confidence further in using ML-based methods in safety-critical applications in power systems such as solving FCUC problems. Meanwhile solving UC with ML-based frequency nadir constraint is considerably faster, results in much less computational expenditure, and allows for more flexible assumptions on system response.

7 Summary, Contributions, and Future Studies

This chapter summarizes the main approaches developed in this thesis and the main findings. It highlights the contributions and future research lines are suggested.

7.1 Problem Statement

Island power systems have some characteristics that make the operation and increment of RES more challenging. The characteristics of islands and the corresponding challenges were discussed in chapter 1. This thesis tried to address those challenges by providing novel solutions. Different methods are suggested in this thesis to make improvements in the following challenges,

- **Reserve scarcity:** in small power systems, usually the number of online units is low. In order to have enough reserve for $N-1$ contingencies, units should keep a considerable percentage of total demand as reserve. RES is unable to provide reserve on its own. So reserve scarcity is getting worse by introducing more RES.

- **Poor frequency response:** inertia is the first support in case of any contingency in the power system. Island power systems already have issues with inertia. Installing RES instead of thermal synchronous units worsens the issues, as RES can't provide inertia. Unit outages usually take out a big percentage of the whole generation in small power systems. And as the system is already suffering from a lack of inertia, frequency response after outages is bad.

- **Stochasticity:** The more popular RES like wind generation and solar generation are hard to forecast. Increasing the share of RES adds to the stochasticity of the scheduling process. Considering stochastic values in the scheduling process makes it complicated.

- **Computational burden:** Both frequency dynamics of the system and stochasticity of RES are mathematically complicated, and including them in the scheduling process imposes a lot of computational burdens.

- **Storage requirement:** The RES generation depends on environmental factors rather than power demand. In reality, in many situations, there is a lot of RES available while the demand is low and vice versa. To avoid such incidents the RES should be stored when it's

abundant, and released when the demand is high. Storage devices can also usually provide reserve and improve the frequency response.

Novel solutions are proposed in this thesis to tackle the aforementioned problems.

7.2 Contributions

7.2.1 Viability of Providing Spinning Reserves by RES

The main objective of chapter 2 is to evaluate the provision of up and down spinning reserves by RES generation. It evaluates the impact of providing spinning reserves on the system operation costs. Simulations are conducted for La Palma (small size) and Tenerife (medium size) islands with various samples of actual and future scenarios to recognize what economic impacts are expected from enabling RES to provide up and down-reserve. The economic operation has been simulated by means of an hourly UC on a weekly basis. The principal characteristics and contributions of this chapter are listed here:

- A deterministic approach considering different scenarios (seasons and years) is employed to assess the viability of providing reserve by RES.
- The methodology of this chapter is applied to two real islands, La Palma and Tenerife, with factual input data.
- Four different approaches to reserve provision are considered (RES providing no reserve, RES providing only down a reserve, RES providing up and down reserve with a fixed constant deloading factor, and RES providing up and down reserve with a variable deloading factor). These approaches are applied to various seasonal scenarios (summer, autumn, winter, and spring), both for current and future time-frames (years 2020, 2025, and 2030).
- Up reserve and down reserve are formulated and analyzed, then the impacts of each on the operation cost are included.
- Deloading is defined as a variable in the UC problem, and the amount of deloading is optimized for each hour in the last approach of RES reserve provision (main contribution).
- A total number of 240 UC weekly simulations are performed for each island.

The concluded points from chapter 2 are categorized in table 7.1. It's also shown how each point contributes to the challenges that were explained in chapter 1. Chapter 2 has been published in [22].

7.2.2 Feasibility of Providing Spinning Reserves by RES

The objective of chapter 3 is to investigate under what circumstances the provision of spinning reserves and inertia by RES provides technical benefits to real island power systems. The assessment is carried out by analyzing the impact of WTG when they operate at a fixed and at a variable deloading percentage under normal conditions. The technical impacts of providing frequency

conclusions	reserve scarcity
Using RES as down reserve providers is always beneficial for a small size island such as La Palma where the scarcity of reserve is more severe and installed RES should immediately be able to provide down reserve to avoid unnecessary spillages.	✓
It is beneficial only for high wind capacity scenarios for a medium size island such as Tenerife. For high penetration levels, providing down reserve reduces more than 40% the amount of thermal generation and more than 30% the system's cost on both islands. For low penetration levels, up spinning reserve provision by wind generation is not justified, but as the availability of wind becomes higher, the benefits of deloading wind generation to participate as up reserve becomes more apparent making 100% renewable generation possible.	✓
Deloading a constant percentage of wind for all hours is not advisable, since it imposes extra expenses and leads to more thermal generation, and can even make economic results worse compared to only providing down reserve	✓
Implementing controllers on RES to enable them to provide down-reserve, always leads to cost reduction. This cost reduction increases, when RES injection goes higher.	✓
Considering the future scenarios, the results suggest that providing reserve by RES is vital to inject more renewable energy when a high share of renewables is available in the system and helps lead to a 100% demand coverage by RES.	✓
In smaller islands, the scarcity of reserve is more severe and the installed capacity of RES should immediately be able to provide down reserve to avoid unnecessary spillages and reduce costs.	✓
For bigger islands like Tenerife, enabling RES to provide down reserve is not urgent but will be required when the share of RES grows in the future.	✓

Table 7.1: Conclusions of chapter 2

regulation by wind turbines on the system frequency response is evaluated. Simulations are carried out for La Palma (small size) and Tenerife (medium size) islands with various samples of actual and future scenarios to recognize what technical impacts are expected from enabling RES to provide reserve and frequency regulation. Simulations without UFLS schemes are presented to evaluate the frequency response quality (frequency nadir, steady-state frequency deviation), whereas simulations with the current UFLS schemes are conducted to assess the impact on load shedding. Chapter 3 uses the hourly generation scenarios of chapter 2 as a starting point. So the contributions of chapter 3 are in addition to chapter 2. The additional contributions are mentioned below,

- By taking the optimal UC schedules obtained in the chapter 2, chapter 3 simulates the dynamic responses of the system to thermal generator and wind outages and assesses the system response by a set of KPIs, such as frequency nadir or the amount of load shedding (main contribution).
- The appropriateness of the commonly used spinning reserve criterion to foster the development of RES in future demand scenarios is evaluated.

Some of the conclusions of chapter 3 are presented in table 7.2. The methodology and results of

conclusions	poor frequency response
For future scenarios of a small island like La Palma, fixed deloading always enhances the frequency quality behavior compared to variable deloading in most scenarios.	✓
Since the expected cost of UFLS is negligible due to typical values of FOR of generators, variable deloading is preferable from a strictly economical point of view.	✓
In a bigger island like Tenerife, variable deloading is only recommended for high demand and wind scenarios. It improves both dynamic response and total system cost.	✓

Table 7.2: Conclusions of chapter 3

Chapter 3 are submitted to the IET Renewable Power Generation journal. It's under the second round of revision.

7.2.3 LAES Model for Scheduling Purposes

Storing the RES on low-demand hours and using them on high-demand hours is economically advisable. In addition, LAES also contributes to spinning reserve. To prevent the overestimation of the operation cost reduction with LAES in the system, a detailed representation of LAES in the UC problem is presented in chapter 4. A detailed model can take other characteristics of LAES, like CSE and DSE into account. Contributions and features are listed below,

- An explicit LAES model has never been investigated in the literature.
- An MILP formulation of LAES, that includes CSE and DSE is developed and presented (main contribution).
- Realistic future scenarios of Tenerife island for the years 2026 and 2030 are used to validate the proposed model by solving weekly UC.
- As wind and solar availability varies from season to season, weekly sample scenarios of winter, spring, summer, and autumn are used, to provide a better insight over each year.
- The model is compared with the general formulation and the differences are pointed out.

Some of the conclusions of chapter 4 are mentioned in the table 7.3. The columns show how each conclusion is related to the challenges. Chapter 4 is published as a paper in Elsevier Energies

conclusions	reserve scarcity	storage requirement
A detailed formulation of LAES will give a more accurate insight to the operator or the planners, for expansion planning purposes.	✓	✓
With the basic model, LAES will be scheduled to start up too many times, which in reality imposes a lot of charging and discharging start energy.	✓	✓
The proposed model gives a realistic awareness of the cost and benefits of LAES.	✓	✓
By considering CSE in the scheduling process, unnecessary start-ups will be prevented to minimize unnecessary energy losses.	✓	✓
The basic model can be used for long-term planning, but it's suggested to use the detailed model for short-term operational planning, to avoid modifications during real-time operation.	✓	✓

Table 7.3: Conclusions of chapter 4

journal on the 22nd of September 2022 [68].

7.2.4 Robust FCUC Using Logistic Regression

Chapter 5 proposes a novel procedure to schedule short-term UC in island power systems. Island power systems usually suffer from a lack of inertia and frequency response capacity, complicating containing frequency within an acceptable range during large disturbances. The proposed method uses an initial dataset to train a linear constraint that takes into account the dynamic response of the system. For the purpose of training this constraint, logistic regression is employed to avoid incidents with undesirable frequency responses as much as possible. Then the logistic regression constraint is included in an adaptive robust formulation. Features and contributions are presented here,

- To build an initial set of data to train the LR model, an adaptive robust UC formulation with reserve constraint is employed and solved for different levels of the reserve requirement. The idea of using different levels of the reserve is to simultaneously determine the level actually needed.
- Every single outage of the obtained results is simulated by an SFR model, which makes the training dataset a proper representative of all acceptable and unacceptable frequency responses.
- From the training dataset, a new constraint is derived using the logistic regression procedure and then included in robust UC instead of conventional reserve constraint to ensure both frequency quality after outages, and feasibility of the result in case of any realization of the stochastic variable.
- Although the linearization happens in the training process, the new constraint does not add to the number of constraints in the UC problem, hence keeping the problem size intact.
- Logistic regression is introduced as a tool to train output data of the SFR model and develops a new constraint to be used in UC problems instead of the reserve constraint (main contribution).
- The proposed formulation does not add any new binary, integer, or free variables to the UC problem and does not enlarge the number of UC constraints, conserving the size and complexity of the problem.
- The procedure of training the new constraint is very fast and can be done by using any computer algebra system.

Some of the conclusions of this chapter are listed in table 7.4. In the columns, it's shown how each point contributes to addressing the challenges that island power systems are facing. This chapter is summarized in [87].

7.2.5 Using ML to Include Frequency Nadir in UC Problem

Chapter 6 uses and compares LR and SVM to classify outages with tolerable and intolerable frequency nadir. Further, these ML-based methods are compared with a piecewise linear approximation of the frequency nadir that uses separable programming. Both the analytical and the ML-based approaches were then tested on the La Palma island in Spain for purposes of formulating and solving frequency-constrained UC problems as mixed-integer linear programming problems. Following the line of research of the data-driven approaches, chapter 6 generates a novel synthetic training dataset and then applies ML methods to the dataset to derive a linear constraint that approximates the original non-linear frequency nadir constraint for all scenarios in the dataset. The contributions and highlights of this chapter are as follows,

- A novel synthetic data generation algorithm is presented that includes feasible operating points. These operating points are sorted by their quadratic generation cost function. Operating points that are cost-efficient are added to the training dataset. Such a dataset is only

conclusions	poor frequency response	stochasticity	computational burden
Results show that by choosing a proper cut-point, the proposed method improves the frequency response, as well as the operation costs, and is able to be employed in a RUC formulation.	✓	✓	
As training data with the LR model is very fast, the size of the training set is not an issue.			✓
A coherent training dataset can better represent the system, leading to a more reliable frequency constraint in comparison to small training datasets.	✓		
The proposed LR approach is compared with OCT in a RUC. Results show that the quality of the results is very close, while the training process of the proposed method is very faster and more cost-efficient.		✓	✓
The operator can use the proposed constraint in the RUC problem to improve the frequency response of the system after outages, instead of lengthy analytical approaches while keeping the solution-time low.	✓		✓

Table 7.4: Conclusions of chapter 5

composed of operating points that are close to the optimal solution of the UC problem, as they are feasible and cheaper. Compared to the proposed datasets in the literature, the data generation algorithm here covers all the feasible generator operating points that are likely to be picked by the solver. An advantage of this dataset is that it's not sensitive to the daily demand and RES forecast. So once it's generated, the models that are obtained from it can be used throughout the year (contribution).

- The training dataset is passed through different ML methods to train a linear constraint that can classify tolerable and intolerable frequency nadirs after any outage. This linear constraint can be directly employed in the UC problem as the frequency nadir constraint (main contribution).

- The performance of the ML methods is compared to the analytical method of predicting frequency nadir. It is shown that the UC is solved considerably faster, whilst still achieving an acceptable frequency response quality after outages ($N - 1$ security criteria). It should be noted that reducing computation times is critical when modeling uncertainties in stochastic or robust UC problems.

Some of the conclusions are listed in table 7.5. This chapter is summarized in [120].

conclusions	poor frequency response	computational burden
The piecewise linearized formulation of frequency nadir is computationally much more demanding.		✓
ML-based methods are statistically as accurate as the piecewise linear formulation, without the added computational burden, in preventing the outages that exceed critical frequency nadir.	✓	✓
While solving UC with ML-based frequency nadir constraint has a considerably lower run-time, it has a good performance and allows for more flexible assumptions on system response.	✓	✓

Table 7.5: Conclusions of chapter 6

7.3 Future Studies

- The last two chapters of the thesis try to reflect the frequency metrics like RoCoF, steady-state frequency, and frequency nadir in the UC problem. Another important measure after outages is the UFLS activation. The amount of UFLS activation not only depends on the frequency dynamics but also on the activation scheme. Usually, UFLS activation is stepwise and discrete, which makes it very hard to formulate and implement it in an MILP problem. In theory, estimating the amount of UFLS for outages and including it in the scheduling process is very useful. Because the amount is in megawatts and can be used directly in some of the constraints and even the objective function.

- Extracting an analytical MILP formulation of UFLS is very complicated, to say the least. As was seen in the last two chapters, ML methods are looking very promising to represent and estimate non-linear quantities with fairly simple constraints. It would be interesting to find suitable ML methods to learn UFLS, so it can be implemented in the UC problem.

- In this thesis, only classical ML methods are used. The natural progression for future studies is to use newer ML methods like DNN and other innovative methods. The use of ML methods in the scheduling of the power systems has a lot of room to explore.

- To maximize the potentials of the ancillary service providers that are introduced in chapter 2, chapter 3, and chapter 4, they should be incorporated in a scheduling process that considers the dynamics of the system. The proposed methods in chapter 5 and chapter 6 can include the inertia and reserve that deloading of the RES offers. The labeling of the ML methods can be updated with the presence of inertia from deloading to optimize the scheduling process of deloading while considering their inertia and additional reserve.

- It's interesting to study how the uncertainty of the wind input affects the scheduling of the deloading and its potential benefits. Using a robust formulation to study this is challenging because another non-linear term will appear in the dual form of the problem, which is the multiplication of the reserve constraint dual variable and the uncertain wind input.
- It's interesting to study the impact of short-term uncertainty of wind and PV on providing reserve. To find out ways to tackle these short-term changes and make sure enough reserve is always available. Also, the potential for demand flexibility seems promising in this line of research. here again, there is uncertainty on whether the forecasted flexible demand will be actually responding as expected. And if not, how it influences the frequency stability of the system.

Acronyms

CAES	compressed air energy storage
CHP	combined heat and power
CSE	charging start energy
CSP	charging start power
CST	charging start time
DC	direct current
DNN	deep neural network
DSE	discharging start energy
DSP	discharging start power
DST	discharging start time
ED	economic dispatch
EES	energy storage system
ESS	energy storage system
FCUC	frequency constrained unit commitment
FOR	forced outage rate
HQFR	high quality frequency response
HSS	hydrogen storage system
HTES	high-temperature thermal energy storage
IUC	interval unit commitment
KPI	key performance indicator
LAES	liquid air energy storage
LNG	liquefied natural gas
LQFR	low quality frequency response
LR	logistic regression
LSC	load shedding cost
MILP	mixed integer linear programming
ML	machine learning
MPPT	maximum power point tracking
MW	megawatt
OC	outage cost
OCT	optimal classifier trees
PHES	pumped hydroelectric energy storage
PHS	pumped hydro storage
PRD	primary response duration
PV	photo voltaic
RES	renewable energy sources

RoCoF	Rate of Change of Frequency
ROM	read-only memory
RRM	renewable reserve multiplier
RUC	robust unit commitment
SFR	system frequency response
SMES	superconducting magnetic energy storage
SUC	stochastic unit commitment
SVM	support vector machine
UC	unit commitment
UFLS	under frequency load shedding
WTG	wind turbine generator

Nomenclature

The Nomenclature section is divided into subsections to make it easier to use. Variables, functions, indices, and sets are mentioned in the definition of each symbol.

Related to Dealoding:

C_t^{UFLS}	cost of UFLS [€]
$CRES$	set of controllable RES
$cres$	index of controllable RES
DF_t	deloading factor at t
DRR_t	down reserve requirement at t [MW]
DW	set of deloading wind units
dw	index of deloading wind units
k_{DR}	down reserve requirement coefficient
k_{RV}	expected renewable output variations
LS_t	total UFLS [MW]
P_t^{RES}	available RES at t [MW]
$p_t^{spilled}$	variable of spilled RES at t [MW]
$r_{t,i}^{down}$	down reserve variable [MW]
$r_{t,i}^{up}$	up reserve variable [MW]
RES	set of RES
res	index of RES
URR_t	up reserve requirement at t [MW]

SFR Model:

Δd	load deviation [p.u.]
Δp	mechanical power deviation [p.u.]
$\Delta \dot{w}_i$	frequency deviation [p.u.]
$\mathcal{H}$	inertia [s]
$\mathcal{K}$	normalized gain of turbine-governor model

$\mathcal{M}$	base rated power of units [MW]
$\mathcal{S}$	base power of the system [MW]
$\widetilde{\Delta d}$	total load deviation [p.u.]
$\widetilde{\Delta p}$	total mechanical power deviation [p.u.]
$a_.$	poles of the second order system
$b_.$	zeros of the second order system
k	inverse of the droop [p.u.]
N	total number of contingencies
n	index of contingency

General UC:this is small

$\mathcal{D}_t$	demand at t [MW]
$\mathcal{I}$	set of all generators
$\mathcal{T}$	set of all time intervals
$\overline{\mathcal{P}}_i$	maximum power output of generator i [MW]
$\overline{\mathcal{R}}_i$	maximum ramp-up of generator i [MW/h]
$\underline{\mathcal{P}}_i$	minimum power output of generator i [MW]
$\underline{\mathcal{R}}_i$	maximum ramp-down of generator i [MW/h]
DT	minimum down-time of generators [hours]
gc	generation costs function [€]
I	number of generators
i	index of generators
ii	alias index for generators
p	power generation variable [MW]
r	online reserve power variable [MW]
S	available solar [MW]
sg	solar generation variable [MW]
$suc(.)$	start-up costs function [€]
T	Number of time intervals
t	index of time intervals
tt	alias index for time intervals
u	commitment variable [$\in\{0,1\}$]

UT	minimum up-time of generators [hours]
v	start-up variable [$\in\{0,1\}$]
W	available wind [MW]
w	shut-down variable [$\in\{0,1\}$]
wg	wind generation variable [MW]

Related to LAES:

$\overline{\mathcal{P}}_{char}$	LAES maximum charging [MW]
$\overline{\mathcal{P}}_{dischar}$	LAES maximum discharging [MW]
$\overline{\mathcal{R}}_{dischar}$	maximum discharge ramp of LAES
$\underline{\mathcal{P}}^{char}$	LAES minimum charging [MW]
$\underline{\mathcal{P}}^{dischar}$	LAES minimum discharging [MW]
ξ^{LAES}	LAES round-trip efficiency
e^{LAES}	LAES energy state variable [MW]
e_0^{LAES}	LAES initial energy state [MW]
e_T^{LAES}	LAES final energy state [MW]
p^{char}	LAES charge power variable [MW]
$p^{dischar}$	LAES discharge power variable [MW]
r^{BESS}	BESS power reserve [MW]
r^{LAES}	LAES power reserve variable [MW]
r^{Ther}	thermal power reserve variable [MW]
u^{char}	LAES charging status variable [$\in\{0,1\}$]
$u^{dischar}$	LAES discharging status variable [$\in\{0,1\}$]
v^{char}	LAES charging start-up variable [$\in\{0,1\}$]
$v^{dischar}$	LAES discharging start-up variable [$\in\{0,1\}$]
w^{char}	LAES charging shut-down variable [$\in\{0,1\}$]
$w^{dischar}$	LAES discharging shut-down variable [$\in\{0,1\}$]

Related to ML:

$\ell(.)$	loss function
$\hat{y}$	predicted label
$\mathcal{X}$	set of all features
$\mathcal{Y}$	set of all labels

$\overline{\mathcal{D}}$	maximum annual thermal generation
Θ	set of θ parameters
θ	coefficients in the linear model
$\underline{\mathcal{D}}$	minimum annual thermal generation
C	regularization coefficient
$f_\theta(x)$	hypothesis function
FC	set of feasible combinations
K_i	number of the steps
M	number of features
m	index of features
N	number of data samples
n	index of data samples
x	features of the dataset
y	labels of the dataset

Logistic Regression:

$\pi(.)$	probability function
ψ	regression cut-point
υ	dependant variable
ξ	independent variable
c	regression coefficient
f^{nadir}	the minimum value of frequency reached during the transient period
f^{qss}	quasi steady-state frequency

Robust UC:

$\mathbb{R}$	set of real numbers
$\mathbb{Z}$	set of integer numbers
$\mathcal{F}$	set of extreme rays
$\mathcal{O}$	set of extreme points
$\phi(.)$	auxiliary variable
θ	set of dual variables
A	integer variable multiplier matrix
B	integer variable multiplier matrix

b	right hand side of integer constraint
c	integer variable cost vector
C_i	cost coefficient of generator i
d	continuous variable cost vector
D	continuous variable multiplier matrix
$f(x)$	value function
g	right hand side of mixed constraints
x	integer variable
$y(.)$	continuous variable
α	dual variable of minimum power constraint
β	dual variable of maximum power constraint
δ	dual variable of up ramp constraint
η	dual variable of power balance constraint
Γ	set of dual variables
γ	dual variable of down ramp constraint
μ	dual variable of minimum reserve constraint
Ω	wind generation scenarios
ω	wind generation uncertainty
ρ	dual variable of LR constraint
ζ	dual variable of maximum wind constraint

Frequency dynamics:

α, β	normalizing coefficients
$\Delta f'_{crit}$	critical rate of change of frequency [Hz/s]
Δf_{crit}^{nadir}	critical frequency nadir [Hz]
Δf_{crit}^{ss}	critical steady state frequency [Hz]
ℓ	index of the lost generator
γ_j	binary operator of affine segments [$\in$\{0,1\}]
λ_j	weight associated with breaking point j
τ	time
a_j	breaking point
D	load damping factor [%/Hz]

$f(t)$	frequency [Hz]
f_0	nominal frequency [Hz]
J	number of the breaking points
j	breaking point index
P_ℓ	lost power [MW]
P_e	electrical power [MW]
P_m	mechanical power [MW]
T_g	delivery time of units [s]
z_1, z_2	auxiliaries for changing variables

Bibliography

1. L. Sigrist, E. Lobato, F. M. Echavarren, I. Egido, and L. Rouco. *Island power systems*. CRC Press, 2016.
2. P. Blechinger, R. Seguin, C. Cader, P. Bertheau, and C. Breyer. "Assessment of the global potential for renewable energy storage systems on small islands". *Energy Procedia* 46, 2014, pp. 325–331.
3. A.-K. Gerlach, E. Gaudchau, C. Cader, V. Wasgindt, and C. Breyer. "Comprehensive country ranking for renewable energy based mini-grids providing rural off-grid electrification". In: *The second international conference on micro perspectives for decentralized energy supply, Berlin, February*. 2013.
4. L. Sigrist, I. Egido, and L. Rouco. "A method for the design of UFLS schemes of small isolated power systems". *IEEE Transactions on Power Systems* 27:2, 2011, pp. 951–958.
5. C. Concordia, L. H. Fink, and G. Poullikkas. "Load shedding on an isolated system". *IEEE Transactions on Power Systems* 10:3, 1995, pp. 1467–1472.
6. L. Sigrist, L. Rouco, and F. M. Echavarren. "A review of the state of the art of UFLS schemes for isolated power systems". *International Journal of Electrical Power & Energy Systems* 99, 2018, pp. 525–539.
7. L. Sigrist. "A UFLS scheme for small isolated power systems using rate-of-change of frequency". *IEEE Transactions on Power Systems* 30:4, 2014, pp. 2192–2193.
8. M. Imanaka, S. Toyoda, S. Sugimoto, and T. Kato. "Coordinated Control of Demand Response for Large Installation of Renewable Energy Sources in Isolated Islands". *Int J Electr Electron Eng Telecommun* 11:05, 2022, pp. 325–332.
9. A. Genave, S. Blancard, and S. Garabedian. "An assessment of energy vulnerability in Small Island Developing States". *Ecological Economics* 171, 2020, p. 106595.
10. H. He, Y. Huang, A. Nakadomari, H. Masrur, N. Krishnan, A. M. Hemeida, A. Mikhaylov, and T. Senjyu. "Potential and economic viability of green hydrogen production from seawater electrolysis using renewable energy in remote Japanese islands". *Renewable Energy* 202, 2023, pp. 1436–1447.
11. C. Hamon. "On frequency control schemes in power systems with large amounts of wind power". PhD thesis. KTH Royal Institute of Technology, 2012.
12. M. Uche-Soria and C. Rodríguez-Monroy. "Special regulation of isolated power systems: The Canary Islands, Spain". *Sustainability* 10:7, 2018, p. 2572.
13. V. Kumar, R. Naresh, and A. Singh. "Investigation of solution techniques of unit commitment problems: A review". *Wind Engineering* 45:6, 2021, pp. 1689–1713.

14. X. Wang, L. Ying, K. Wen, and S. Lu. "Bi-level non-convex joint optimization model of energy storage in energy and primary frequency regulation markets". *International Journal of Electrical Power & Energy Systems* 134, 2022, p. 107408.
15. D. Rebollal, M. Chinchilla, D. Santos-Martín, and J. M. Guerrero. "Endogenous approach of a frequency-constrained unit commitment in islanded microgrid systems". *Energies* 14:19, 2021, p. 6290.
16. A. Darbandsari and T. Amraee. "Under frequency load shedding for low inertia grids utilizing smart loads". *International Journal of Electrical Power & Energy Systems* 135, 2022, p. 107506.
17. K. S. Ratnam, K. Palanisamy, and G. Yang. "Future low-inertia power systems: Requirements, issues, and solutions-A review". *Renewable and Sustainable Energy Reviews* 124, 2020, p. 109773.
18. M. H. Athari and Z. Wang. "Modeling the uncertainties in renewable generation and smart grid loads for the study of the grid vulnerability". In: *2016 IEEE Power & Energy Society Innovative Smart Grid Technologies Conference (ISGT)*. IEEE. 2016, pp. 1–5.
19. A. Belderbos and E. Delarue. "Accounting for flexibility in power system planning with renewables". *International Journal of Electrical Power & Energy Systems* 71, 2015, pp. 33–41.
20. Y. Rivera-Durán, C. Berna-Escriche, Y. Córdova-Chávez, and J. L. Muñoz-Cobo. "Assessment of a Fully Renewable Generation System with Storage to Cost-Effectively Cover the Electricity Demand of Standalone Grids: The Case of the Canary Archipelago by 2040". *Machines* 11:1, 2023, p. 101.
21. M. S. Javadi, M. Lotfi, M. Gough, A. E. Nezhad, S. F. Santos, and J. P. Catalao. "Optimal spinning reserve allocation in presence of electrical storage and renewable energy sources". In: *2019 IEEE International Conference on Environment and Electrical Engineering and 2019 IEEE Industrial and Commercial Power Systems Europe (EEEIC/I&CPS Europe)*. IEEE. 2019, pp. 1–6.
22. M. Rajabdorri, L. Sigrist, E. Lobato Miguélez, M. d. C. Prats Soriano, and F. Echavarren Cerezo. "Viability of providing spinning reserves by RES in Spanish island power systems". *IET Renewable Power Generation*, 2021.
23. C. W. Hansen and A. D. Papalexopoulos. "Operational impact and cost analysis of increasing wind generation in the Island of Crete". *IEEE Systems Journal* 6:2, 2011, pp. 287–295.
24. H. C. Gils and S. Simon. "Carbon neutral archipelago–100% renewable energy supply for the Canary Islands". *Applied energy* 188, 2017, pp. 342–355.
25. J. Schallenberg-Rodriguez. "Photovoltaic techno-economical potential on roofs in the Canary Islands". *Journal of Sustainable Development of Energy, Water and Environment Systems* 2:1, 2014, pp. 68–87.
26. J. Schallenberg-Rodriguez and N. G. Montesdeoca. "Spatial planning to estimate the offshore wind energy potential in coastal regions and islands. Practical case: The Canary Islands". *Energy* 143, 2018, pp. 91–103.

27. T. Adefarati and R. Bansal. "Integration of renewable distributed generators into the distribution system: a review". *IET Renewable Power Generation* 10:7, 2016, pp. 873–884.

28. R. Yan, T. K. Saha, N. Modi, N.-A. Masood, and M. Mosadeghy. "The combined effects of high penetration of wind and PV on power system frequency response". *Applied Energy* 145, 2015, pp. 320–330.

29. I. D. Margaris, S. A. Papathanassiou, N. D. Hatziargyriou, A. D. Hansen, and P. Sorensen. "Frequency control in autonomous power systems with high wind power penetration". *IEEE Transactions on sustainable energy* 3:2, 2012, pp. 189–199.

30. J. Liu, S. Feng, K. Wang, X. Guo, and L. Xu. "Method to determine spinning reserve requirement for a grid with large-scale wind power penetration". *The Journal of Engineering* 2017:13, 2017, pp. 1686–1691.

31. M. Bucksteeg, L. Niesen, and C. Weber. "Impacts of dynamic probabilistic reserve sizing techniques on reserve requirements and system costs". *IEEE Transactions on Sustainable Energy* 7:4, 2016, pp. 1408–1420.

32. M. Hedayati-Mehdiabadi, K. W. Hedman, and J. Zhang. "Reserve policy optimization for scheduling wind energy and reserve". *IEEE Transactions on Power Systems* 33:1, 2017, pp. 19–31.

33. J. B. Cardell and C. L. Anderson. "A flexible dispatch margin for wind integration". *IEEE Transactions on Power Systems* 30:3, 2014, pp. 1501–1510.

34. M. Asensio and J. Contreras. "Stochastic unit commitment in isolated systems with renewable penetration under CVaR assessment". *IEEE Transactions on Smart Grid* 7:3, 2015, pp. 1356–1367.

35. H. Gu, R. Yan, T. K. Saha, E. Muljadi, J. Tan, and Y. Zhang. "Zonal inertia constrained generator dispatch considering load frequency relief". *IEEE Transactions on Power Systems* 35:4, 2020, pp. 3065–3077.

36. Y. Wang, H. Bayem, M. Giralt-Devant, V. Silva, X. Guillaud, and B. Francois. "Methods for assessing available wind primary power reserve". *IEEE Transactions on Sustainable Energy* 6:1, 2014, pp. 272–280.

37. V. Gevorgian, Y. Zhang, and E. Ela. "Investigating the impacts of wind generation participation in interconnection frequency response". *IEEE transactions on Sustainable Energy* 6:3, 2014, pp. 1004–1012.

38. J. Dai, Y. Tang, Q. Wang, and P. Jiang. "Aggregation frequency response modeling for wind power plants with primary frequency regulation service". *IEEE Access* 7, 2019, pp. 108561–108570.

39. F. Teng and G. Strbac. "Assessment of the role and value of frequency response support from wind plants". *IEEE Transactions on Sustainable Energy* 7:2, 2016, pp. 586–595.

40. M. Dreidy, H. Mokhlis, and S. Mekhilef. "Inertia response and frequency control techniques for renewable energy sources: A review". *Renewable and sustainable energy reviews* 69, 2017, pp. 144–155.

41. C. Pradhan and C. N. Bhende. "Enhancement in primary frequency regulation of wind generator using fuzzy-based control". *Electric Power Components and Systems* 44:15, 2016, pp. 1669–1682.

42. L.-R. Chang-Chien, W.-T. Lin, and Y.-C. Yin. "Enhancing frequency response control by DFIGs in the high wind penetrated power systems". *IEEE transactions on power systems* 26:2, 2010, pp. 710–718.

43. S. Liao, J. Xu, Y. Sun, Y. Bao, and B. Tang. "Wide-area measurement system-based online calculation method of PV systems de-loaded margin for frequency regulation in isolated power systems". *IET Renewable Power Generation* 12:3, 2018, pp. 335–341.

44. S. I. Abouzeid, Y. Guo, and H.-C. Zhang. "Dynamic control strategy for the participation of variable speed wind turbine generators in primary frequency regulation". *Journal of Renewable and Sustainable Energy* 11:1, 2019, p. 013304.

45. G. Shu-Feng, Z. Jie-Tan, A. Philip, H. Li-Li, and J. Jing. "A review of wind turbine deloaded operation techniques for primary frequency control in power system". In: *2018 China International Conference on Electricity Distribution (CICED)*. IEEE. 2018, pp. 63–71.

46. K. Vidyanandan and N. Senroy. "Primary frequency regulation by deloaded wind turbines using variable droop". *IEEE transactions on Power Systems* 28:2, 2012, pp. 837–846.

47. D. Kumar, P. Sharma, H. Mathur, S. Bhanot, and R. Bansal. "Modified deloading strategy of wind turbine generators for primary frequency regulation in micro-grid". *Technology and Economics of Smart Grids and Sustainable Energy* 5:1, 2020, pp. 1–12.

48. G. de Canarias. *Anuario energético de Canarias*. 2020.

49. L. Sigrist, E. Lobato, L. Rouco, M. Gazzino, and M. Cantù. "Economic assessment of smart grid initiatives for island power systems". *Applied Energy* 189, 2017, pp. 403–415.

50. E. B. Hedo. "Real Decreto 738/2015, de 31 de julio, por el que se regula la actividad de producción de energíaeléctrica y el procedimiento de despacho en los sistemas eléctricos de los territorios no peninsulares". *Actualidad Juridica Ambiental* 49, 2015, pp. 54–55.

51. M. de Industria turismo comercio. "Real decreto 738/2015, de 31 de julio, por el que se regula la actividad de producción de energía eléctrica y el procedimiento de despacho en los sistemas eléctricos de los territorios no peninsulares". *BOE-A-2015-8646, 2015. Retrieved March 20th, 2019*, 2015.

52. D. Rajan, S. Takriti, et al. "Minimum up/down polytopes of the unit commitment problem with start-up costs". *IBM Res. Rep* 23628, 2005, pp. 1–14.

53. J. Ostrowski, M. F. Anjos, and A. Vannelli. "Tight mixed integer linear programming formulations for the unit commitment problem". *IEEE Transactions on Power Systems* 27:1, 2011, pp. 39–46.

54. A. J. Conejo and L. Baringo. *Power system operations*. Vol. 11. Springer, 2018.

55. E. L. Miguélez, I. E. Cortés, L. R. Rodríguez, and G. L. Camino. "An overview of ancillary services in Spain". *Electric Power Systems Research* 78:3, 2008, pp. 515–523.

56. C. Pradhan and C. Bhende. "Enhancement in primary frequency contribution using dynamic deloading of wind turbines". *IFAC-PapersOnLine* 48:30, 2015, pp. 13–18.

57. H. Wang, J. Yang, Z. Chen, W. Ge, Y. Ma, Z. Xing, and L. Yang. "Model predictive control of PMSG-based wind turbines for frequency regulation in an isolated grid". *IEEE Transactions on Industry Applications* 54:4, 2018, pp. 3077–3089.

58. A. K. Mishra, P. Mishra, and H. Mathur. "A deep learning assisted adaptive nonlinear deloading strategy for wind turbine generator integrated with an interconnected power system for enhanced load frequency control". *Electric Power Systems Research* 214, 2023, p. 108960.

59. A. Hosseinipour and H. Hojabri. "Virtual inertia control of PV systems for dynamic performance and damping enhancement of DC microgrids with constant power loads". *IET Renewable Power Generation* 12:4, 2018, pp. 430–438.

60. A. B. T. Attya and J. L. Dominguez-Garcia. "Insights on the provision of frequency support by wind power and the impact on energy systems". *IEEE Transactions on Sustainable Energy* 9:2, 2017, pp. 719–728.

61. T. Nielsen and M. Windolf. "GRANI: A full scale "Live Lab" for new intelligent solutions within renewable energy". In: *3rd NESSIS Euroelectric conference toward a sustainable energy future for island systems*. 2010, pp. 26–27.

62. D. M. Gioutsos, K. Blok, L. van Velzen, and S. Moorman. "Cost-optimal electricity systems with increasing renewable energy penetration for islands across the globe". *Applied energy* 226, 2018, pp. 437–449.

63. Y. Tan, L. Meegahapola, and K. M. Muttaqi. "A suboptimal power-point-tracking-based primary frequency response strategy for DFIGs in hybrid remote area power supply systems". *IEEE Transactions on Energy Conversion* 31:1, 2015, pp. 93–105.

64. G. Ramtharan, N. Jenkins, and J. Ekanayake. "Frequency support from doubly fed induction generator wind turbines". *IET Renewable Power Generation* 1:1, 2007, pp. 3–9.

65. L. Sigrist. "Design of underfrequency load-shedding schemes of small isolated power systems", 2010.

66. K.-b. Kwon, H. Park, J.-K. Lyu, and J.-K. Park. "Cost analysis method for estimating dynamic reserve considering uncertainties in supply and demand". *Energies* 9:10, 2016, p. 845.

67. L. Sigrist, I. Egido, E. L. Miguélez, and L. Rouco. "Sizing and controller setting of ultracapacitors for frequency stability enhancement of small isolated power systems". *IEEE Transactions on Power Systems* 30:4, 2014, pp. 2130–2138.

68. M. Rajabdorri, L. Sigrist, and E. Lobato. "Liquid Air Energy Storage Model for Scheduling Purposes in Island Power Systems". *Energies* 15:19, 2022, p. 6958.

69. S. Koohi-Fayegh and M. A. Rosen. "A review of energy storage types, applications and recent developments". *Journal of Energy Storage* 27, 2020, p. 101047.

70. A. Olabi, C. Onumaegbu, T. Wilberforce, M. Ramadan, M. A. Abdelkareem, and A. H. Al–Alami. "Critical review of energy storage systems". *Energy* 214, 2021, p. 118987.

71. J. Wei, Y. Zhang, J. Wang, L. Wu, P. Zhao, and Z. Jiang. "Decentralized Demand Management Based on Alternating Direction Method of Multipliers Algorithm for Industrial Park with CHP Units and Thermal Storage". *Journal of Modern Power Systems and Clean Energy* 10:1, 2022, pp. 120–130.

72. Z. Wang, W. Xiong, R. Carriveau, D. S.-K. Ting, and Z. Wang. "Energy, exergy, and sensitivity analyses of underwater compressed air energy storage in an island energy system". *International Journal of Energy Research* 43:6, 2019, pp. 2241–2260.

73. M. Budt, M. Hadam, and E. Schischke. "Low-temperature Adiabatic Compressed Air Energy Storage for Island Applications". In: *2019 Offshore Energy and Storage Summit (OSES)*. IEEE. 2019, pp. 1–8.

74. E. Borri, A. Tafone, A. Romagnoli, and G. Comodi. "A review on liquid air energy storage: History, state of the art and recent developments". *Renewable and Sustainable Energy Reviews* 137, 2021, p. 110572.

75. M. V. P. Menezes, I. F. Vilasboas, and J. A. M. da Silva. "Liquid Air Energy Storage System (LAES) Assisted by Cryogenic Air Rankine Cycle (ARC)". *Energies* 15:8, 2022, p. 2730.

76. S. B. Mousavi, M. H. Nabat, A. R. Razmi, and P. Ahmadi. "A comprehensive study and multi-criteria optimization of a novel sub-critical liquid air energy storage (SC-LAES)". *Energy Conversion and Management* 258, 2022, p. 115549.

77. M. H. Nabat, M. Zeynalian, A. R. Razmi, A. Arabkoohsar, and M. Soltani. "Energy, exergy, and economic analyses of an innovative energy storage system; liquid air energy storage (LAES) combined with high-temperature thermal energy storage (HTES)". *Energy Conversion and Management* 226, 2020, p. 113486.

78. M. Qi, J. Park, J. Kim, I. Lee, and I. Moon. "Advanced integration of LNG regasification power plant with liquid air energy storage: Enhancements in flexibility, safety, and power generation". *Applied energy* 269, 2020, p. 115049.

79. J. Park, S. Cho, M. Qi, W. Noh, I. Lee, and I. Moon. "Liquid air energy storage coupled with liquefied natural gas cold energy: focus on efficiency, energy capacity, and flexibility". *Energy* 216, 2021, p. 119308.

80. Z. Gao, W. Ji, L. Guo, X. Fan, and J. Wang. "Thermo-economic analysis of the integrated bidirectional peak shaving system consisted by liquid air energy storage and combined cycle power plant". *Energy Conversion and Management* 234, 2021, p. 113945.

81. Y.-Y. Hong, G. F. D. Apolinario, T.-K. Lu, and C.-C. Chu. "Chance-constrained unit commitment with energy storage systems in electric power systems". *Energy Reports* 8, 2022, pp. 1067–1090.

82. M. Sedighizadeh, M. Esmaili, and S. M. Mousavi-Taghiabadi. "Optimal joint energy and reserve scheduling considering frequency dynamics, compressed air energy storage, and wind turbines in an electrical power system". *Journal of Energy Storage* 23, 2019, pp. 220–233.

83. S. Nojavan, A. Najafi-Ghalelou, M. Majidi, and K. Zare. "Optimal bidding and offering strategies of merchant compressed air energy storage in deregulated electricity market using robust optimization approach". *Energy* 142, 2018, pp. 250–257.

84. C. Damak, D. Leducq, H. M. Hoang, D. Negro, and A. Delahaye. "Liquid Air Energy Storage (LAES) as a large-scale storage technology for renewable energy integration–A review of investigation studies and near perspectives of LAES". *International Journal of Refrigeration* 110, 2020, pp. 208–218.

85. A. Vecchi, Y. Li, P. Mancarella, and A. Sciacovelli. "Integrated techno-economic assessment of Liquid Air Energy Storage (LAES) under off-design conditions: Links between provision of market services and thermodynamic performance". *Applied Energy* 262, 2020, p. 114589.

86. REE. "Estudios de prospectiva del sistema y necesidades para su operabilidad", 2020. URL: https://www.ree.es/sites/default/files/01_ACTIVIDADES/Documentos/Prospectiva_y_Operabilidad_Reunion_GSP29Sep20.pdf.

87. M. Rajabdorri, E. Lobato, and L. Sigrist. "Robust frequency constrained uc using data driven logistic regression for island power systems". *IET Generation, Transmission & Distribution* 16:24, 2022, pp. 5069–5083. DOI: https://doi.org/10.1049/gtd2.12658. eprint: https://ietresearch.onlinelibrary.wiley.com/doi/pdf/10.1049/gtd2.12658. URL: https://ietresearch.onlinelibrary.wiley.com/doi/abs/10.1049/gtd2.12658.

88. A. F. Zobaa and S. A. Aleem. *Uncertainties in Modern Power Systems*. Academic Press, 2020.

89. C. Ning and F. You. "Data-driven adaptive robust unit commitment under wind power uncertainty: A Bayesian nonparametric approach". *IEEE Transactions on Power Systems* 34:3, 2019, pp. 2409–2418.

90. M. Zhang, J. Fang, X. Ai, B. Zhou, W. Yao, Q. Wu, and J. Wen. "Partition-combine uncertainty set for robust unit commitment". *IEEE Transactions on Power Systems* 35:4, 2020, pp. 3266–3269.

91. Y. Cho, T. Ishizaki, and J.-I. Imura. "Three-stage Robust Unit Commitment Considering Decreasing Uncertainty in Wind Power Forecasting". *IEEE Transactions on Industrial Informatics*, 2021.

92. M. Habibi, V. Vahidinasab, J. Aghaei, and B. Mohammadi-Ivatloo. "Assessment of energy storage systems as a reserve provider in stochastic network constrained unit commitment". *IET Smart Grid* 4:2, 2021, pp. 139–150.

93. H. Huang, M. Zhou, and G. Li. "An endogenous approach to quantifying the wind power reserve". *IEEE Transactions on Power Systems* 35:3, 2019, pp. 2431–2442.

94. V. Prakash, P. Kushwaha, K. C. Sharma, and R. Bhakar. "Frequency response support assessment from uncertain wind generation". *International Journal of Electrical Power & Energy Systems* 134, 2022, p. 107465.

95. V. Trovato, A. Bialecki, and A. Dallagi. "Unit commitment with inertia-dependent and multispeed allocation of frequency response services". *IEEE Transactions on Power Systems* 34:2, 2018, pp. 1537–1548.

96. L. Badesa, F. Teng, and G. Strbac. "Simultaneous scheduling of multiple frequency services in stochastic unit commitment". *IEEE Transactions on Power Systems* 34:5, 2019, pp. 3858–3868.

97. M. Paturet, U. Markovic, S. Delikaraoglou, E. Vrettos, P. Aristidou, and G. Hug. "Stochastic unit commitment in low-inertia grids". *IEEE Transactions on Power Systems* 35:5, 2020, pp. 3448–3458.

98. F. Pérez-Illanes, E. Álvarez-Miranda, C. Rahmann, and C. Campos-Valdés. "Robust unit commitment including frequency stability constraints". *Energies* 9:11, 2016, p. 957.

99. S. M. Mousavi-Taghiabadi, M. Sedighizadeh, M. Zangiabadi, and A. S. Fini. "Integration of wind generation uncertainties into frequency dynamic constrained unit commitment considering reserve and plug in electric vehicles". *Journal of Cleaner Production* 276, 2020, p. 124272.

100. P. Rabbanifar and N. Amjady. "Frequency-constrained unit-commitment using analytical solutions for system frequency responses considering generator contingencies". *IET Generation, Transmission & Distribution* 14:17, 2020, pp. 3548–3560.

101. M. Shahidehpour, T. Ding, Q. Ming, J. P. Catalao, and Z. Zeng. "Two-Stage Chance-Constrained Stochastic Unit Commitment for Optimal Provision of Virtual Inertia in Wind-Storage Systems". *IEEE Transactions on Power Systems*, 2021.

102. D. Lagos and N. D. Hatziargyriou. "Data-Driven Frequency Dynamic Unit Commitment for Island Systems with high RES penetration". *IEEE Transactions on Power Systems*, 2021.

103. Y. Zhang, C. Chen, G. Liu, T. Hong, and F. Qiu. "Approximating trajectory constraints with machine learning–microgrid islanding with frequency constraints". *IEEE Transactions on Power Systems* 36:2, 2020, pp. 1239–1249.

104. Y. Zhang, H. Cui, J. Liu, F. Qiu, T. Hong, R. Yao, and F. Li. "Encoding frequency constraints in preventive unit commitment using deep learning with region-of-interest active sampling". *IEEE Transactions on Power Systems* 37:3, 2021, pp. 1942–1955.

105. Y. Shen, W. Wu, B. Wang, Y. Yang, and Y. Lin. "Data-Driven Convexification for Frequency Nadir Constraint of Unit Commitment". *Journal of Modern Power Systems and Clean Energy*, 2022.

106. H.-W. Chiu, L.-R. Chang-Chien, and C.-C. Wu. "Construction of a frequency compliant unit commitment framework using an ensemble learning technique". *Energies* 14:2, 2021, p. 310.

107. J. M. Hilbe. *Practical guide to logistic regression*. crc Press, 2016.

108. P. Khosravi, Y. Liang, Y. Choi, and G. V. d. Broeck. "What to expect of classifiers? reasoning about logistic regression with missing features". *arXiv preprint arXiv:1903.01620*, 2019.

109. S. Lahaie. "How to take the Dual of a Linear Program". *Columbia University, New York*, 2008.

110. P. Bonami, D. Salvagnin, and A. Tramontani. "Implementing Automatic Benders Decomposition in a Modern MIP Solver." In: *IPCO*. 2020, pp. 78–90.

111. D. Bertsimas, E. Litvinov, X. A. Sun, J. Zhao, and T. Zheng. "Adaptive robust optimization for the security constrained unit commitment problem". *IEEE transactions on power systems* 28:1, 2012, pp. 52–63.

112. G. Morales-España, Á. Lorca, and M. M. de Weerdt. "Robust unit commitment with dispatchable wind power". *Electric Power Systems Research* 155, 2018, pp. 58–66.

113. Z. C. Taşkin. "Benders Decomposition". *Wiley Encyclopedia of Operations Research and Management Science* January 2011, 2011. DOI: 10.1002/9780470400531.eorms0104.

114. R. Fletcher and S. Leyffer. "Solving mixed integer nonlinear programs by outer approximation". *Mathematical programming* 66:1, 1994, pp. 327–349.

115. D. G. Kleinbaum, L. L. Kupper, A. Nizam, and E. S. Rosenberg. *Applied regression analysis and other multivariable methods*. Cengage Learning, 2013.

116. F. L. Huang and T. R. Moon. "What are the odds of that? A primer on understanding logistic regression". *Gifted Child Quarterly* 57:3, 2013, pp. 197–204.

117. A. E. de Canarias. "Consejería de Transición Ecológica, Lucha contra el Cambio Climático y Planificación Territorial". *Gobierno de Canarias*, 2019.

118. H. Pandzic, Y. Dvorkin, T. Qiu, Y. Wang, and D. Kirschen. "Unit Commitment under Uncertainty -GAMS Models", 2015. DOI: 10.13140/RG.2.1.1180.0485.

119. D. Bertsimas and J. Dunn. "Optimal classification trees". *Machine Learning* 106:7, 2017, pp. 1039–1082. ISSN: 15730565. DOI: 10.1007/s10994-017-5633-9.

120. M. Rajabdorri, B. Kazemtabrizi, M. Troffaes, L. Sigrist, and E. Lobato. "Inclusion of Frequency Nadir constraint in the Unit Commitment Problem of Small Power Systems Using Machine Learning". *arXiv e-prints*, arXiv:2210.01540, 2022, arXiv:2210.01540. arXiv: 2210.01540 [eess.SY].

121. C. Ferrandon-Cervantes, B. Kazemtabrizi, and M. C. Troffaes. "Inclusion of frequency stability constraints in unit commitment using separable programming". *Electric Power Systems Research* 203, 2022, p. 107669.

122. Y. Yang, J. C.-H. Peng, C. Ye, and Z.-S. Ye. "Optimal Reserve Allocation With Simulation-driven Frequency Dynamic Constraint: A Distributionally Robust Approach". *IEEE Transactions on Circuits and Systems II: Express Briefs*, 2022.

123. A. Jung. *Machine Learning: The Basics*. Springer Nature, 2022.

124. F. Pedregosa, G. Varoquaux, A. Gramfort, V. Michel, B. Thirion, O. Grisel, M. Blondel, P. Prettenhofer, R. Weiss, V. Dubourg, et al. "Scikit-learn: Machine learning in Python". *the Journal of machine Learning research* 12, 2011, pp. 2825–2830.